February 2005 • NREL/SR-520-37660

Subcontractor Report

# Implementation of a Comprehensive On-Line Closed-Loop Diagnostic System for Roll-to-Roll Amorphous Silicon Solar Cell Production

## Annual Report, Year Two
## 1 September 2003—31 August 2004

T. Ellison
*Energy Conversion Devices, Inc.*
*Troy, Michigan*

**National Renewable Energy Laboratory**
**1617 Cole Boulevard, Golden, Colorado 80401-3393**
**303-275-3000 • www.nrel.gov**

Operated for the U.S. Department of Energy
Office of Energy Efficiency and Renewable Energy
by Midwest Research Institute • Battelle

Contract No. DE-AC36-99-GO10337

February 2005 • NREL/SR-520-37660

# Implementation of a Comprehensive On-Line Closed-Loop Diagnostic System for Roll-to-Roll Amorphous Silicon Solar Cell Production

## Annual Report, Year Two
## 1 September 2003—31 August 2004

T. Ellison
*Energy Conversion Devices, Inc.*
*Troy, Michigan*

NREL Technical Monitor: R. Matson

Prepared under Subcontract No. ZDO-2-30628-11

**National Renewable Energy Laboratory**
**1617 Cole Boulevard, Golden, Colorado 80401-3393**
**303-275-3000 • www.nrel.gov**

Operated for the U.S. Department of Energy
Office of Energy Efficiency and Renewable Energy
by Midwest Research Institute • Battelle

Contract No. DE-AC36-99-GO10337

## CONTENTS

## BACKGROUND and EXECUTIVE SUMMARY

Energy Conversion Devices, Inc. (ECD) has developed and built 7 generations of roll-to-roll amorphous silicon PV production equipment. In the ECD/United Solar Ovonic production process we deposit about a 1 μm-thick 12-layer coating consisting of a metal/oxide backreflector, a 9 layer a-Si/a-SiGe alloy triple junction solar cell, and a top transparent conductive oxide coating onto 125 μm thick, 35.5 cm wide stainless steel webs in a series of three roll-to-roll deposition machines. Figure 1 shows a schematic of the United Solar 30 MW a-Si deposition machine; a photograph of the machine is shown in Fig. 2.

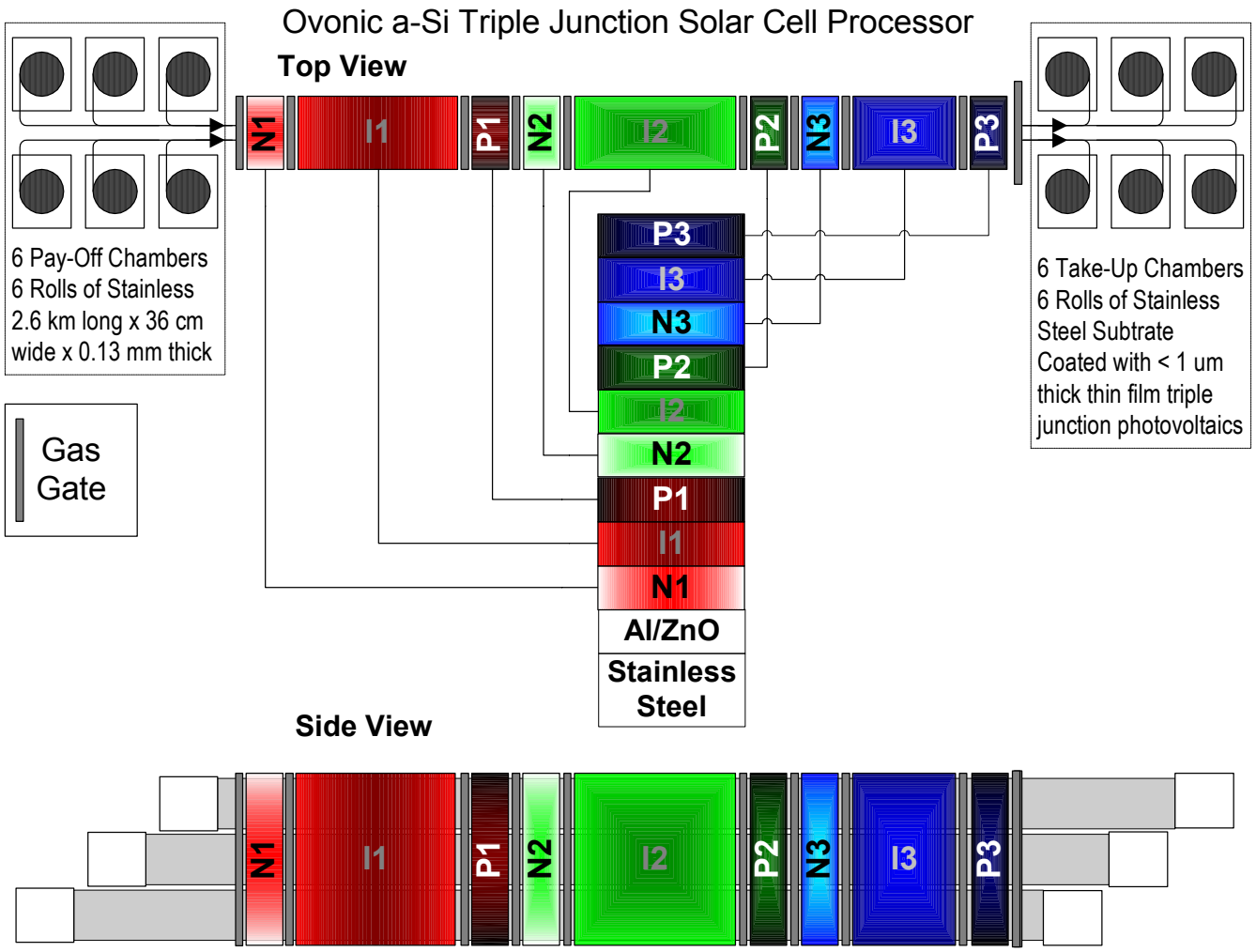


**Fig. 1.** Schematic of the United Solar 30 MW/yr a-Si deposition equipment.

All the developments of the PVMaT 5A program have been incorporated into this machine:

- A substrate heating and monitoring system, using durable NiChrome heater elements;
- Reactive sputtering for low-cost deposition of the Al/ZnO backreflector;
- A new PECVD cathode providing uniform deposition over large areas and reduced germane usage;
- "Pinch Valves" that allow the rolls of substrate to be installed and removed while keeping the deposition regions of the machine under vacuum; and

- Hardware for online diagnostic systems, including the non-contacting PV Capacitive Diagnostic (PVCD) system, which can measure the a-Si solar cell electrical properties in-situ without an ITO top coating[4], and reflection spectrometers to measure the cell thickness.

"Included in the machine" might be an understatement: many of these technologies are essential to the machine. For example, the a-Si machine processes about ½ MW of material in a single "batch" of six 2500 m long coils. Offline Q/A-Q/C may not be available for another 1 – 2 batch-cycles: it is difficult envisioning operating such a machine without the online diagnostic systems (e.g. PVCD and spectrometers) developed in the PVMaT 5A program.

**Fig. 2**. Side view of the United Solar 30 MW/yr a Si processor.

In the PV Manufacturing R&D Inline Diagnostics Solicitation, ECD is building upon these accomplishments to enhance the operation of the present production machine, and lay the foundation for improvements in the next generation machine. The four major work areas undertaken by ECD and United Solar in the present PV Manufacturing R&D program are described below:

1. Development of closed loop thickness control systems for the ZnO, ITO layers, and a-Si component layer thicknesses (the last is an expansion of this program) (Tasks 1, 5 and 9);
2. Continued development of the PVCD, and the initiation of online optimization using these devices (Tasks 2, 6 and 10);
3. The development of plasma monitoring systems to further optimize the i-layer deposition process, and for possible online implementation (Tasks 3, 7 and 11);
4. Yield improvements by investigating online yield measurement systems, investigations into sources of reduced yield, and mitigation of these sources (Tasks 4, 8 and 12).

United Solar has been expanding its manufacturing capability at a rate of about 30%/yr – doubling capacity every 3 years. The PV Manufacturing R&D Program is playing a key roll in the incubation of this Roll-to-Roll manufacturing technology allowing ECD/United Solar to develop new technologies to enhance the present equipment and lay the foundation for the next generation machines.

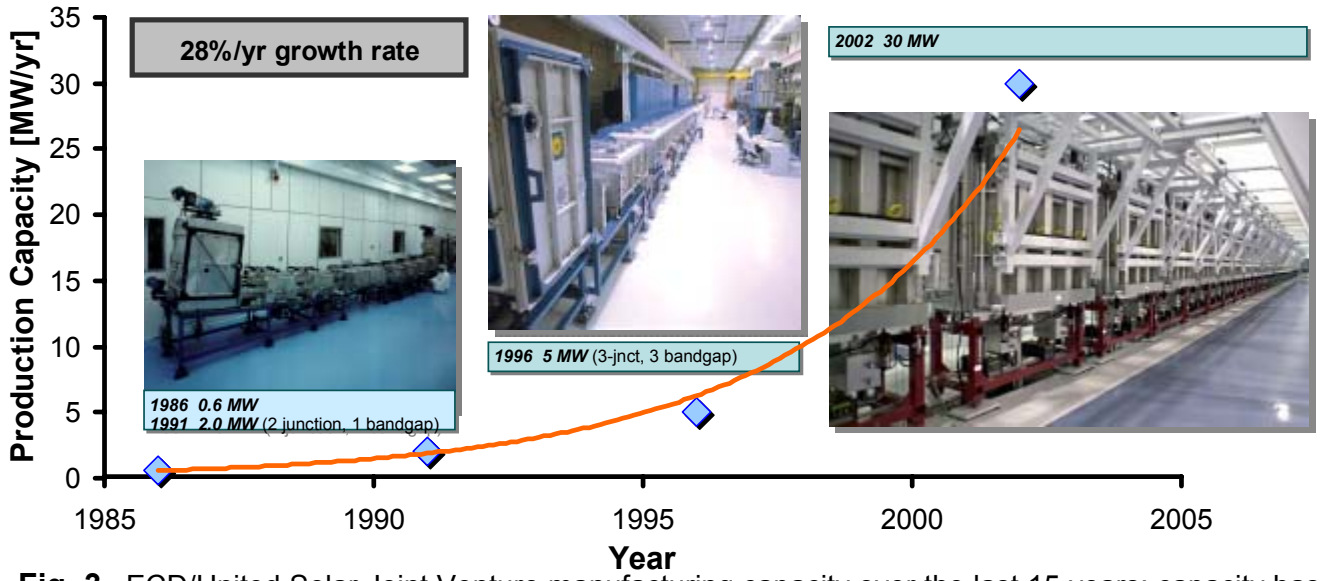


**Fig. 3**. ECD/United Solar Joint Venture manufacturing capacity over the last 15 years; capacity has expanded at about 30%/year, with more rapid expansion in the last 5 years.

ECD has now completed the Phase II work for this program. In the following report we summarize the Phase II work in each of these tasks.

We have involved United Solar production personnel in each of these Tasks. This is important for two reasons:

- Firstly, the collaboration of ECD and United Solar personnel keep the projects responsive to the developing needs at United Solar;
- Secondly, most of the tasks affect operations and consequently need the support of United Solar production and QA/QC managers.

In the process, we have developed a good working relationship between the production personnel and good balance between optimizing production while also "adiabatically" improving the manufacturing equipment.

*Note: Many of the figures in this report show "screen displays" taken from diagnostic system computer displays. Color is used extensively in these displays to convey information. If your are viewing a black and white copy of this report, some of this information will be lost, and we encourage you to view the color PDF file on the NREL website.*

## TASK 5: Development of Closed-Loop Control of Film Thickness – II

-- **Jeff Karn (ECD)** and Rujiang Liu (United Solar)

### 1.1 Introduction

Thickness is one of the most basic properties of deposited films. In the first phase of this project, thickness measuring spectrometers were developed and installed on the Backreflector (BR), amorphous silicon (a-Si), and top conductive oxide (ITO) deposition machines. These spectrometers provided valuable information during the commissioning process of the 30 MW equipment, and now serve as important tools providing online process monitoring and control. While this thickness information is provided real-time to the operator, it still requires interpretation and corrective action by the operator using the appropriate control set points. Under the second phase of this project this process was automated and the spectrometers have been successfully integrated into a closed-loop thickness control system (CLTC.) In addition, a new generation of spectrometer hardware has been successfully installed inside the more hostile environment of the a-Si deposition chambers. These new systems are now providing the opportunity to characterize the individual layers of the triple cell device.

The 1st generation CLTC system was installed in the ZnO Deposition Machine and was immediately adopted by the United Solar production team as at standard operating procedure. The ZnO Machine was chosen first since it is the most understood and easily-controlled of the three machines. The thickness control system on the ITO Machine has grown from one spectrometer to six spectrometers and multiple-control points as uniformity and color issues continue to be characterized. To address this more complex system a 2nd generation CLTC system was been developed. This system has been installed on the ITO Machine and is being commissioned.

The thickness control system on the a-Si Machine originally consisted of two spectrometers: one in the Pay-Off chamber monitoring the input material and one in the Take-Up chamber measuring the complete device. To measure individual layers a 2nd generation spectrometer was designed for installation in the deposition chambers. This new design had to overcome issues including high temperature, coating of optics, and accessibility. A prototype system was installed in a deposition chamber at the end of the middle layer. Experience from the operation of this system drove the design of a 3rd generation spectrometer. Two of these systems have been reliably operating and providing the thickness of the bottom cell and the "bottom + middle" cells. Installation of seven additional systems is progressing. The use of these spectrometers as part of a CLTC system on the a-Si Machine is being designed.

### 1.2 2nd Generation ITO/ZnO CLTC System

#### *1.2.1 ZnO Deposition Process and Control Points*

A 2nd generation CLTC system has been running on the Al/ZnO reactive sputtering Backreflector (BR) Machine for five months. This system maintains the thickness of the ZnO layer by controlling the oxygen flows to the plasma in this reactive sputtering process. The BR Machine has six plasma emission monitors (PEMs) at various locations in the deposition chamber. These devices use a PID controller to regulate the oxygen flow and maintain the plasma emission intensity at a set point. The six PEMs are collectively calibrated (using off-

line measurements) to produce uniform deposition. However, while the uniformity remains constant during operation, the overall ZnO thickness varies over time. The change in thickness can be corrected by scaling all six PEMs accordingly. The initial operational mode for the ZnO Machine required the operator to monitor ZnO thickness with the spectrometer and make corrections using the PEMs. Plotted in Fig. 1.1 is the variation in ZnO through such a production run. The saw-tooth pattern is produced as the thickness drifts beyond the established tolerance and the operator makes a corrective PEM change.

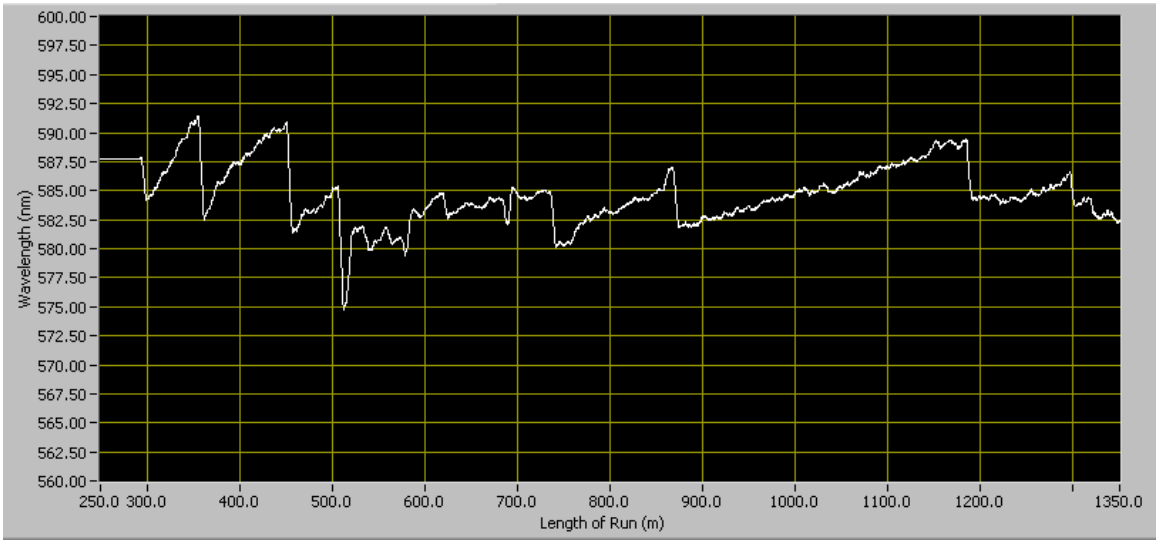


**Fig. 1.1.** Variation in ZnO through a production run prior to closed-loop control operation.

To quantify the change in thickness due to a PEM change, an experiment was performed that stepped the PEM settings to ± 9% and ± 18% of nominal. The reflection spectra from the spectrometer are plotted in Fig. 1.2 and the resulting shift in the ZnO interference maximum is plotted in Fig. 1.3.

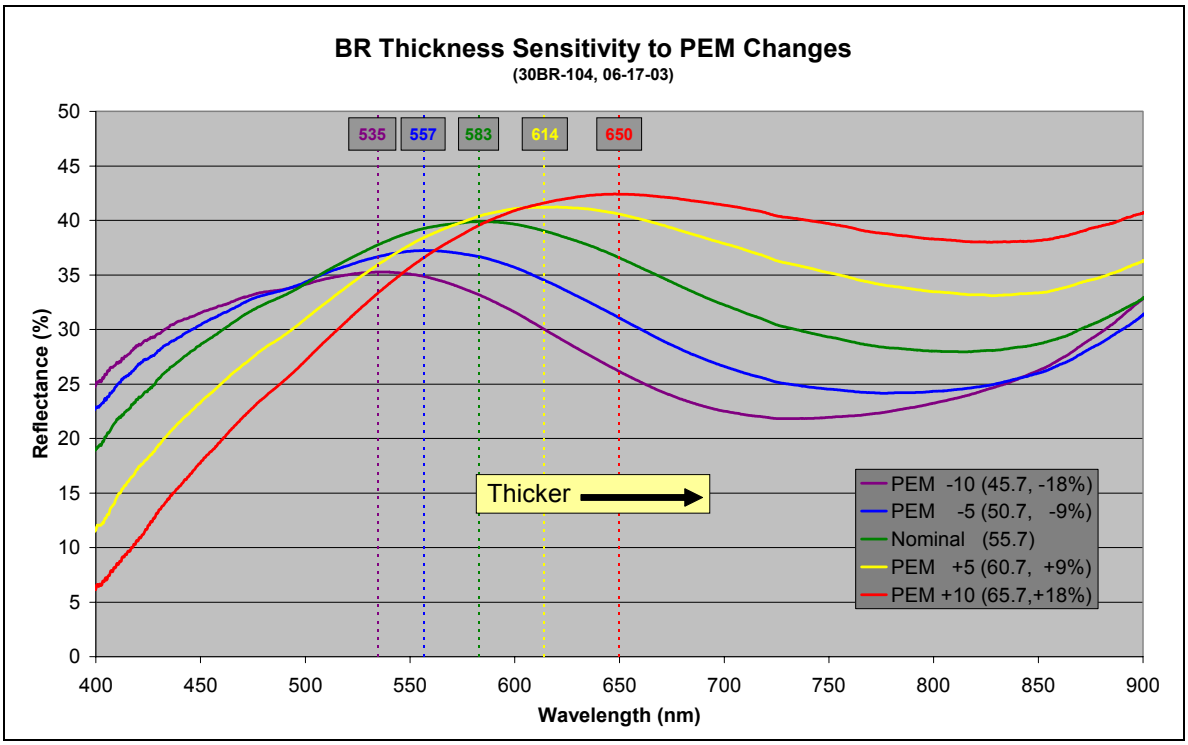


**Fig. 1.2.** Shift in the reflection spectrum resulting from PEM set-point changes.

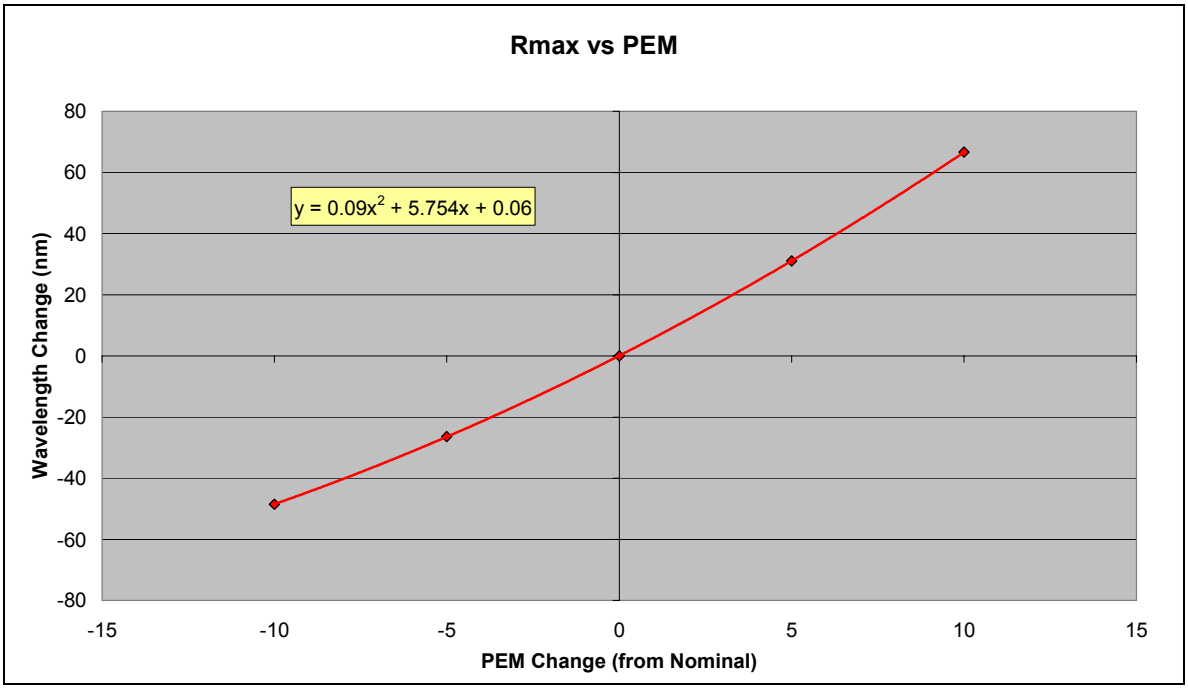


**Fig. 1.3.** Shift in ZnO reflection spectrum maximum due to PEM set-point changes

### *1.2.2 Closed Loop Control Software*

The modular layout of the closed loop software is shown in Fig. 1.4. The feedback algorithm resides on the PLC that runs the ZnO Machine. The algorithm is written in the S7 flowchart language of the Siemens PLC which provides a CPU efficient and robust framework. Communication between the PLC and the Controls Computer, PEM Computer, and Diagnostic Computer is accomplished by a mix of network protocols.

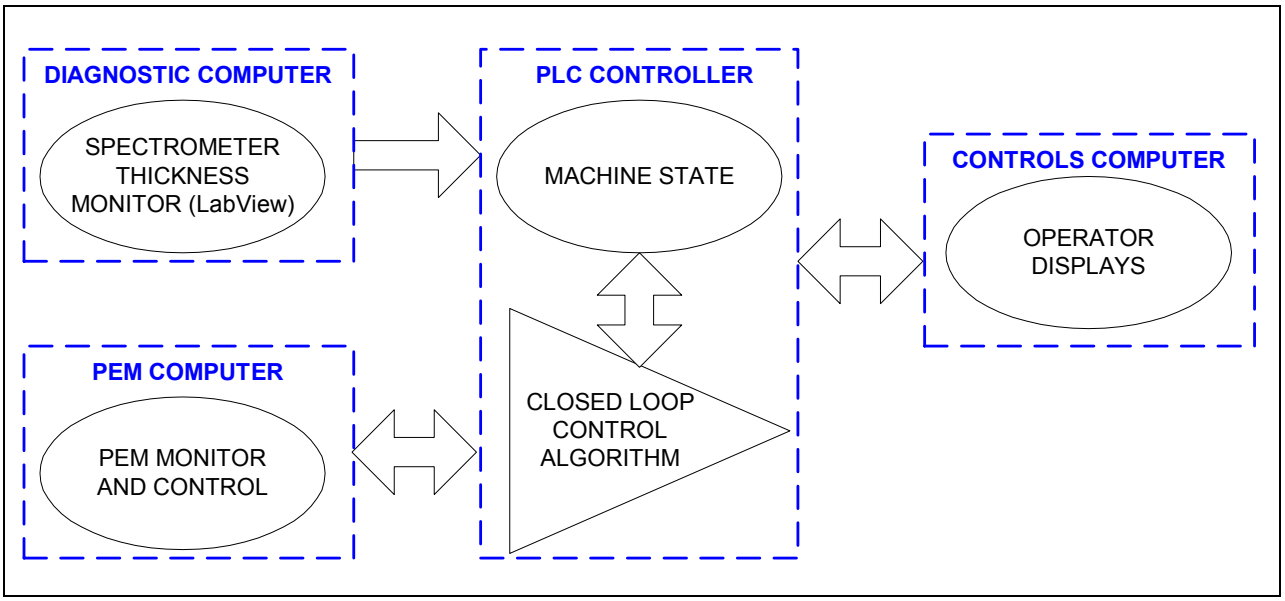


**Fig. 1.4.** Modular layout of the CLTC software

The operator interface for CLTC Is shown in Fig. 1.5. Features of the interface include:

- It is easy to switch between closed-loop and open-loop control modes by just clicking on the button in the PEM Control Modes group. The selected control mode will be turned green for indication purpose.
- The ZnO thickness set-point and measurement values are displayed in the $R_{MAX}$ group. The set-point can be changed but the measurement value is read-only.
- The control settings related to the control algorithm are displayed and adjustable on the interface screen.
- The Process Mode and communication with spectrometer, the two pre-requisite conditions to run the closed-loop control system, are displayed on the screen.
- For the purpose of monitoring the behavior of the CLTC system, historical data for thickness set-point and measurement, PEM set-point as well as PEM set-point increments are plotted.

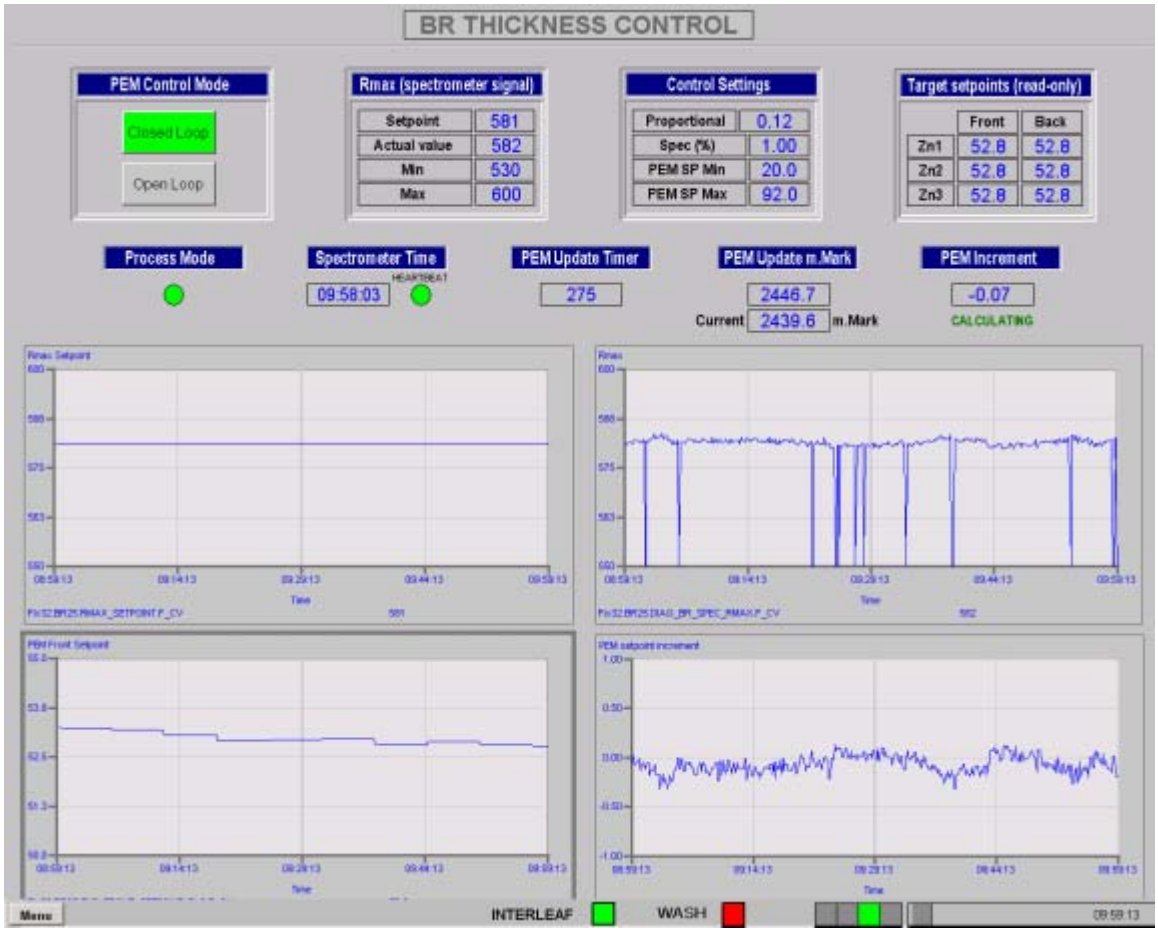


**Fig. 1.5.** BR CLTC Interface Screen.

### *1.2.3 Operation of the ZnO CLTC System*

Shown in Figs. 1.6a and 1.6b are the ZnO thickness profiles from two production runs. In Fig. 1.6a the machine is run in open loop mode with the operator periodically changing PEM settings. In Fig. 1.6b the CLTC system is running, demonstrating improved thickness consistency.

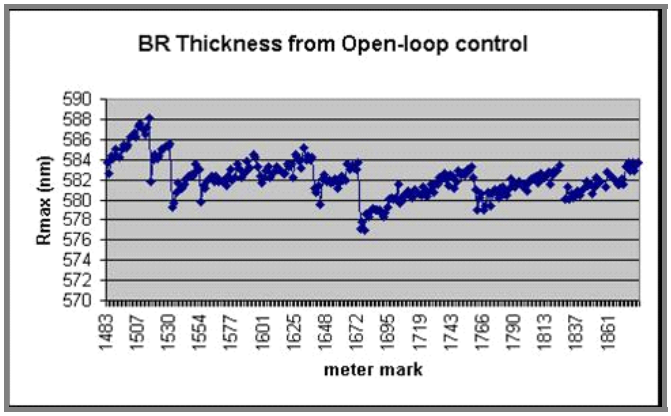


**Fig. 1.6a.** Open Loop

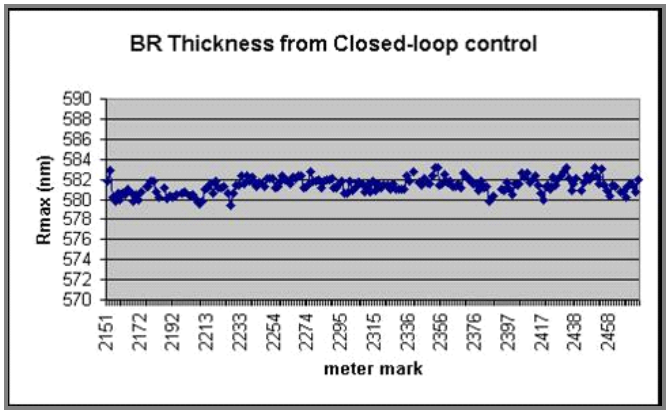


**Fig. 1.6b.** Closed Loop

## 1.3 3rd Generation ITO/ZnO CLTC System

### *1.3.1 Introduction*

When we wrote our proposal in the year 2000 we envisioned a CLTC system for the ITO Machine with a single measurement point and a single control point – much like we have implemented for the ZnO Machine. In the meantime, the 30 MW ITO machine has grown in complexity to control transverse web color uniformity to include 5 measurement points and 6 control points (2 PEM's and 4 gas valves) – as such, this system is significantly more complex than we envisioned, and the system developed for the ZnO machine cannot be trivially implemented on the ITO machine. ECD and United Solar have committed the additional resources needed to complete this work and all milestones by the end of this Phase at no additional cost to the program.

### *1.3.2 ITO Deposition Process and Control Points*

The ITO system is a Multi-Input and Multi-Output (MIMO) system with six inputs and five outputs. The layout of these devices is shown schematically in Fig. 1.7. The five output devices are thickness measuring spectrometers located transversely across the three webs. The six input devices consist of four valves controlling oxygen flow and two plasma emission monitors. The complexity of the system is driven by determining the coupling amongst the input and output variables of the MIMO system.

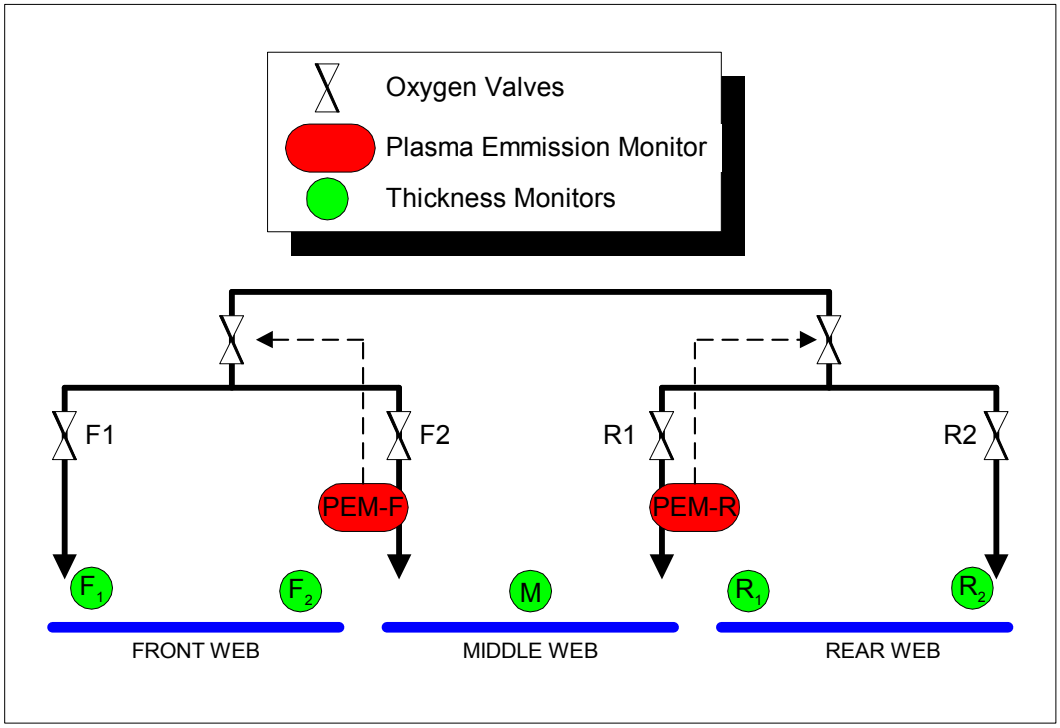


**Fig. 1.7.** Schematic layout of the ITO CLTC inputs and outputs

Data collected from past runs has been analyzed to determine this coupling. This analysis has shown that the MIMO systems can be divided into two subsystems: one for the Front Web and one for the Rear Web. Each subsystem will consist of two inputs and two outputs. The two

subsystems will also receive a global correction signal from the Middle Web output. Using the labeling convention denoted in Fig. 1.7 the three parts of the control strategy are:

- Front Web Subsystem
  - Inputs: PEM-F, valve $F_1$, and valve $F_2$
  - Outputs: Spectrometer $F_1$ and $F_2$
- Rear Web Subsystem
  - Inputs: PEM-R, valve $R_1$, and valve $R_2$
  - Outputs: Spectrometer $R_1$ and $R_2$
- Middle Web Correction
  - Output: Spectrometer M

### *1.3.3 ITO Closed Loop Control Software*

The main control panel for the ITO CLTC is shown in Fig. 1.8. The section of controls labeled *$R_{MIN}$'s* are the readbacks and setpoints of the five thickness monitoring spectrometers. The units for the spectrometer values are given as a percent of a defined thickness. This provides more flexibility to the spectrum processing software to use different interference extrema to derive deposition thickness. Each spectrometer also provides a "Burn Detection" indicator to warn the Operator and the CLTC algorithm that an a-Si burn is present and that no changes should be made to the ITO deposition. The section of controls labeled "PEMs" and "O2 Valves" are the readbacks and setpoints for the six input devices. The PEM controls for both targets will be ganged together and provide a front and rear input.

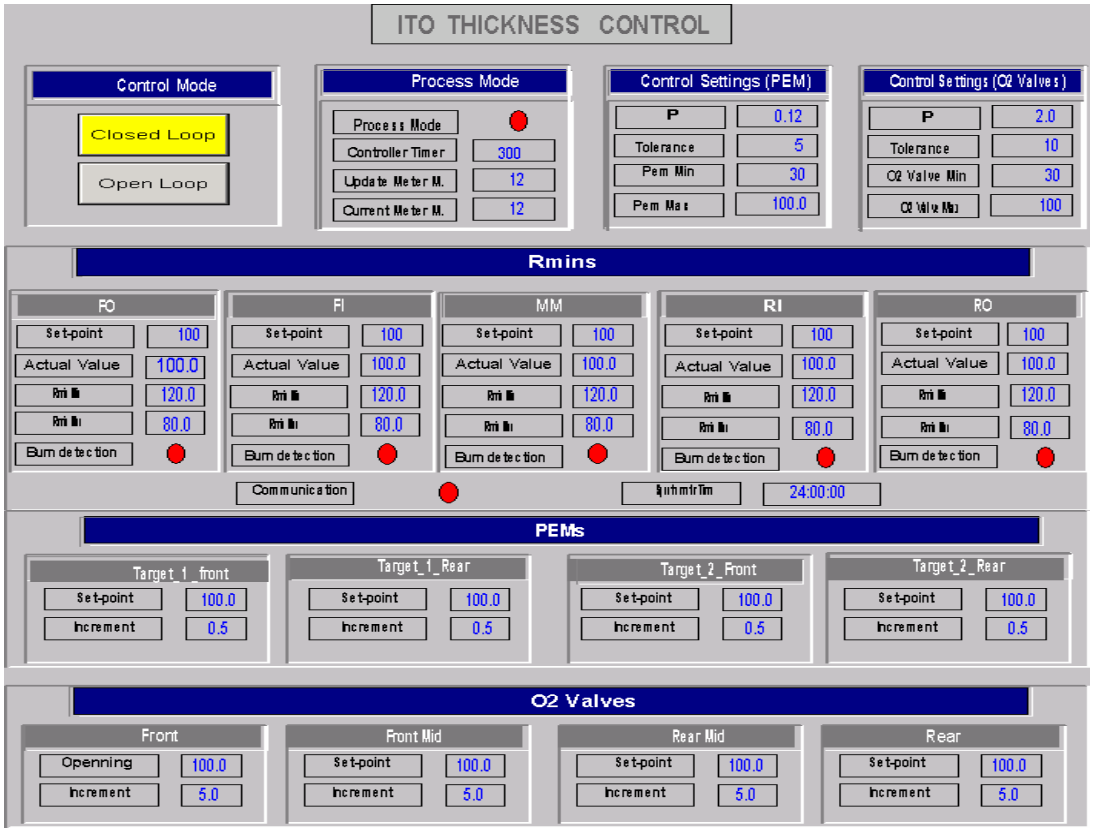


**Fig. 1.8.** ITO Machine CLTC Operator Interface Panel

### *1.3.4 Changing Emphasis: From Closed-Loop Thickness Control to Closed Loop Process Control*

Thickness is one of the most fundamental properties of thin films – but it is not the only property that affects the PV device efficiency. For example, other important properties of the ITO coating include conductivity and transparency; and other properties of the Backreflector include reflectivity, transparency, and texture. We have documented significant changes in film properties while only operating the process to keep film thickness constant both in the BR machine and the ITO machine. For example, Fig. 1.9 shows a situation where we observe a 3% and 1% change respectively in the measured offline $P_{MAX}$ and $V_{OC}$ while no change was observed in any of the online PVCD or spectrometer signals in the a-Si machine. This change was traced to a process change in the ITO machine that was not correlated with ITO optical thickness *per se*. In our future thinking, to maximize the performance of our devices we need to:

- ***Begin focusing on closed loop process control, not just closed loop thickness control;***
- ***Develop complete online cell characteristic diagnostics for use after ITO deposition;***
- ***Join the BR and ITO machines to the a-Si machine for online optimization of the complete device.***

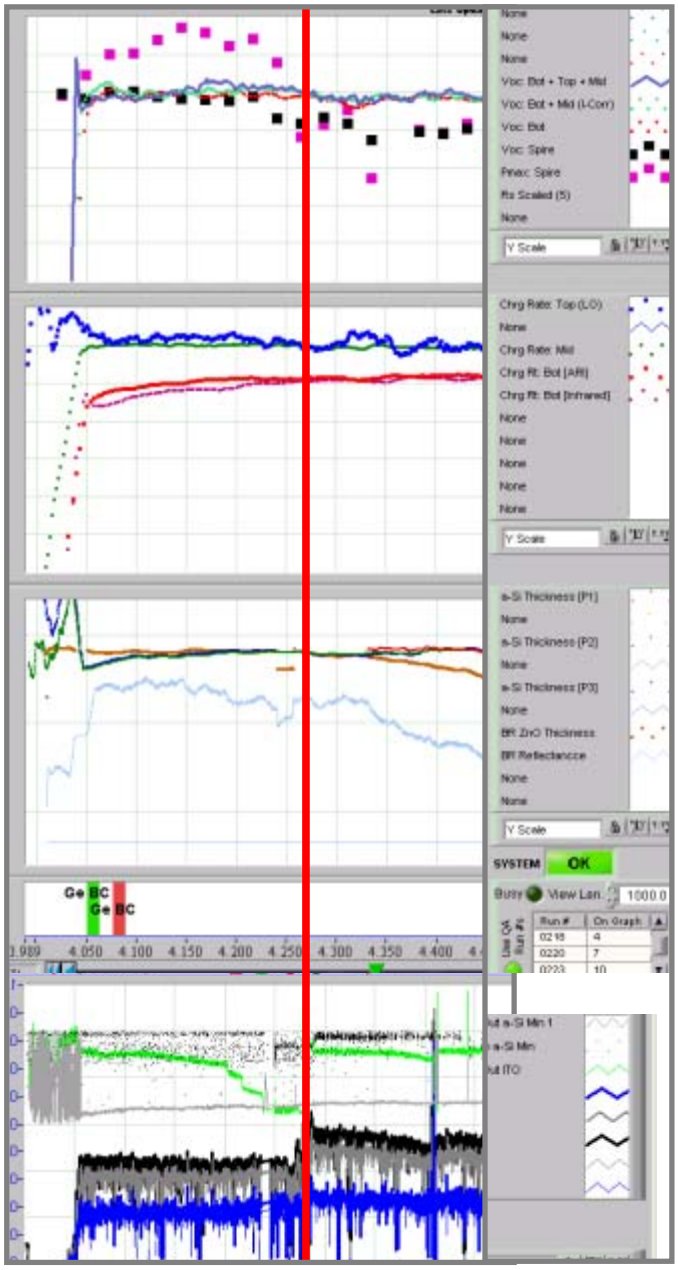


**Fig. 1.9.** Online data from a-Si and ITO machines along with offline QA/QC data.

## 1.4 2nd and 3rd Generation a-Si Spectrometers

### *1.4.1 2nd Generation Operation and 3rd Generation Design Changes*

A 2nd generation spectrometer was installed and briefly operated in the P2C (end of the middle layer) deposition chamber. Operational experience with this system led to several improvements and the development of the 3rd generation spectrometer. Several of these changes were retrofitted into the existing P2C spectrometer while all features were incorporated into a new installation in the P1C (end of bottom layer) chamber. Both P1C and P2C have been operating with high degree of reliability for four months. We now have online measurements of the thickness of each cell in the triple-junction device. Installation of seven additional 3rd generation systems at new locations is in progress; this additional capability will provide online measurement of each n, i, and p layer for all three cells.

The quality of the measured reflectance spectrum is driven by the alignment and stability of the spectrometer detection lens to the traversing web. To address this issue three primary design changes were instituted and are outlined below:

- Web Stability: The 2nd generation system used a Vespel-tipped finger to push on the back side of the web at the location of the spectrometer. Once adjusted, this finger significantly reduced the noise from web movements. However, the softer Vespel material was observed to wear and required periodic adjustment to maintain an effective force on the web. The 3rd generation system use two hardened rollers that wrap around the existing mag-roller and press against the traversing web (Fig. 1.10.) The rollers are adjusted into the web to remove the contact with the mag-roller locally in the vertical region where the spectrometer acquires the reflection spectrum.
- Spectrometer Stability: The 2nd generation system was also observed to make abrupt alignment changes in between production runs. This was believed to be caused by the extreme thermal cycles of the deposition chambers between runs. To minimize the high temperatures seen by the spectrometer a blower was configured to increase the air flow through the quartz tube. In addition, the 3rd generation spectrometer mount included extra vent holes to improve the added flow.
- Internal Reflection Reduction: Aligning the 2nd generation spectrometer proved to be a challenge due to the fact that it is hidden deep inside the deposition chamber and out of view. Ideally, the detection lens is focused to create a small spot and thus a stronger reflected signal. However, this smaller spot increases the difficulty in aligning the reflection back into the detection fiber. By defocusing the lens and creating a larger spot the alignment gets easier but the signal strength drops. In addition, the larger spot assures that some of the emitted light will strike the quartz tube perpendicularly and be reflected directly back into the detection fiber – thus creating an offset baseline. To minimize this internal reflection from the quartz tube the 3rd generation system offset the detection lens from the centerline of the tube. Due to the already tight dimensional constraints this required a significant redesign of the detection optics.

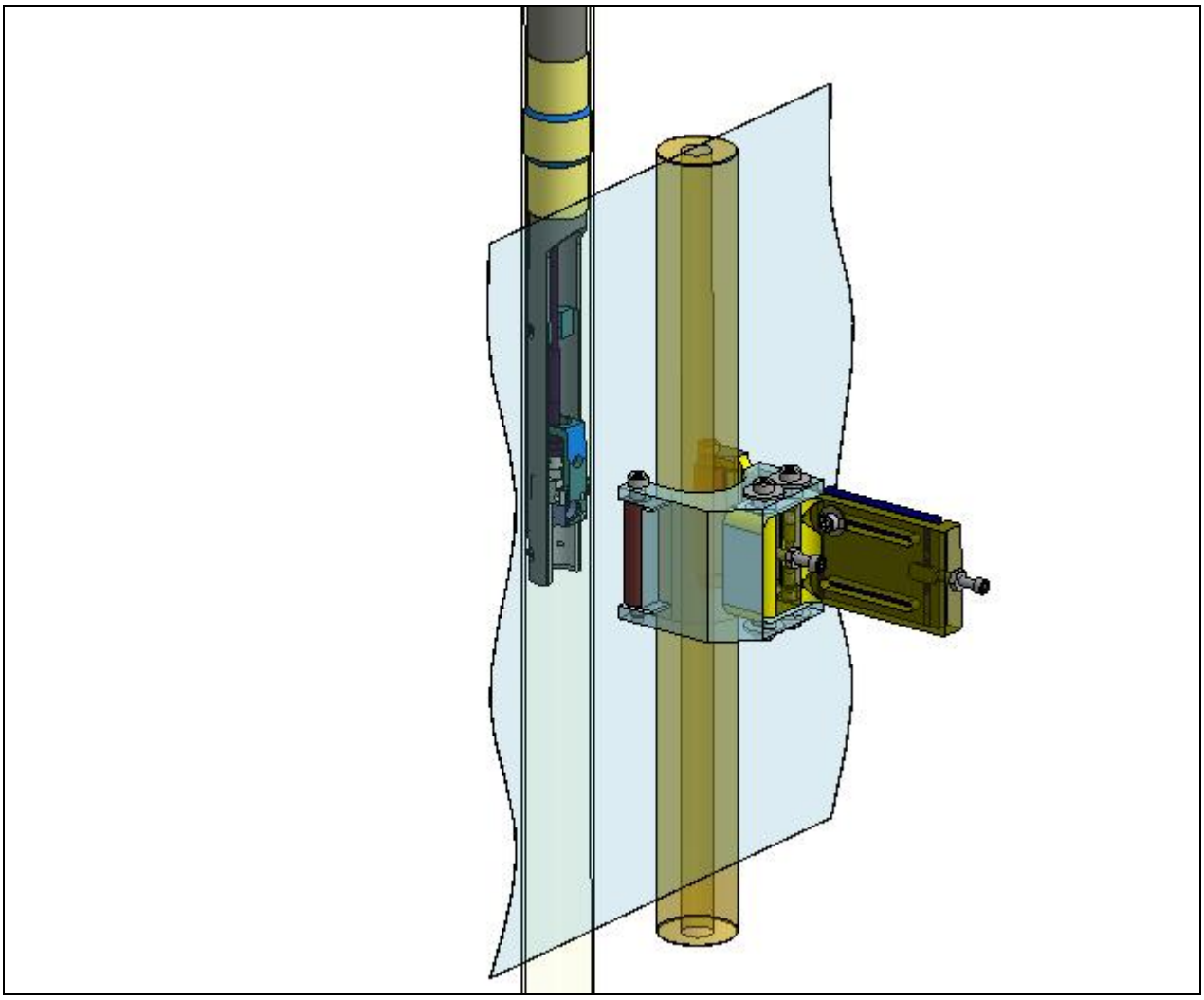

**Fig. 1.10.** Model of 3rd generation Spectrometer's new web stabilizer. Two hardened rollers wrap around the existing mag-roller (vertical gold cylinder) and press against the web (light blue.)

### *1.4.2 3rd Generation Spectrometer Operation*

The new web-stabilization and spectrometer temperature stabilization systems have resulted in extremely stable signals for the a-Si quartz-tube-mounted spectrometer systems. Plotted in Fig. 1.11 is the amplitude of the reflectance over two production runs: Run #201 and Run #202 as denoted by the color bars on the x-axis. Prior to Run #201 the web stabilizer was positioned at a time when the heaters were off in the deposition machine. It can be seen that as this run progressed the amplitude drifted upwards. The abrupt changes at 700 meters and 1500 meters occur when the machine was cooled down. At 2100 meters, while Run #202 was in progress, the web stabilizer was readjusted. This resulted in a larger reflectance signal and did not demonstrate the observed shift when the machine was again cooled at 2700 meters.

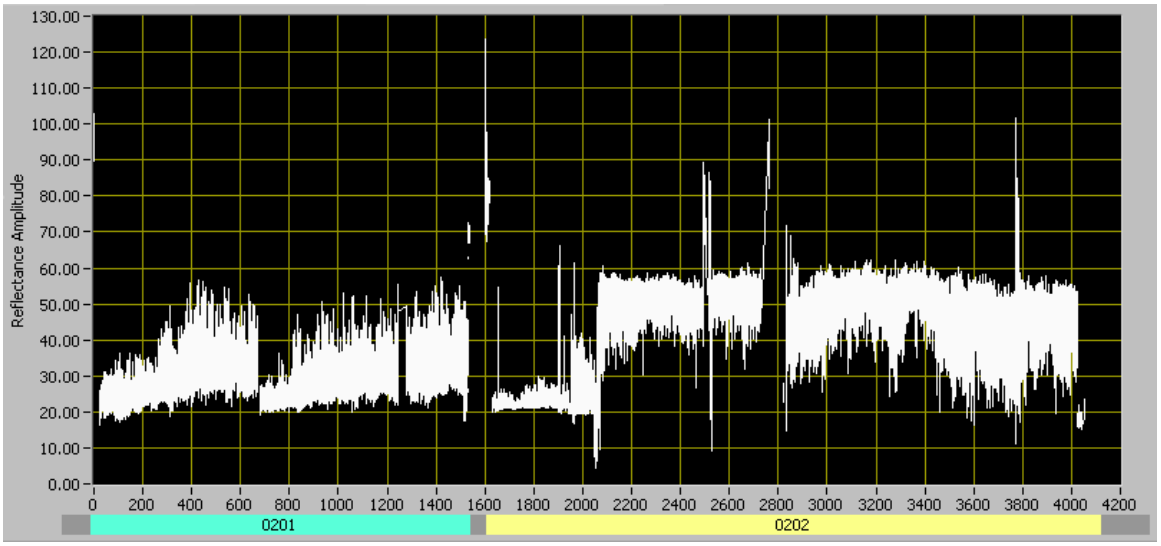


**Fig. 1.11.** Reflectance amplitude from two production runs. System realigned at 2700 meters when machine was at operating temperature.

The amplitude signal serves as a sensitive means for monitoring spectrometer stability but it is the wavelength that is proportional to thickness. The significant noise level observed in the amplitude has a minimal effect on the measured wavelength. Plotted in Fig. 1.12 is the thickness from a one minute static burn as measured by P2C and a second spectrometer located in the Take-Up Chamber. This plot demonstrates that the precision and signal to noise of P2C system is now comparable to that of the long-established Take-Up spectrometer; this is further demonstrated in Fig. 1.13 which shows thickness measurements of the total cell thickness (blue) and thickness of the bottom and middle cells (green) over an 8000 m length of operation.

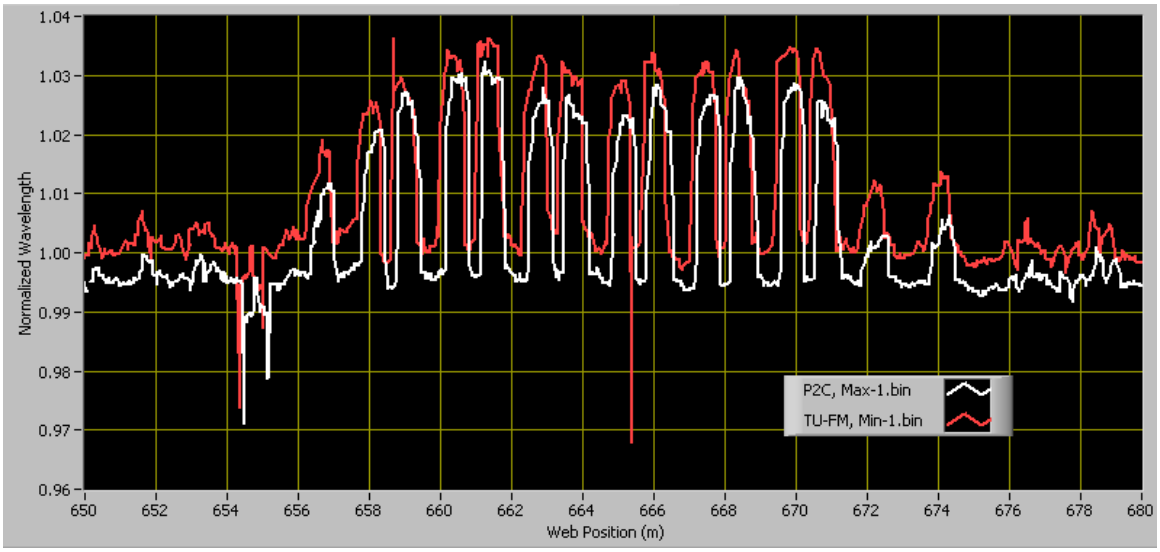


**Fig. 1.12.** Wavelengths of P2C and Take-Up Spectrometers demonstrating comparable precision and stability.

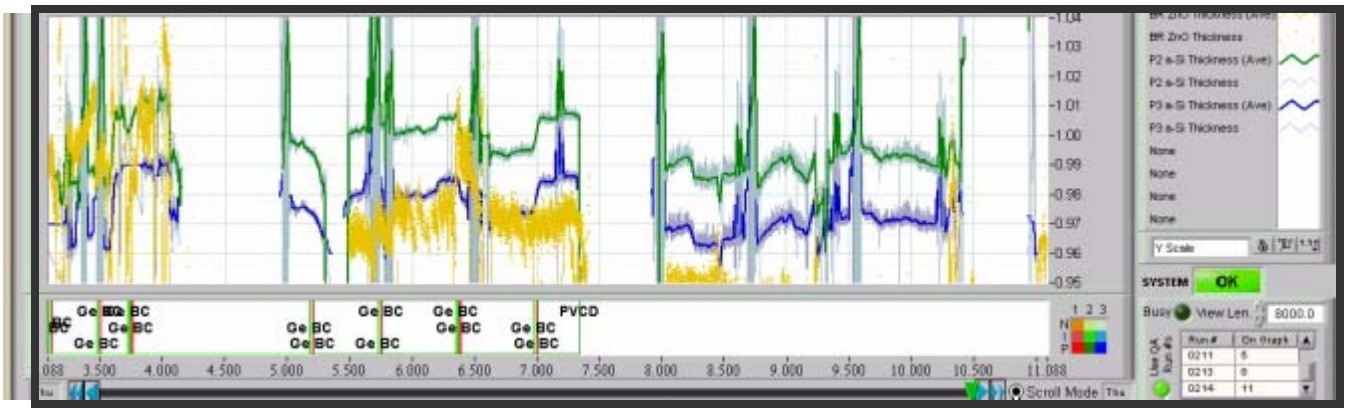


**Fig. 1.13.** Online thickness measurements of the Bottom + Middle Cells, and the Bottom + Middle + Top Cells over 8,000 m of production. Vertical: 1%/div. The darker lines in the middle are running averages of the real time data (lighter-colored signals).

## 1.5 1st Generation a-Si CLTC System

### *1.5.1 Introduction*

The ZnO closed-loop thickness control (CLTC) system described in section 1.2 uses one spectrometer to measure thickness and one control point for adjustment. The 3rd generation of this system for the ITO Deposition Machine, describe in section 1.3, is much more complex with five spectrometers and six control points. In the a-Si Deposition Machine the CLTC system will have to control the thickness of 12 layers using 13 spectrometers and choose from ~ 70 control points. The varying complexity of the CLTC systems for these three machines is summarized in Table 1.1.

| Machine | Deposition Layers | Spectrometers | Primary Control Points |
|---|---|---|---|
| ZnO | 2 | 1 | 1 |
| ITO | 1 | 5 | 6 |
| a-Si | 12 | 13 | ~ 70 |

**Table 1.1.** CLTC Complexity for ZnO, ITO, and a-Si Machines

Spectrometers are being installed to measure the thickness of the N, I, $P_{etch}$, and $P_{dep}$ layers for each of the bottom, middle, and top cells. These locations, and the present installation status, are shown schematically in Fig. 1.14.

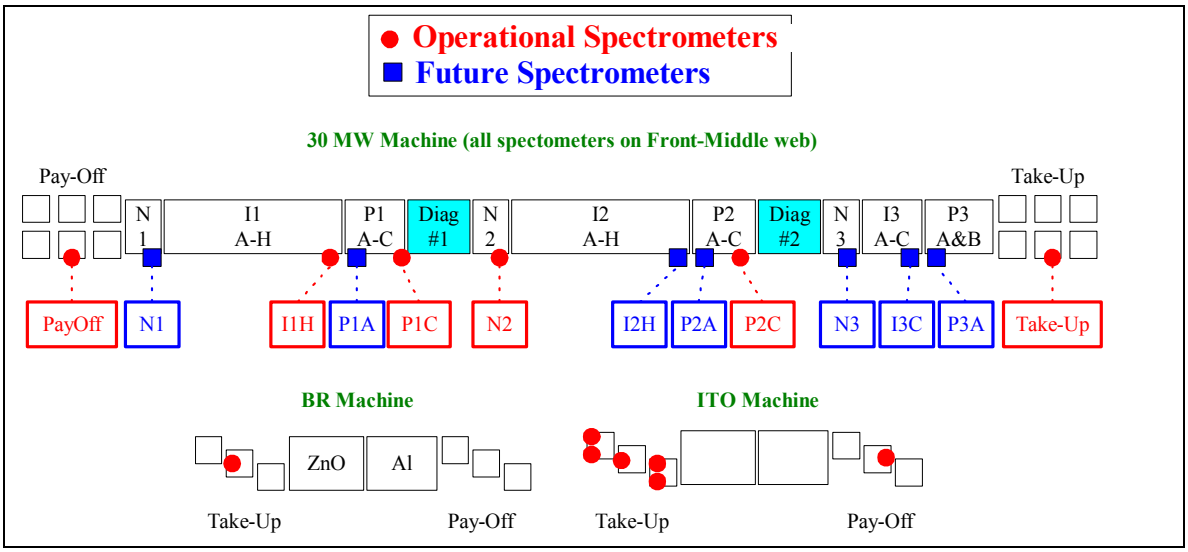


**Fig. 1.14.** Layout of operational and future spectrometers.

### *1.5.2. CLTC Design*

Due to the complexity of the a-Si deposition process the design of the CLTC system is being approached from two directions: bottom cell thickness control and top cell thickness control. Each approach has pros and cons that will require detailed analysis and experimentation to characterize the closed-loop algorithms. Pursuing each approach in parallel will assure the fastest path to success and a more immediate impact on improving machine performance.

A source of yield loss is the color of the final PV product. Measurements have shown that this color can be affected by not only the top ITO layer thickness, but also the top a-Si cell thickness. Consequently controlling the thickness of the top cell would offer immediate benefits. Another favorable issue for top cell control is the reduced number of control points: either via a single gas flow control or a single RF power control. Control of the bottom layer is more complex due to the use of multiple gases, silicon/germanium grading, and coupling between RF-driven thickness changes and cell current.

The primary drawback to top cell control is the complexity of determining the actual top cell thickness. In theory, a spectrometer located before the top layer provides the thickness of the "bottom + middle" layers and a spectrometer located after the top layer provides the thickness of the "bottom + middle + top" layers. A simple subtraction provides the top cell thickness. However, past analysis has shown that the perceived thickness is affected by absorption and index changes in the lower layers. These two spectrometers are not adequate to quantify changes in the top cell thickness. Rather, information from additional upstream spectrometers will have to be integrated into the algorithm for calculating top cell thickness. This added complexity does not exist for the bottom cell.

A summary of the pros & cons for each approach is listed in Table 1.2. While top cell thickness control is the most important it is complicated by variations in the bottom and middle layers. Controlling bottom layer thickness, while offering minimal immediate performance benefits, is the systematic starting point for complete device thickness control, measurements are relatively easy, but control is difficult. Thus, the adopted two-pronged approach will be pursued.

| Issue | Bottom Cell Control | Top Cell Control |
|---|---|---|
| Importance to overall device performance | less important | most important |
| Complexity in determining cell thickness | easier | complicated |
| Complexity in controlling thickness | more difficult | less difficult |

**Table 2.** Pros & Cons of Top Cell versus Bottom Cell Thickness Control

Experiments have been scheduled to vary potential control points (RF and gas flows) in the both the top and bottom cells. Analysis of these data will provide the necessary sensitivity matrices for closed-loop thickness control and will quantify effects related to overall device performance. In addition, spectrometer data from past runs will be analyzed and used for development of an algorithm for calculating the thickness of individual layers. Static burns provide a controlled test for evaluating algorithm effectiveness.

## TASK 6: PV Capacitive Diagnostic (PVCD) Design and Fabrication for Bottom and Middle Cells

**– Tim Ellison**, Rob Kopf, Jeff Karn and Wayne Messing (ECD); Dave Dodge (Focus Software)

### 2.1 Introduction and Background

In the PVMaT 5A program we developed the PV Capacitive Diagnostic (PVCD) [1]. This device has proven its capability to make precise (≈ 0.1%) in-line measurements [2,3] of the PV device open circuit voltage, $V_{OC}$, and short circuit current divided by cell capacity, $J_{SC}/C$. It also provides information on the cell series resistance, $R_S$. This non-contacting device works on material both before and after application of the top ITO coating, and has become an essential online diagnostic for production QA.

The goal of this program was to extend this technology to be able to characterize each component cell of the triple-junction device. While the original PVCD can precisely measure the triple-junction device $V_{OC}$, it could not unambiguously tell us which of the three cells had changed. We envisioned a series of three PVCD's, one following each completed cell.

The original PVCD was developed to operate in the Take-Up chamber of the a-Si machine. This was "simple" in that in the Take-Up chamber:

- There are few space constraints;
- The device is far from any EMI-generating plasmas and heaters;
- The device can easily be shielded from extraneous light and ionized gas generated by plasmas;
- The device design did not require the use of ultra-high purity vacuum materials and techniques necessary to install the device inside the deposition part of the machine.
- The device was easily accessible for service, modifications, and calibration.

The Component Cell PVCD developed in this program had all these additional constraints – and it was not clear whether it could even be made to operate in such an environment.

The Component Cell PVCD's (Fig. 2.1) are now operating for both the Bottom and Middle cells as online Quality Assurance (QA) tools and are a tremendous success:

- The devices provides measurements of the bottom cell and bottom + middle cells open circuit voltage, $V_{OC}$, about every meter with an rms noise of about 0.05%. They also provide, at the same repetition period, two measurements of the bottom cell charging rate (one signal provides information on the cell $J_{SC}$ and $R_S$, and the other signal provides information about the cell bandgap) and one measurement of the middle cell charging rate.

---

[1] Tim Ellison, "Non-contacting PV Capacitive Diagnostic (PVCD) System for real-time in-situ analysis, QA/QC, and optimization", *Proc. 28th IEEE Photovoltaic Specialists Conference* (Anchorage Alaska, 15 – 22 Sept 2000).

[2] Greg DeMaggio et al., "Development of Online Diagnostic Systems for Roll-to-Roll a-Si Production: ECD's PV Manufacturing R&D Program", Proceedings of the 2003 NCPV Review Meeting (Denver, 24 – 26 March 2003).

[3] Masat Izu and Tim Ellison, "Roll-to-roll manufacturing of amorphous silicon alloy solar cells with in-situ cell performance diagnostics" in Solar Energy Materials and Solar Cells, Elsevier Science B.V., Amsterdam.

- Online troubleshooting is becoming much easier – rather than saying we have a problem, we are now often able to quickly pinpoint problems to specific cathodes, online, and adjust the process online to compensate.
- Even in offline QA/QC testing, we only obtain a $V_{OC}$ for the complete device; online we now have precise information on the $V_{OC}$ for each of the component cells. This is changing the language that we use – if the $V_{OC}$ changes, one now asks, "which $V_{OC}$?".
- To ensure reliability, the devices have two calibration systems:
  -- An online calibration system that tests and calibrates the entire electronics system every few minutes with a precision of 0.01%.
  -- There is also an offline calibration system that can test the device at a more fundamental level.
  -- There are also other system-diagnostics, such as a continuous measurement of the substrate temperature, data-logging of the LED light source current, and measurement of the light pulse amplitude.
- Finally, with reliable voltage, current [and thickness] measurements of each component cell in the triple-junction device, we can now envision a significant continuous online optimization program.

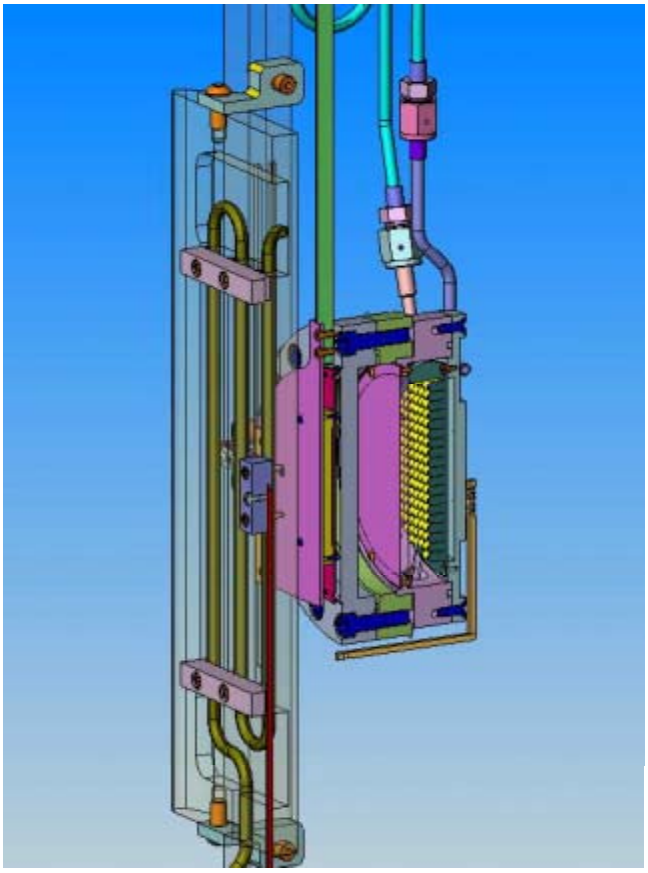

**Fig. 2.1.** Close-up view section view of the PVCD sensor head, shutter, and transparent view of the "pusher plate".

In the following sections we summarize Phase II work in the following areas:

- Further improvements in the Bottom (Component) Cell PVCD (installed October 2002, and commissioned towards the end of Phase I) and examples of uses of this device for online QA (e.g., germane gas concentration, bottom cell $R_S$);
- Installation and optimization of the Middle (Component) Cell PVCD and its use as an online QA device;
- In progress work to change the PVCD temperature stabilization systems;
- Development of diagnostics for the diagnostic systems and the development of a new Alarms/Warning/Expert system; and, finally,
- The initial use and future prospects of using these systems for optimization.

## 2.2. Bottom (Component) Cell PVCD

The 2nd Generation Component Cell PVCD installed after the bottom cell in the 30 MW production machine is now in use as an online QA device to decide the course of runs. Figure 2.2 is a screen capture of the Data Diagnostics Display in the 30 MW control room. This particular display shows $V_{OC}$ data from 3 sources:

- The Take-Up chamber PVCD which measures the $V_{OC}$ of the complete triple junction device [grey closely-spaced dots];
- The Bottom Component Cell PVCD which measures the $V_{OC}$ of just the bottom cell [red closely spaced dots]; and
- Offline $V_{OC}$ measurements from a Spire solar simulator [widely-spaced blue squares].

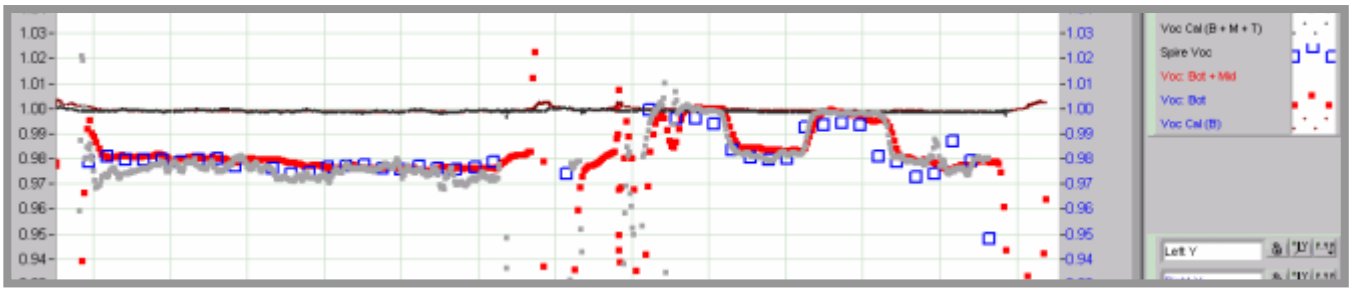


**Fig. 2.2.** Screen capture of a portion of the Control Room Data Diagnostic Display (DDD): [Grey closely-spaced dots: TU PVCD relative $V_{OC}$; Red closely-spaced dots: Bottom Component Cell PVCD relative $V_{OC}$; Large widely-space blue squares: relative offline spire measurements of the complete device $V_{OC}$]; 1/%/div].

In this 1300 m record most changes in the device $V_{OC}$ were due to deliberate changes in the germane gas flow to the bottom cell reactors and, consequently, changes in the $V_{OC}$ in the device due mostly to changes in the bottom cell. In this online plot one can clearly see the degree of precision and accuracy of this device.

The signal-to-noise ratio for this device is illustrated in Fig. 2.3. A few observations:

- Throughout this 500 m section the bottom cell $V_{OC}$ signal stays within a range of ± 0.2%, showing both the stability of the diagnostic system, as well as the production machine.
- The rms noise for the measurement, looking at 20 successive data points, is less than 0.05%. The source of this noise is not yet determined; by contrast, the noise level for the Calibration Signal, which tests all the electronics, is 5 times lower.

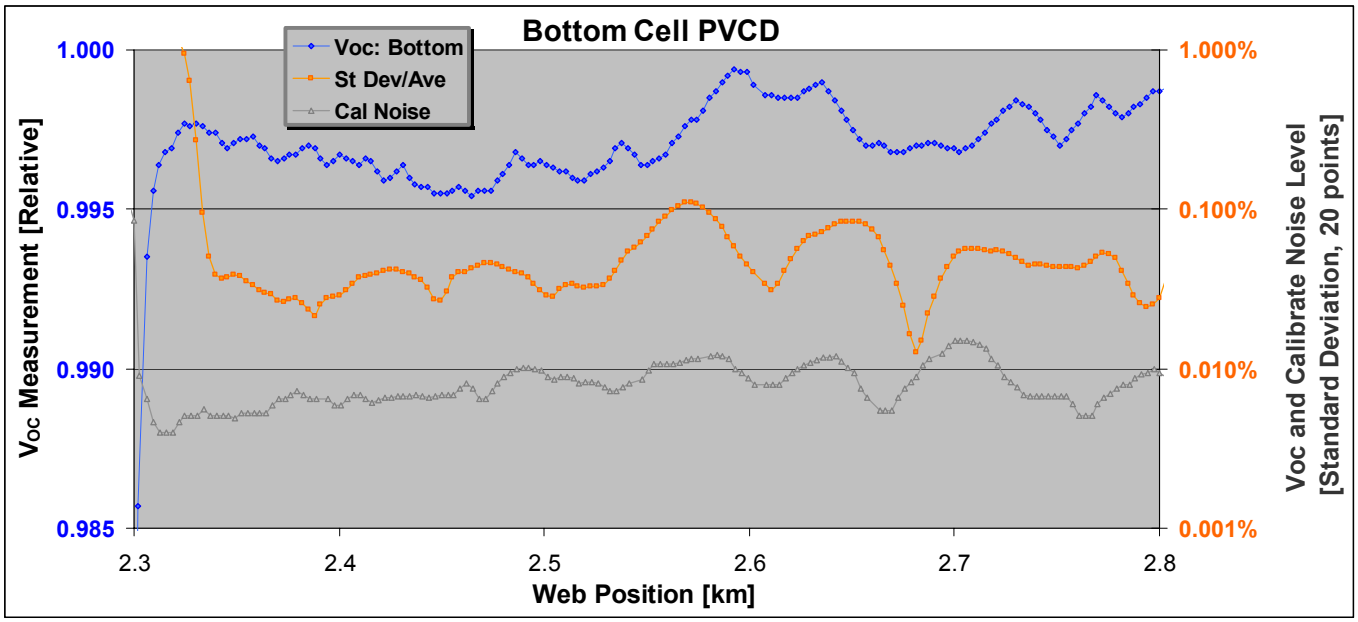


**Fig. 2.3.** Normalized bottom cell $V_{OC}$ measurements from the bottom (component) cell PVCD. Also shown are the standard deviations, or rms noise levels, for both the $V_{OC}$ signal and the Electronics Calibration signals.

### *2.2.1. Use of Bottom (Component) Cell PVCD to Measure Germane Concentration*

The PVCDs have demonstrated the ability to detect changes in the germane concentration of the bottled $GeH_4/H_2$ gas at the level of about 0.1% when bottles are changed.

We initially calibrated the PVCD $V_{OC}$ vs. Ge flow as shown in Fig. 2.4. The standard deviation of the PVCD $V_{OC}$ measurement corresponds to a 1% change in Ge concentration; a 20 minute average of the PVCD amplitude reduces this value to 0.3%.

To further increase our precision in this measurement, and to discern between cell thickness or $R_S$ changes and changes in bandgap, we added a new measurement to the Bottom Cell PVCD program: a charging rate measurement using long-wavelength IR light pulse at 860 nm. This signal is shown in Fig. 2.5, a Data Diagnostics Display screen-capture during a recent 2400 m run.

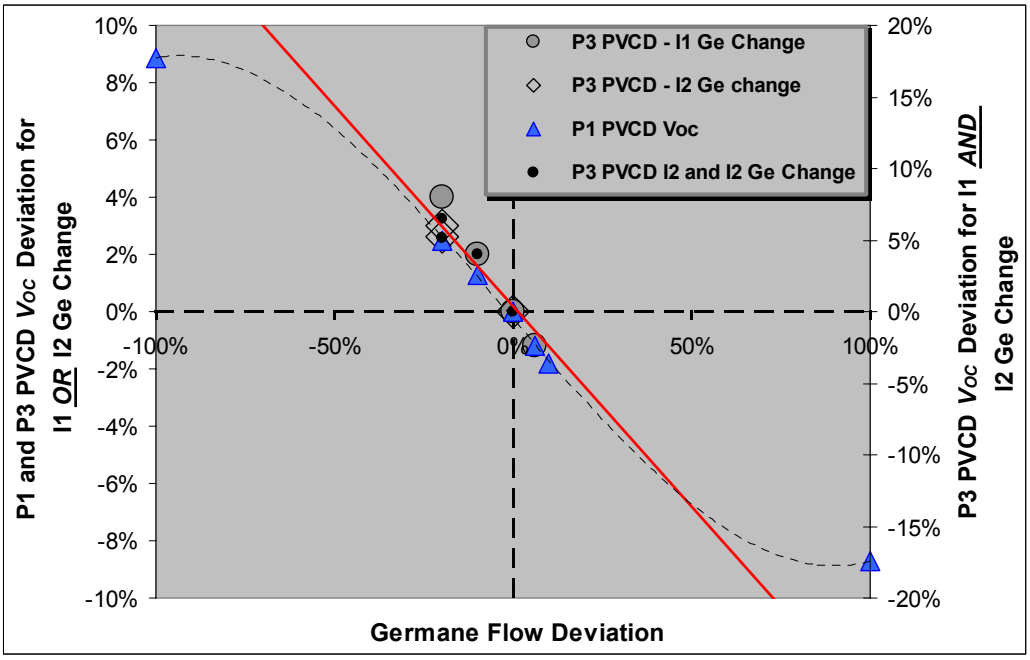


**Fig. 2.4.** Data from experiments with changes in germane gas flow. Four sets of measurements are displayed: the P1 PVCD can measure changes in the bottom cell $V_{OC}$; since the changes pass through the P3 PVCD serially, it can measure changes in the bottom, middle, and bottom + middle layer; this latter change is plotted on the right-hand scale.

Explanation of Fig. 2.5:

- The upper plot shows the open circuit voltages, $V_{OC}$, 1%/div, ±3% full scale. Red: bottom cell; Grey: complete triple junction device.
- The middle plot shows cell charging rates, 2%/div, ± 10% full scale. Blue: top cell; Blue-green: top cell normalized to PVCD photo-detector output; Light Red: bottom cell charging rate using amber, red, and infrared light; Dark Red (new signal): bottom cell charging rate with only an infrared light pulse.
- The bottom plot shows online spectrometer thickness measurements, 2%/div, ± 6% full scale. Gold: ZnO thickness; Grey: total cell thickness – towards the right hand side one observes one of the one-minute burns providing us with deposition rate measurements for each cathode.
- The very bottom plot shows the now-automated mapping of germanium bottle changes. The green bar shows the region over which the changes take place for the middle cell; the red bar the region over which changes take place for the bottom cell.

In this display we see 3 germane bottle changes. In the first bottle change the germane concentration was increased by about 3%. The sub-percentage decreases in the device $V_{OC}$ can be easily observed in the upper plot. Even clearer, however, is the 9% increase in the new bottom cell infrared charging rate signal.

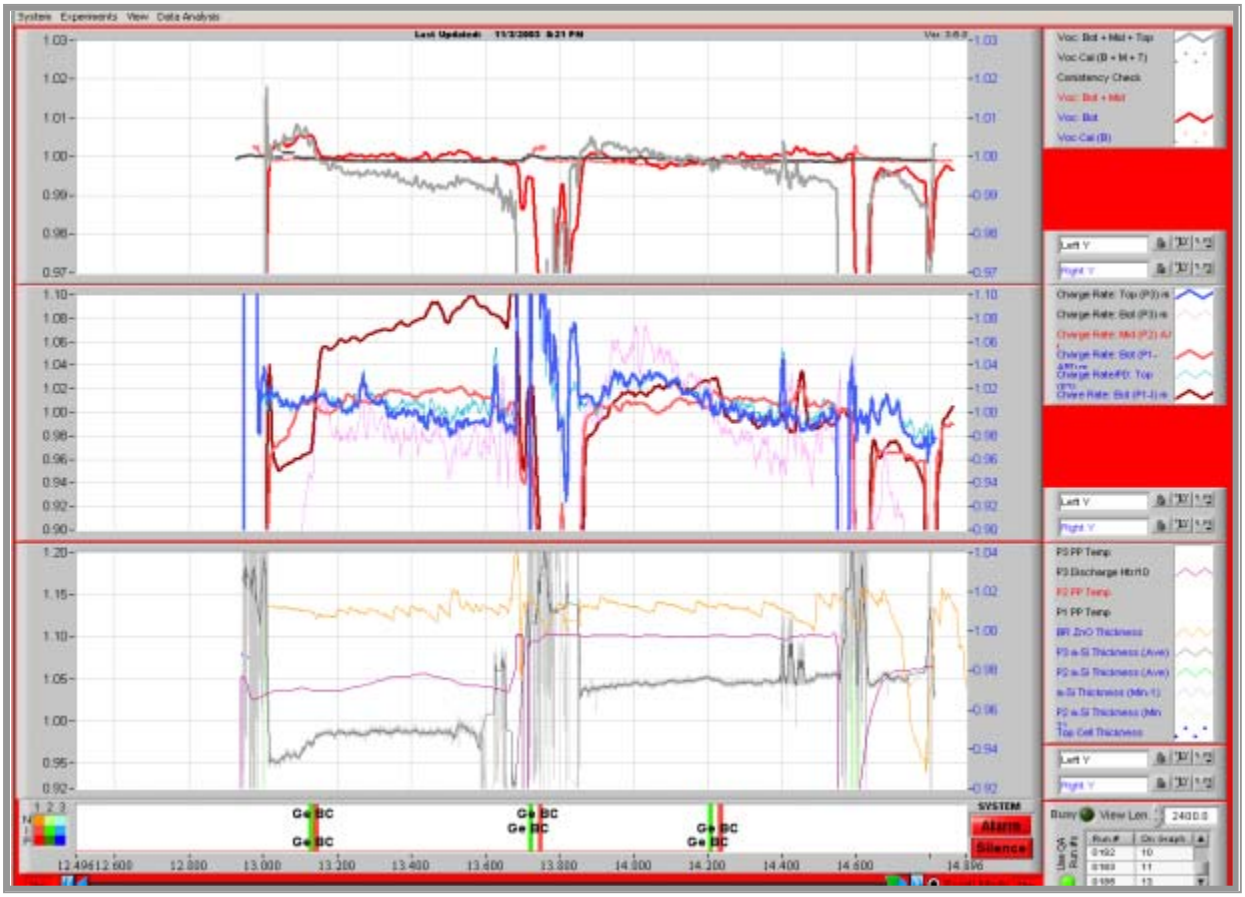

**Fig. 2.5**. Online DDD showing three germane bottle changes. See text for explanation.

### *2.2.2. Use of Bottom (Component) Cell PVCD to Measure Bottom Cell $R_S$*

Figure 2.6 shows the cell charging-rate signal from the bottom (component) cell PVCD at 3 consecutive start-ups of the 30 MW production machine. While we see an increase in the bottom cell charging rate at the beginning of runs following the machine being open to air, no such increase is observed between runs where the machine was not opened to air. This reduced charging rate, while not so clear in offline QA/QC data, is indeed observed as a slight decrease in device efficiency for charging rates below 0.9.

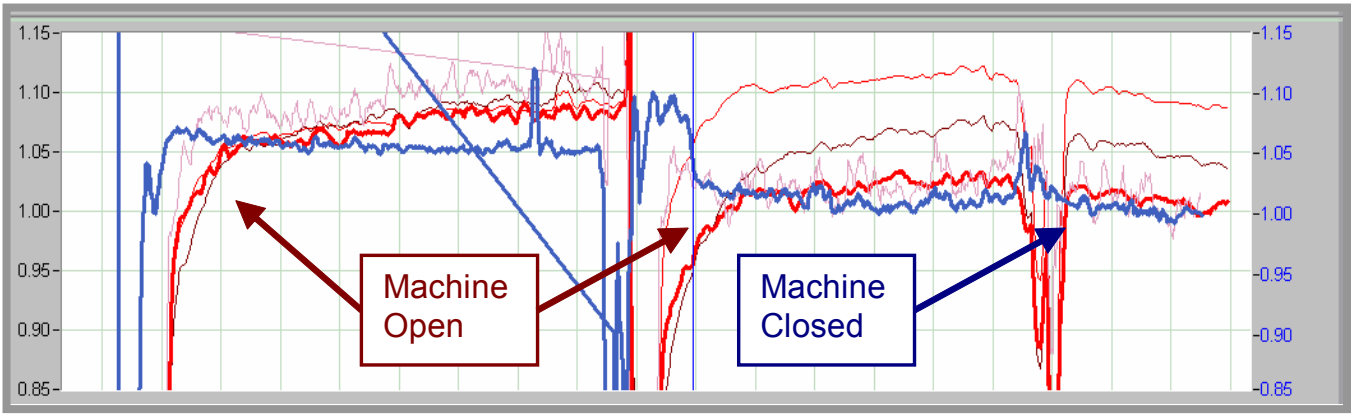


**Fig. 2.6.** Cell charging rate measurements of the top (thick blue line) and bottom cell (thick red line) in the 30 MW production equipment. The bottom Si/Ge alloy cell appears to be more affected by small amounts of contamination than the top a-Si cell. [Horizontal: 2 km full scale].

This diagnostic has allowed to optimize the machine start-up procedure to eliminate an increase in the device $R_S$ due to contamination and temperature effects.

## 2.3 Middle Component Cell PVCD Status

The next-generation Component Cell PVCD, which contained numerous improvements over the first-installed Bottom (Component) Cell PVCD, took place in early November 03.

Figure 2.7 shows raw data from this detector soon after its installation. The system was clearly working: one observes the cell charging as the LED light source is pulsed, and sees the characteristic initially fast, and later slow, discharge of the cell.

On the other hand, there were clearly some problems that needed work:

- The degree of noise in the signal was clearly unacceptable. We needed to average a few hundred pulses to get a reasonable signal from detector. This high degree of averaging cost a lot in terms of bandwidth.
- We also saw a high degree of EMI from the LED light source (notice the “steps” in the red waveform in the areas circled by the bright green ellipses.


**Fig. 2.6.** Raw data from middle (component) cell PVCD soon after installation. The 4 traces are as follows: Blue and Gold: signals from photo-detectors showing the light pulse. The blue signal has 10 times the bandwidth as the gold signal. White and Red signals: the white signal shows the last (raw) data take from the detector; the red signal has is the average taken over the last 5 minutes.

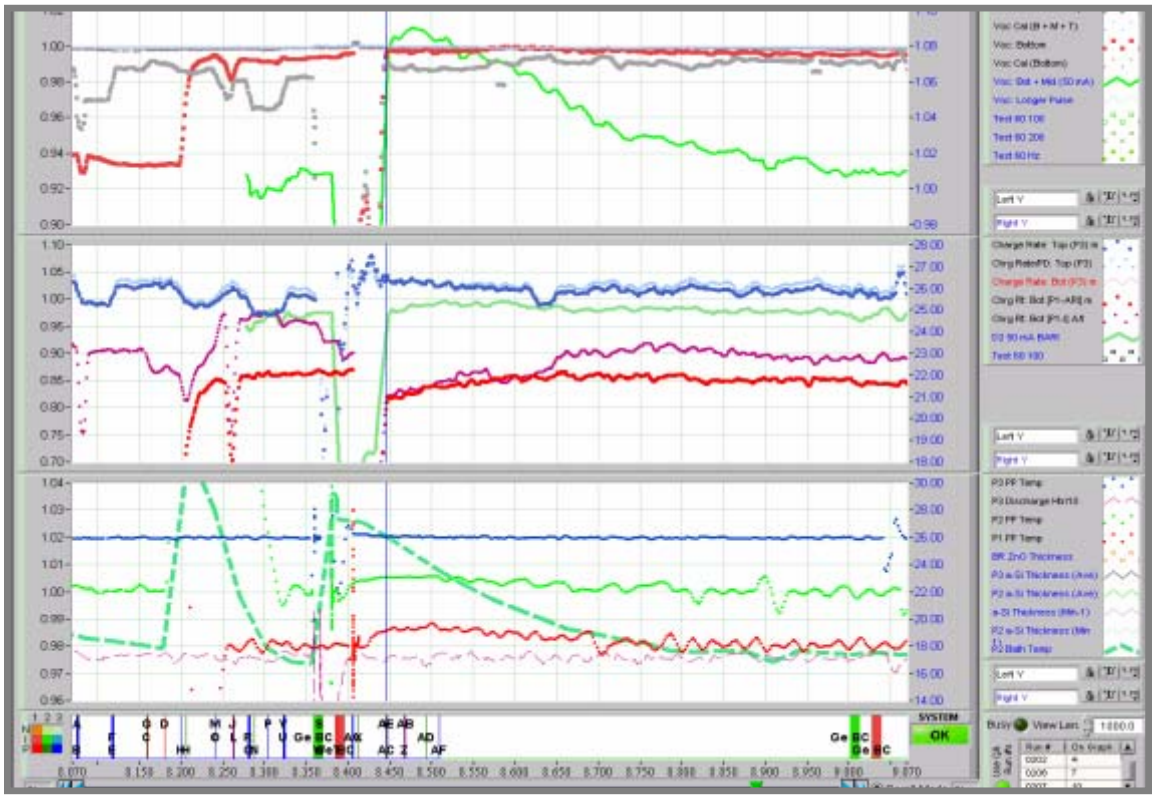

**Fig. 2.7.** Data showing about a 7% decrease in the Bottom + Middle cells $V_{OC}$ [top plot, green]. This change appears correlated with the temperature of the water used to stabilize the Pusher Plate temperature [thick dashed line, bottom plot, 2 $^{o}$C/div], even though the pusher plate temperature is well-controlled [bottom plot, light green line, 0.25 $^{o}$C/div.

After reducing the noise and EMI from the pulsed LED light source we began to observe other problems not observed on the bottom cell PVCD as shown in Fig. 2.7, a screen capture of the Control Room Data Diagnostics Display. The top plot shows the measured $V_{OC}$'s for the three PVCD's: **bottom**, **bottom + middle**, and **bottom + middle + top**. While it is clear that the system was basically working (e.g. the signal comes up when good material begins to pass the detector [blue vertical cursor in Fig. 2.7]), we see a significant drop in the material $V_{OC}$ measured by this detector during a run; this drop is not confirmed by either the bottom, or bottom + middle + top detectors. This drop in measured $V_{OC}$ appears to be related to a temperature increase in the area of the detector, as evidenced by the drop in the water temperature used to stabilize the temperature of the Pusher Plate which in turn stabilizes the temperature of the web. While this trend of temperatures is seen in the bottom cell PVCD, it does not have the reduced $V_{OC}$ problem.

We first conjectured that though the pusher plate temperature was stabilized, there may not have been good thermal coupling between the pusher plate and the web.

The machine was opened and the system was inspected. The mounting for the pusher-plate, which stabilizes the position and temperature of the web, was modified, and the plate re-positioned for better contact with the web. All the electronics were scrutinized and tested. We found and corrected two errors: a wire that connects the FET-pre-amp circuit board to the case

was not making a good connection; we also found a jumper wire in the wrong place that by-passed a resistor controlling the amplifier time-constant. So – two things that could be affecting the signal reduction (pusher plate adjustment and time constant resistor), were identified and corrected; however, further tests in operation showed that corrections did not have any impact on the problem, though the re-connection of the ground-wire removed almost all the line noise and LED light-source EMI.

We finally recognized that in the course of a production run, as the machine temperature increased in the vicinity of the detector, the PVCD waveforms changed (Figs. 2.8-2.9). While we originally suspected this change was due to the electronics, we found that it was due to an increased conductivity of the gas in the region of the detector.

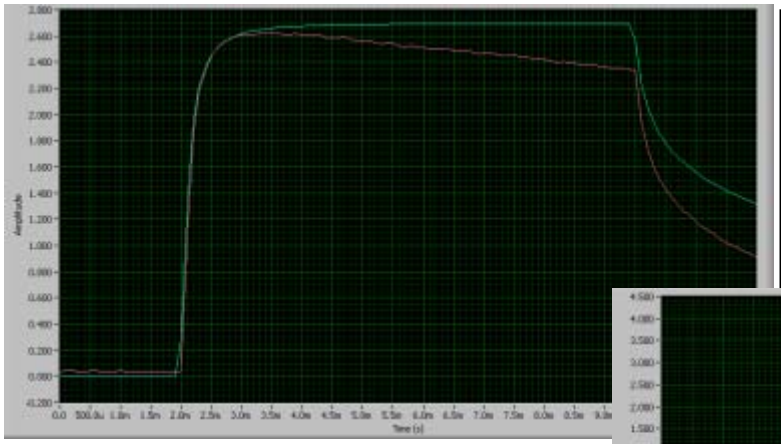

**Fig.2.8**. PVCD waveform with plasmas off. The red curve is raw data; the blue curve is averaged and corrected for the amplifier time constant. The cell charges, reaches steady-state $V_{OC}$, and then discharges [at first rapidly, and then more slowly] when the light pulse is terminated.

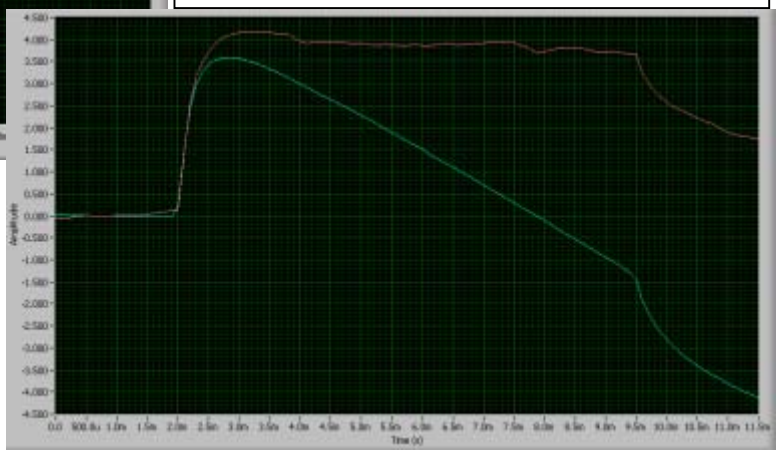

**Fig.2.9**. PVCD waveform with plasmas on. We see a steady decrease in the measured voltage. This signal changes as a run progresses. For shorter pulses, it was interpreted incorrectly as a change in the amplifier time-constant.

We modified the Test Schedule (high level programming) for the diagnostic system which resulted in an immediate “90+%” correction of this problem. We have long suspected that there may possibly still be a drift of on the order of < 1%. We have only recently finally solved this last 1%-level error by adding an additional correction using a measurement of the difference between the supply and return temperature of the water stabilizing the web temperature. Since direct off-line measurements of the bottom + middle cell $V_{OC}$ cannot be made, this second order correction was not trivial.

The Bottom+Middle Cell PVCD is now operating with 0.1% resolution providing the United Solar operations group with online measurements of the bottom, middle, and top cells as shown in Fig. 2.10.

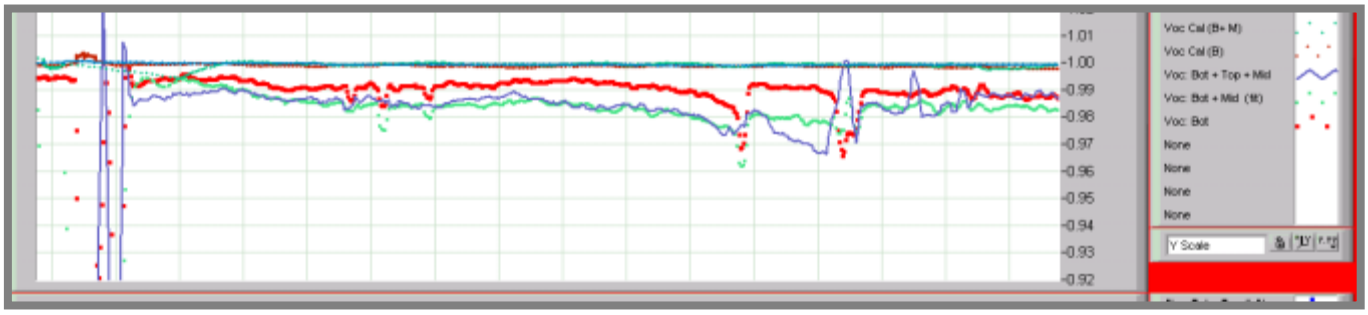


**Fig 2.10:** Online $V_{OC}$ measurements for the Bottom Cell, Bottom + Middle Cells, and Bottom + Middle + Top Cells in the United Solar 30 MW a-Si Production Machine. Vertical: 1% per division; all signals normalized to nominal triple-junction $V_{OC}$; Horizontal: 800 m Full Scale.

We now have all PVCD detectors operating with about 0.1% resolution. We have been continually pushing to improve the signal-to-noise ratio of the detectors since that translates into increased measurement bandwidth. Every improvement, however, also allows us to measure smaller and smaller discrepancies and systematic errors – making this an almost endless process leading to perfection! We are now reaching the point of diminishing returns:

- The precision of the systems matches or exceeds the precision of offline measurements;
- They bandwidth of the systems exceeds the bandwidth of offline measurement systems by more than an order of magnitude;
- As shown in Fig. 1.9, there are discrepancies between online (PVCD) measurements and offline measurements of up to a few percent, or an order of magnitude above the online PVCD stability and accuracy, caused by downstream processing (e.g. ITO deposition conditions).

This performance will be useful in future work:

- The high degree of precision allows us to perform experiments that yield precise results while not significantly affecting the material properties:
- The high bandwidth allows us to perform very short experiments:
- The high degree of accuracy allows us to identify changes in material quality resulting from downstream processes.

### 2.4 PVCD Temperature Stabilization System

We have also begun to make measurements to determine whether it might be possible to remove the water stabilization systems from the PVCD devices, and instead apply temperature corrections to the measured PVCD quantities. This is somewhat ambitious: the temperature of the web and PVCD device will vary by as much as 50 $^{o}$C during a run as the system heats up and heat is transported to the device by the web if the water temperature stabilization system is removed. There are many benefits if this work is successful:

- The system will be simpler, more reliable, and lower cost by eliminating the temperature stabilization bath, refrigerator, water circulation system, feedback loops, etc.
- We shall be able to remove all water cooling from the machine – a possible source of a water leak – which is a severe production problem (as discussed in Task 7, we have also developed a new system allowing us to remove the water cooling from the p-deposition zones in the machine).

We presently use a servo-system to stabilize the temperature of the web. The PV material has a $V_{OC}$ temperature coefficient of about -0.5% per $^{o}$C. As shown in Fig. 2.11, we presently stabilize the temperature of the web "pusher plate" to < ± 0.05 $^{o}$C. The servo-system uses an RTD (Resistive Thermal Device – a platinum resistor) to measure the temperature to the "pusher plate" (PP) which stabilizes the position and temperature of the web. We then adjust the temperature to the water flowing through the PP using a bath that has refrigeration, heaters, and an auto-fill mechanism to stabilize the temperature of the PP.

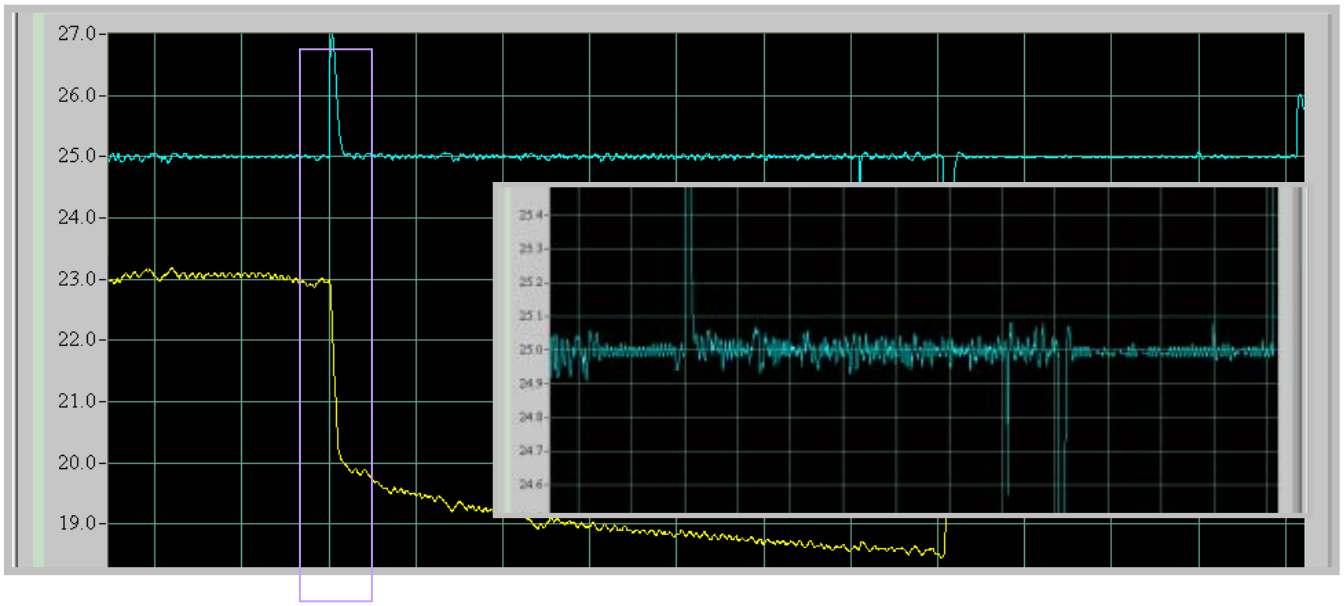


**Fig. 2.11.** Recorded Pusher Plate (PP) [blue trace] and Bath [gold trace] temperatures as a function of time during a Run Segment. At the start of a run [boxed in lavender] when the heat-load to the PP increases, the Bath begins to cool and the PP temperature is kept stabilized to better than ± 0.05 $^{o}$C [Horizontal: 3 hours/div].

While this system works extremely well, one can envision a much simpler system in which we measure the temperature of the web and PVCD and use these data to temperature-compensate the cell measurements. We have experimented with temperature compensation of the Bottom [Component] Cell PVCD. During these experiments the temperature of the Pusher Plate was changed by – 5 $^{o}$C to + 45 $^{o}$C from its nominal operating temperature of 30 $^{o}$C [i.e. 25 to 75 $^{o}$C]. We were able to reduce deviations by almost an order of magnitude by adjusting the raw data with a correction derived from the PP temperature. The most significant remaining deviations were not related to the PP temperature, but rather to the rate-of-change of the PP temperature. This is indicative of different thermal time constants for different components in the system. We have now added software to also data-log the derivative of the temperature change.

Figure 2.12 shows a correction made using both the temperature and derivative of the temperature for the pusher plate. While the correction is not yet perfect, we are for now concluding that this approach is doable – especially when we consider that in steady-state operation the derivative term should be very small.

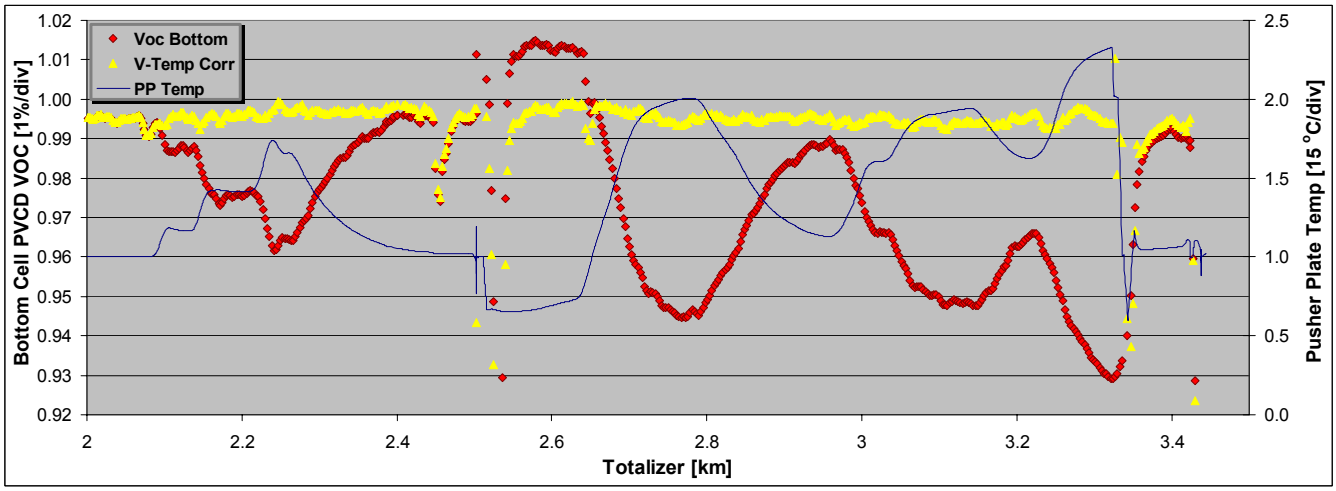


**Fig. 2.12**. Bottom Component Cell PVCD $V_{OC}$ measurement vs. pusher plate temperature: raw data, and data corrected with the pusher plate temperature and temperature derivative.

As a next step we shall install an additional RTD on the PP body and see whether this added data will eliminate the need for incorporating temperature-rate-of-change data. We shall also investigate the easiest way to incorporate the time-rate-of-change correction into the software.

## 2.5 Using the PVCD's for Optimization

The PVCD system, besides being useful for online QA, has been useful in a number of machine optimization programs, e.g.:

- Bottom and middle cell germane concentration optimization;
- Start-up procedure optimization;

Here we show an interesting new technique for optimization that we discovered. The 1-minute stop-and-go measurements that are used to measure the longitudinal deposition profile in the a-Si machine (see Fig. 1.12) also provide us with already-having-been-performed-experiments showing the effect of increasing the deposition thickness in each cathodes in the machine. While the PVCD data are not taken at a high enough repetition rate to measure this effect, we gathered all data from all past stop-and-go's and carefully aligned them using the spectrometer data. From this compilation we can quantify changes in $V_{OC}$ and charging rate for thickness increases in each deposition area. An example of these data is shown in Fig. 2.13. From these data we have identified a few "prime suspects" for detailed optimization studies.

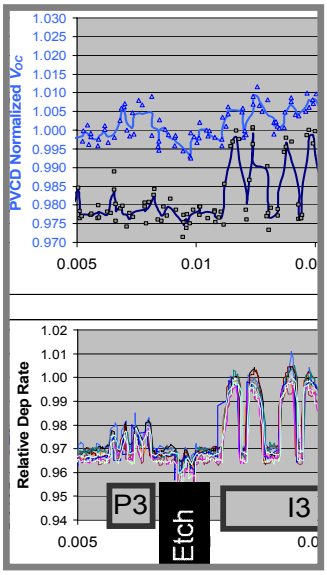


Fig. 2.13. Top: online PVCD $V_{OC}$ [light blue] and charging rate [dark blue] signals vs. change in deposition thickness [bottom plot].

One "prime suspect" for increasing the device efficiency was to increase the thickness of the n3 layer. Recent experiments in the 30 MW machine using offline QA/QC confirmed this prediction – providing a couple of percent increase in device efficiency as shown in Fig. 2.14.

We are now operating the machines in the regime where we will make significant (e.g. 10%) increases in efficiency not by finding a couple of large improvements, but by making many fine tweaks, and keeping the machine at this operating point. In this regime, and with the "month-long" feedback period that results when relying upon offline QA, we have in some senses reached a limit. The feedback rate will slow down further if we were to begin looking for smaller effects on efficiency.

While the online diagnostics can provide the data with a couple of order-of-magnitude improvement in feedback rate, since they do not make full V-I tests using an AM 1.5 spectrum, they cannot be relied upon alone for this optimization process. In addition, the online diagnostic systems view only one of the 6 webs. As can be seen in Fig. 2.14, there are significant differences between webs. So, where do we go?

- In the short term, we can us the online diagnostics to increase the probability of choosing good targets for study using offline QA. On the other hand, the motivation and resources to systematically do experiments with the necessary statistical significance to find sub-1% improvements, even for prime candidates, is not high. We may investigate the possibility of performing such optimization independent from offline QA/QC feedback.
- In the longer term we need to speed up the rate at which full I-V measurements can be made offline, or performing full I-V measurement online in the ITO machine – or better still – in an ITO deposition chamber installed at the end of the a-Si machine.

We shall be investigating various strategies for the short-term in the near future.

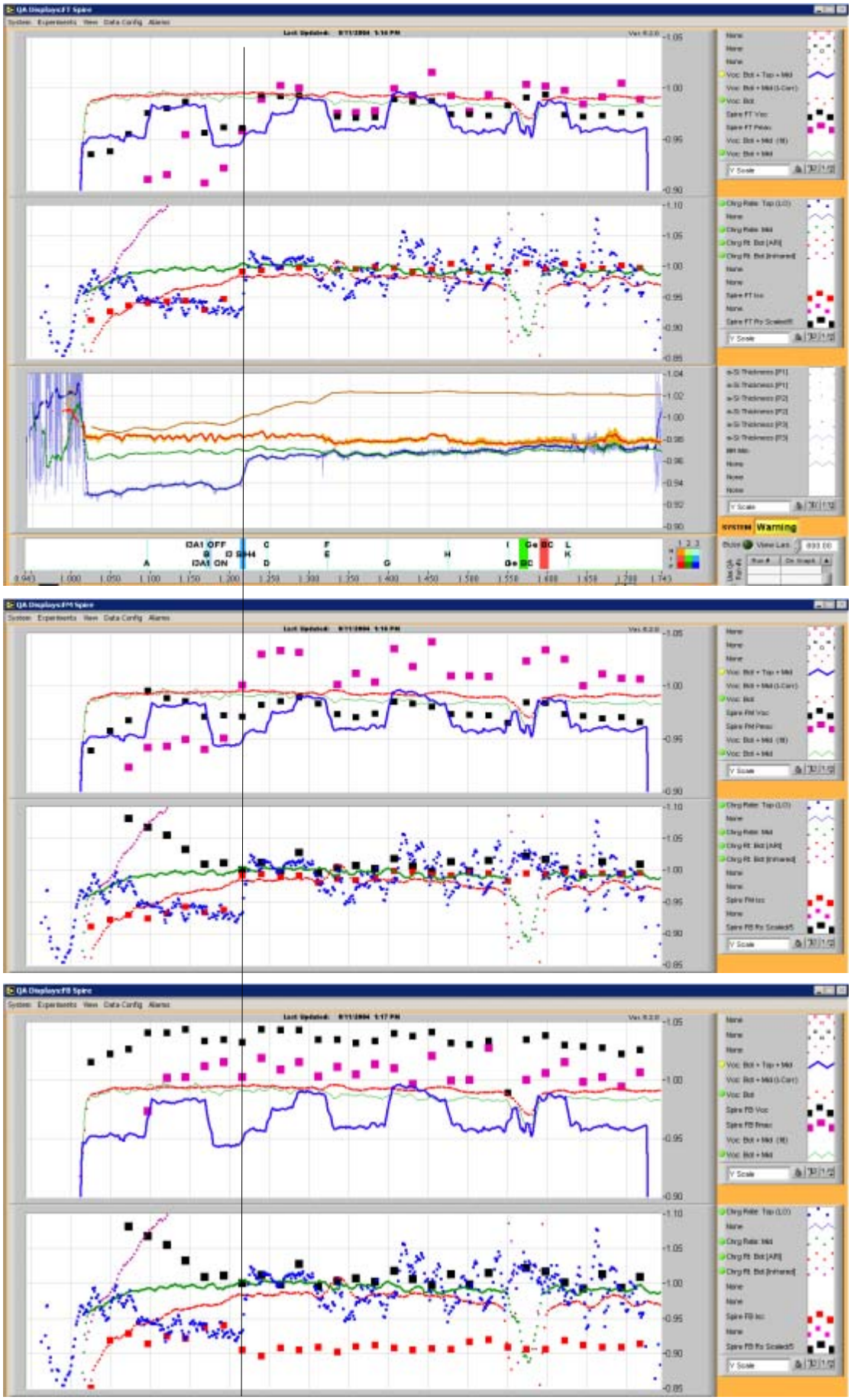

Black Line
I3 thickness increased
Compensate for I3A off

| | $I_{SC}$ | $P_{MAX}$ |
|---|---|---|
| Top | 5% | 7% |
| Middle | 5% | 7% |
| Bottom | -3% | 0% |

N3 Experiments
Where PVCD $V_{OC}$ (Blue Line, Top) has square wave structure

Top Web
$V_{OC}$ Agrees w PVCD
$P_{MAX}$ 2.5% improvement

Middle Web
$V_{OC}$ Less Var than PVCD
$P_{MAX}$ 3% improvement

Bottom Web
$V_{OC}$ Much less variation
$P_{MAX}$ No change

**Fig. 2.14**.

Results of n3 thickness optimization measurements.

## 2.6 The Diagnostics Data Display [DDD] and Alarm Package

The new Data Diagnostic Display [DDD] alarms program is being constantly improved. One of the new features is the ability to display “Virtual Channels”. A Virtual Channel is created by an arbitrary mathematical function using an arbitrary number of “real” or other Virtual Channels. The DDD calculates these real-time and for all archived data, regardless of non-synchronous data acquisition rates for the different channel.

We have also developed a program with alarms and warnings, along with a “Virtual Expert” to explain the meaning of the alarms in order to help the operators make use of the myriad of signals bombarding them from the online diagnostic systems. A small indicator “lamp” appears on the screen for any displayed channel that also has an associated alarm. The “lamp” is green for “good”, amber for “warning”, and red for “alarm”. When this lamp is selected by the cursor, the warning and alarms levels are displayed, as shown in Fig. 2.15. Alarms are active whether or not the channel is displayed. When a channel is in “warning” or “alarm”, the system “lamp” in the lower right-hand corner will change from “OK” to “Warning” or “Alarm”. Hitting this indicator will bring up a screen showing the alarms. This alarms screen also provides an explanation of the alarms to the operator as shown in Fig. 2.16.

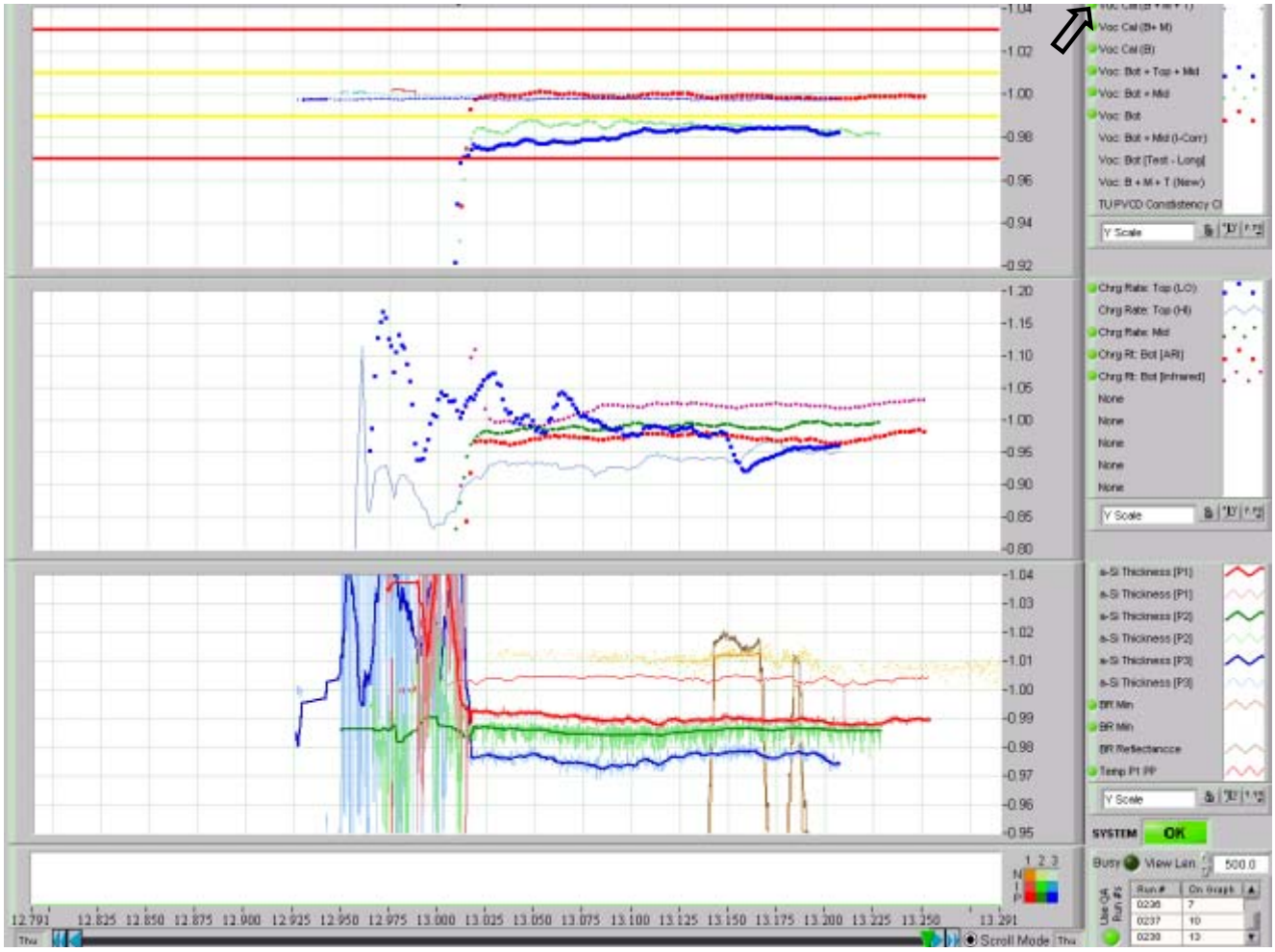


**Fig. 2.15.** New “Alarm DDD” display. The system is operating in the mode.

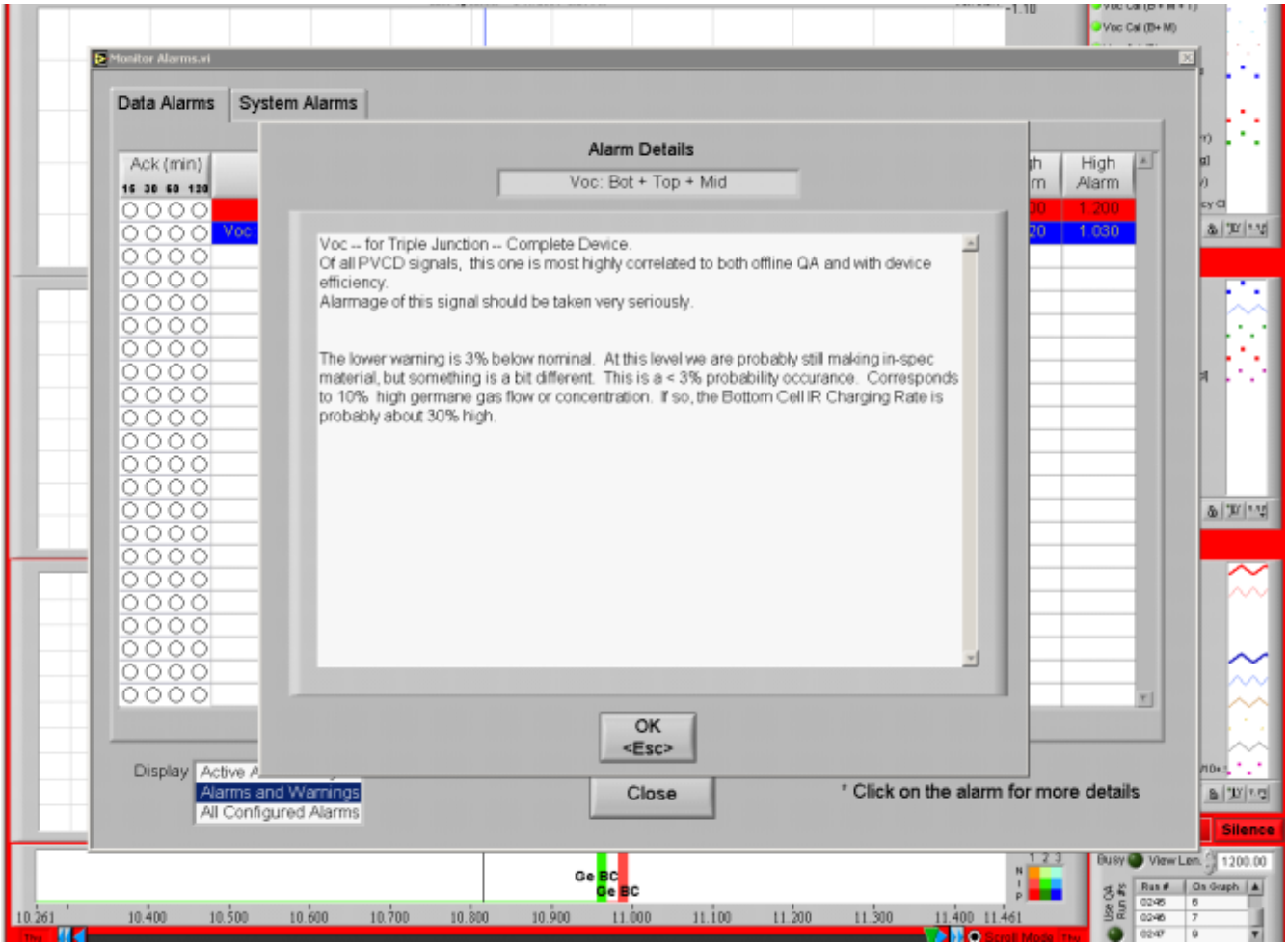


**Fig. 2.16.** Example of a warning explanation associated with a system warning.

## TASK 7: Deposition Optimization and Plasma Diagnostics

**– Tim Ellison**, Scot Jones, Tongyu Liu, Mark Lycette, Joe Doehler [ECD], **Gautam Ganguli** (United Solar)

### 3.1 Introduction and Summary

We have concentrated on three principle areas to improve the plasma deposition and our understanding of the plasma. These areas are:

- Studying the usefulness of an RGA (Mass Spectrometer Residual Gas Analyzer) on the exhaust gas of the production machine upstream of the nitrogen purge and burn box. These studies are continuing. Thus far we have not been able to correlate logged RGA data with PV device performance, or machine malfunctions (i.e. water or air leaks).
- We have made significant improvements in the p-layer deposition hardware, and our understanding of the heat dynamics in this area of the machine.
- We have developed and are data-logging data from RGA and OES (Optical Emission Spectrometer) on our pilot deposition line. Our hope is to be able to correlate measurements with cell quality that will lead to increased feedback in optimizing new higher rate deposition systems. As yet no firm correlations to help us in this effort have been identified. We are also developing a “moving wire” Langmuir Probe to allow fundamental plasma property measurements in a deposition plasma.

### 3.2 Improved p-Deposition Hardware

We have modified the cathode and chamber in the test system to enable us to study the high intensity p-chamber plasmas as well as the different intrinsic a-Si:Ge layers. A window was made which allowed for observation of the entire plasma region [See Fig. 3.2].

**Fig. 3.1.** Photograph of the test chamber showing the newly-installed p-type cathodes and gas lines.

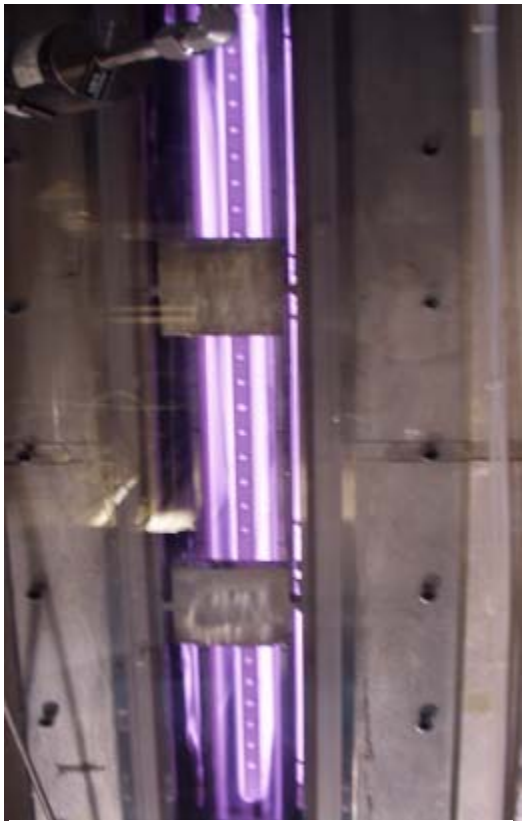

**Fig. 3.2.** View of the plasma from the p-style cathodes installed in the test chamber. The window allows direct observation of the plasma –impossible in the production machine.

The p-cathodes along with gas and RF feedlines are shown in Fig. 3.1. The p-chamber cathodes operate with considerably higher power than most other cathodes in the production equipment. Studies of the high-power p-chamber plasmas have two areas in which the p-cathode geometry design can be improved: temperature regulation; and rf grounding. We also developed new cathode-supporting insulators that could withstand the high power p-plasmas.

### *3.2.1 Temperature Stabilization and rf Grounding*

The quality of the p-layers depends on the substrate temperature. In the p-chambers, the rf plasmas, rather than the heaters, are the primary heat source for the substrate. The standard heating and temperature measurement and regulation systems, developed in the PVMaT 5 program, are not applicable in this regime. In particular, studies have shown that the substrate temperature may vary by more than 100 °C moving through the p-deposition zones. The high power plasmas also lead to arcing which can damage the thin film PV material. We have developed a conceptual design for a new capacitive cooling system that:

- Eliminates the potential of water leaks by remove water from the system;
- Eliminates the extreme temperature of the substrate as it moves through the p-deposition area;
- Provides accurate web temperature monitoring;
- Removes cool surfaces close to the web
- Provides a capacitive rf ground to eliminate arcing problems; and
- Will simplifies and reduce the cost of future machines

This substrate-cooling and rf-grounding system has undergone several design iterations and at one time was even abandoned. The first few iterations addressed only the problem of web temperature stabilization; we later added the function of an rf ground. Another fundamental design change was changing the primary heat resistor from the gap between the web and cooling plate to easily-changeable shims to allow optimization of the temperature uniformity.

This system (Fig. 3.4 on the following page) was tested at full power in the Test Chamber at Pant 2 and the design iterated. Results of the last test are shown below in Fig. 3.3.

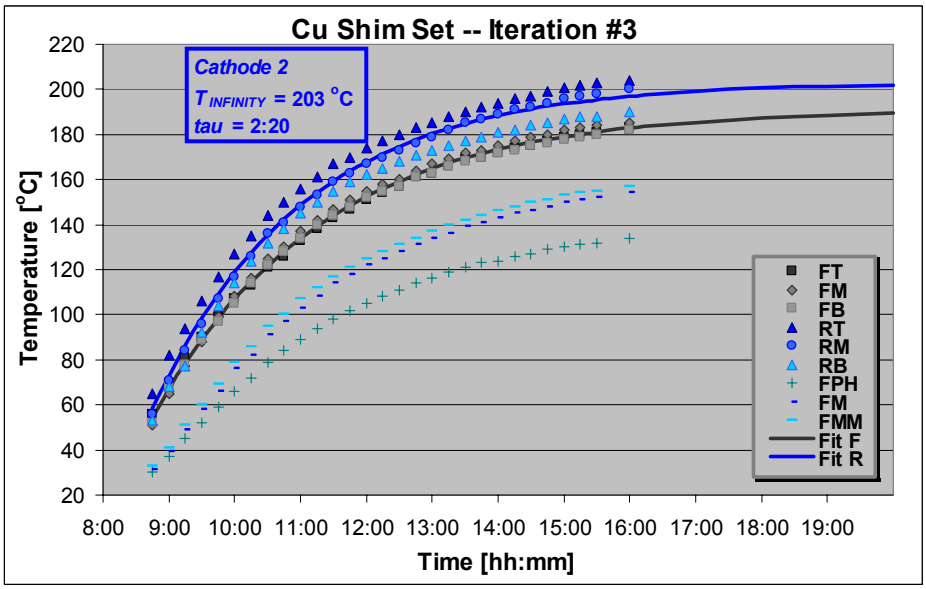


**Fig. 3.3.** Temperature measurements of the web [blue-fit] and other cooling system parts during a test in the Test Chamber.

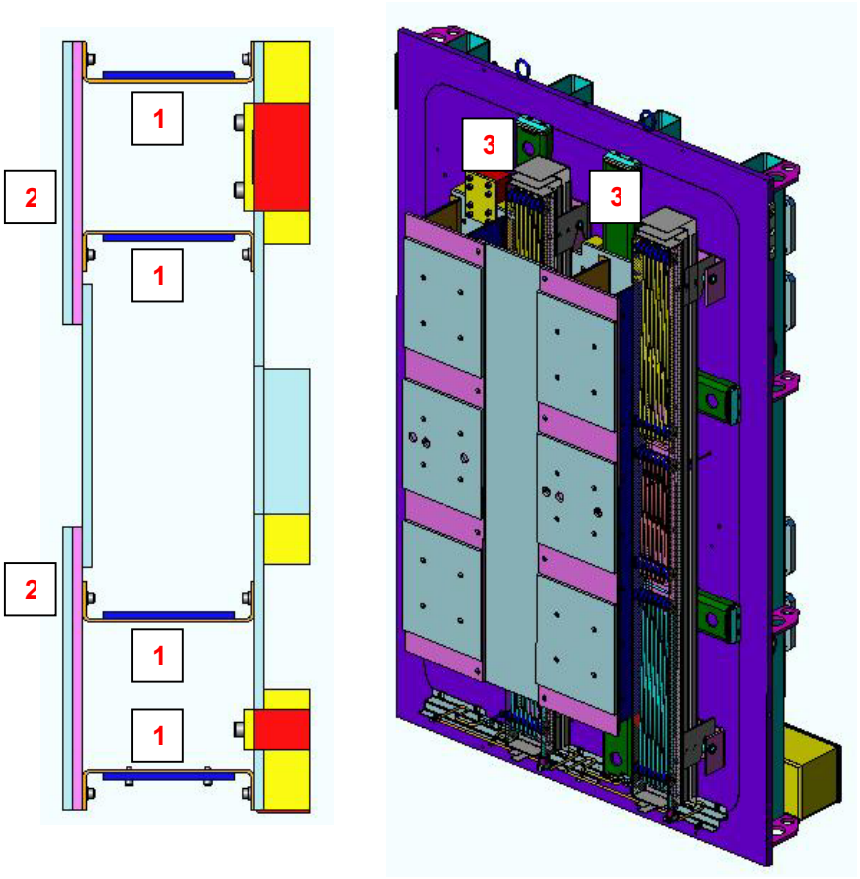


**Fig. 3.4.** Renderings of the new p-cooling/rf grounding system. [Side view, looking in the direction web transport direction, on the LHS, and view normal to the substrate surface on the RHS]. The aluminum plates close to the backside of the web [2] provide uniform substrate temperature. Heat is transferred to the door via the thin stainless steel channels [1]; aluminum shims on these plates are used to adjust the temperature. This system also functions as an rf grounding system; rf conductivity and thermal conductivity can be separately adjusted since the rf current flows only on the surface of the conductors.

We now have a design that satisfies all the technical requirements. The system has been tested in the Test Deposition Chamber and we are now waiting for an opportunity to install it in the production machine for testing. After the first test installation the system will be further optimized to minimize the cost, and maximize the ease-of-installation [e.g., overall cost].

### *3.2.2 Successful Testing of New Ceramic Cathode Supports*

In the test chamber we observed that the cathode supports comprised of a carbon-based (polymer) material are a source of carbon contamination when subjected to the high intensity plasma used in the p-chambers. Consequently we developed and tested a new type of ceramic material for the cathode supports. It was found that this material did not release measurable contaminants and is more resilient to the high intensity hydrogen-rich plasmas. Short-term testing looks very promising; to further increase our confidence in this new material, we are procuring more of these new ceramic supports for long term testing in a few select regions of the 30 MW manufacturing line. We expect they will be used as the new standard support for the next generation machine.

## 3.3 Residual Gas Analyzer (RGA) for Production Monitoring

In order to investigate the apparent relationship between decreased bottom cell charging rate, with resulting reduced efficiency [see Section 2.2.2 and Fig. 2.6] and possible low levels of contamination, we installed an RGA in the exhaust manifold of the 30 MW production machine. The RGA must operate at a much lower pressure than the exhaust manifold pressure; we used a needle valve and ion pump to provide this reduced pressure and have tested the system. Initial tests have shown the following:

- In order to safeguard the system against over pressure, the needle valve was adjusted to ensure safe operation of the RGA when the 30 MW production machine exhaust manifold was brought up to atmosphere. This reduces the sensitivity of the device when the exhaust manifold is under vacuum.
- The nitrogen purge in the exhaust manifold prevents measurement of air-leaks.
- The ion pump is unsuitable, reaching argon instability as a consequence of operating modes resulting in high concentrations of argon in the exhaust manifold.

We then designed a 2$^{nd}$ generation system that will eliminate these identified shortcomings:

- The new system will uses a small turbo pump to eliminate the ion pump argon instability, and increase throughput and sensitivity;
- The system was moved upstream of the $N_2$-purge in the exhaust to proved sensitivity to air leaks;
- The needle valve was be set at operating pressure in the exhaust manifold; a pressure monitor and interlocked valve instead provides a safeguard for the RGA and turbo pump. This further increases the system sensitivity.

During the Holiday Shutdown [December 03] there was a failure with the RGA system: both the turbo pump and RGA unit became non-operational. The entire unit was removed from the United Solar production equipment and brought back to ECD's Plant 2 to be taken apart and analyzed. We found that:

- The turbo-pump apparently failed due to powder entering the exhaust port of the turbo pump apparently happening when the a-Si exhaust manifold was let-up to atmospheric pressure. One proposed solution was to back the turbo pump with a separate backing pump with a separate exhaust. While technically straight-forward, it becomes complicated from a safety standpoint since we are dealing with process gasses.

Another solution was proposed and implemented using a series of filters in the exhaust line.

- The RGA failed due to a burnt-out filament. We believe this happened after the fact when repeated attempts were made to turn on the filament while the turbo pump was not operating. We addressed this problem by more fully-instrumenting the system.

The system was re-assembled at Plant 2 with new ***LabView*** software. We then encountered a number of problems beginning with a burnt filament. After the filament repair the system displayed occasional erratic behavior. We changed out the filament a second time, with no success, and even more erratic behavior. Before sending the system back, we tried re-building the ionizer section (filament, repeller, anode and focus plate) of the RGA. This was successful. The data are now integrated with the DDD in the control for constant monitoring.

We now suspect that out-gassing from the rolls of stainless and interleaf in the Pay-Off and Take-Up chambers, which are pumped through the same manifold as the deposition chambers, will probably prevent us from detecting small leaks that would affect material quality. On the other hand, the system will still be useful for identifying the occasional gusher. Our goal now is to prove reliable operation of the system for the next year or two – and modify as necessary. We shall then have a reliable tool which can be used in future machines to also detect small leaks if a separate pumping manifold for the deposition chambers is available, as will likely be the case.

### 3.4 OIS and RGA for Plasma Characterization

As shown in Fig. 3.5, RGA measurements of the ratio of $Si_3Hx$ to SiHx, and plasma emission spectroscopy of the ratio of Si* to SiH* may provide an indication, online, of the quality of the deposited film[4]. We developed plans to install these two diagnostic systems in the test deposition chamber at ECD's Plant 2 for testing.

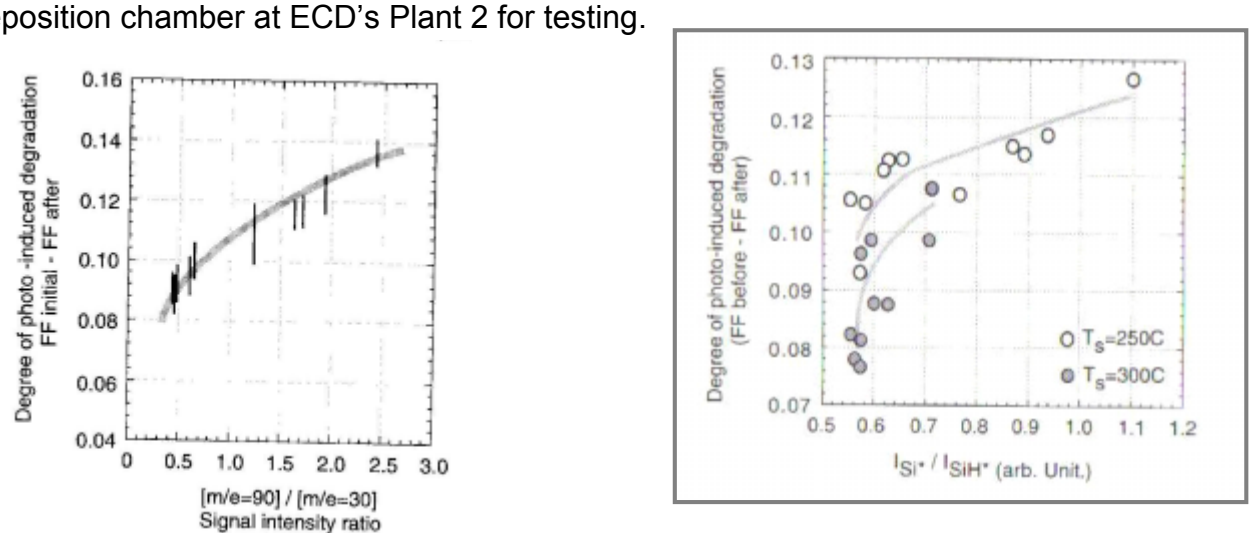


**Fig. 3.5.** Data from Matsuda showing correlations between material quality and measurements made with RGA and OES systems.

[4] A. Matsuda et al., Solar Energy Materials and Solar Cells, **78** (2003)]

### *3.4.1 The RGA System*

An RGA system for measuring the $Si_3H_x$ to SiH ratios in deposition chambers was designed. We developed method employing two separate flow constrictors, with one adjustable; this system will allow us to operate in the regime where we can use a photo-multiplier to minimize signal drift due to coating the electron emission cathode with the reactive gases, and also be able to make hopefully-equivalent measurements on systems operating at different pressures. The first fixed flow constrictor, at the sampling point, allows rapid movement of gas from the process chamber to the RGA.

### *3.4.2 The Optical Emission Spectrometer System (OES)*

The optical spectrometer was also mounted on the test deposition chamber at Plant 2 and is in operation. We have identified the SiH* and Si* peaks (where the "*" indicates excited states of the species) – though the latter is just out of the noise. We are working to improve the system S/N and have looked at rf and VHF plasmas (Figs. 3.6-7).

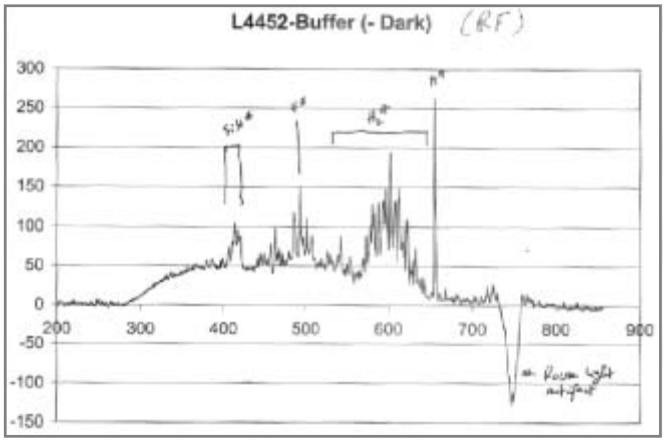


**Fig. 3.6**. Emission spectrum from an rf plasma.

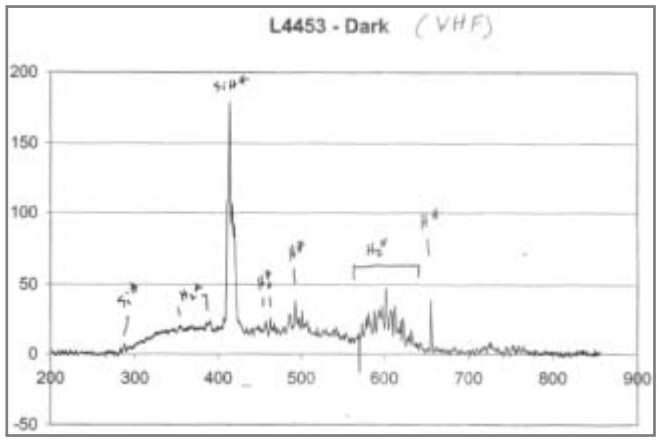


**Fig. 3.7**. Emission spectrum from a VHF plasma.

There are clear differences in the signals from rf and VHF plasmas - the SiH* lines are much stronger and Si* is visible indicating stronger silane. The higher frequency reduces electron loss rate and hence results in higher electron density.

The strong SiH* line in the VHF spectrum and its ratio with the Si* is an indication of the electron temperature (the lower the Si* to SiH* ratio, the lower the electron temperature, and the better the quality of material). The lines within the SiH* family have all different relaxation mechanisms and the ratios between them depend on the actual pressure, etc.

We conjecture that the system has some absorption in the U.V. region that is not allowing us to measure the Si* peak well. We are investigating whether this is true.

While a few pictures can provide a qualitative picture, we realized the need to data-log all these peaks, and then correlate their ratios with measured offline QA (e.g. Fill Factor and degree of degradation). We installed a ***LabView*** Software system, modified from the software developed for the online diagnostic systems, to log and analyze these data.

### *3.4.3. LabView Data Acquisition/Data-Logging System*

We adapted the spectrometer and RGA ***LabView*** programs from the 30 MW systems for data acquisition for the OES and RGA systems on the test deposition system as shown in Figs. 3.8-9.

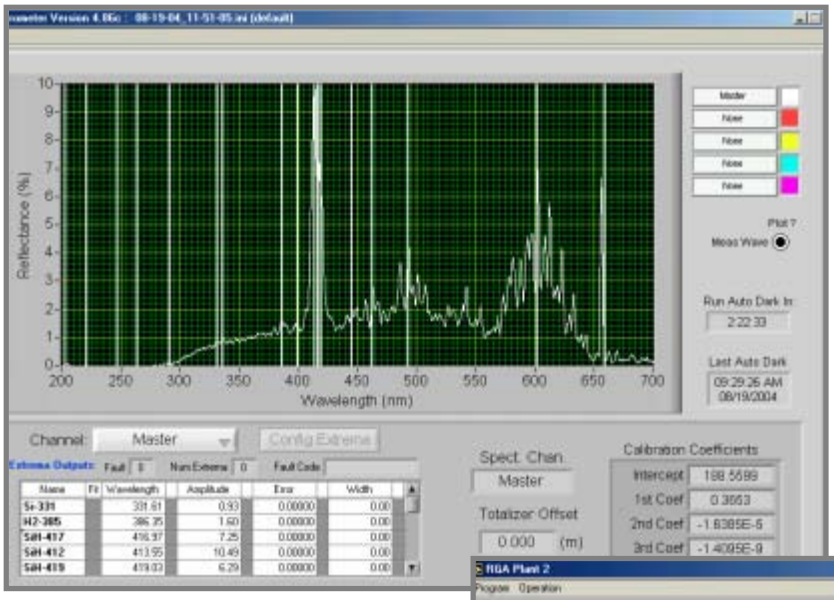


**Fig. 3.8**. LabView program for data-logging various peaks in the plasma emission spectrum.

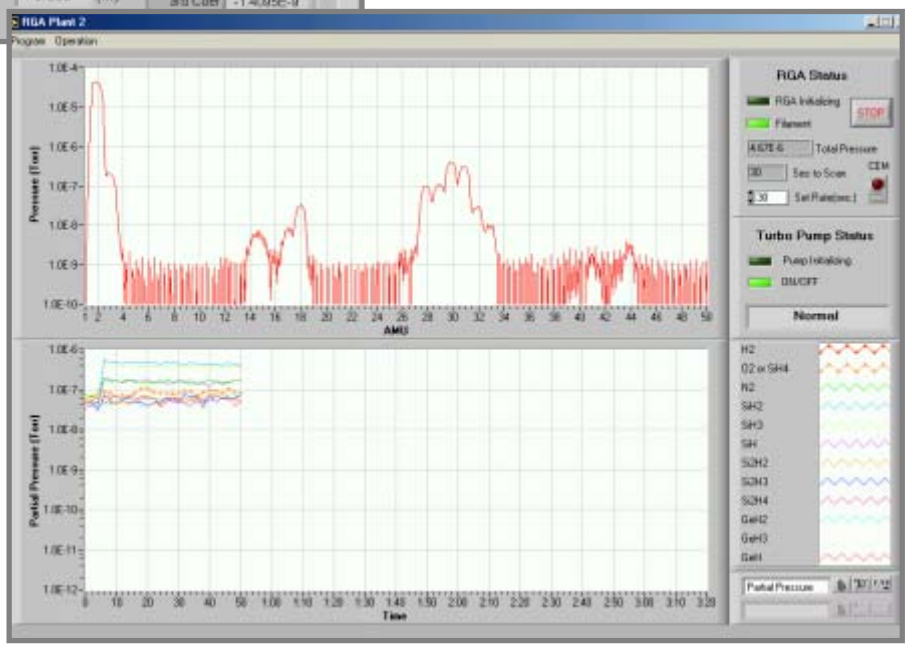


**Fig. 3.11**. LabView program for data-logging peaks in the RGA spectrum.

We also adapted the DDD to display and correlate these signals as shown in Fig. 3.10.

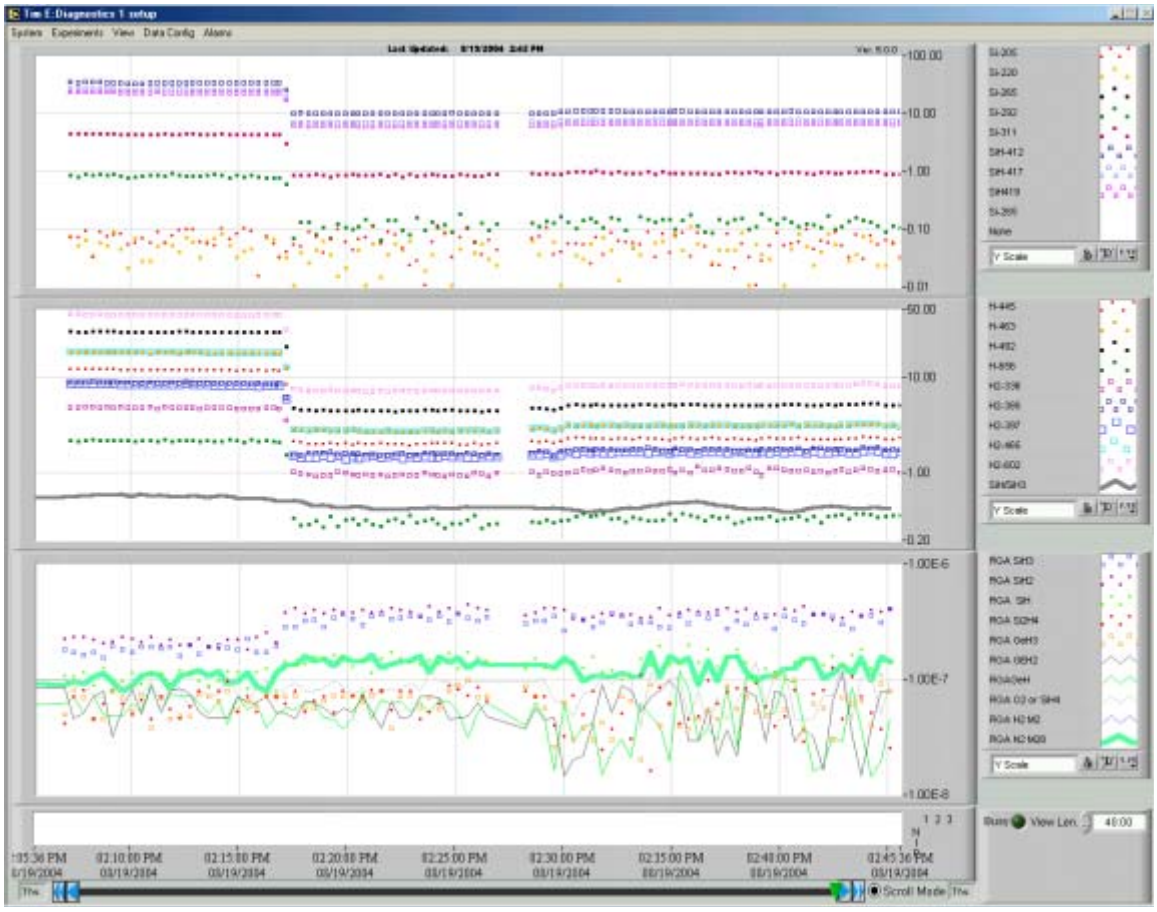

**Fig. 3.10.** Adapted DDD program to display RGA and OES signals as a function of deposition conditions.

We are now set-up to be able to data-log signals as a function of deposition parameters to see whether we can find any useful signals to help with future optimization studies.

### 3.5. "Moving-Wire" Langmuir Probe

A Langmuir probe measures the most fundamental properties of a plasma, including electron temperature, plasma potential, floating potential, electron density, ion density, and electron energy distribution function. As such, one would expect to see them in common use in PECVD reactors. However, in plasmas where deposition takes place, the probes become coated with films and cease to provide useful information. In typical plasmas used for rf a-Si deposition, this coating time is on the order of 1 minute; for high rate deposition processes, the coating time would be only a few seconds. While there are commercially-available "self-cleaning" probes, these probes only remove some absorbed gas contaminants by operating at high temperature, and will not clean off deposition. In fact, the high temperatures would induce thermal CVD, consequently exacerbating the coating problem.

We are designing a Langmuir probe (Fig. 3.11) with an electrode that is part of a long spool of wire. The wire will be moved at a rate of about 1 – 10 cm/min from one reel to another, so that a there is always a fresh uncoated wire that can be used for measuring the plasma properties. The first proto-type system has been built and is being bench-tested for mechanical operation. The electronics have been build and tested.

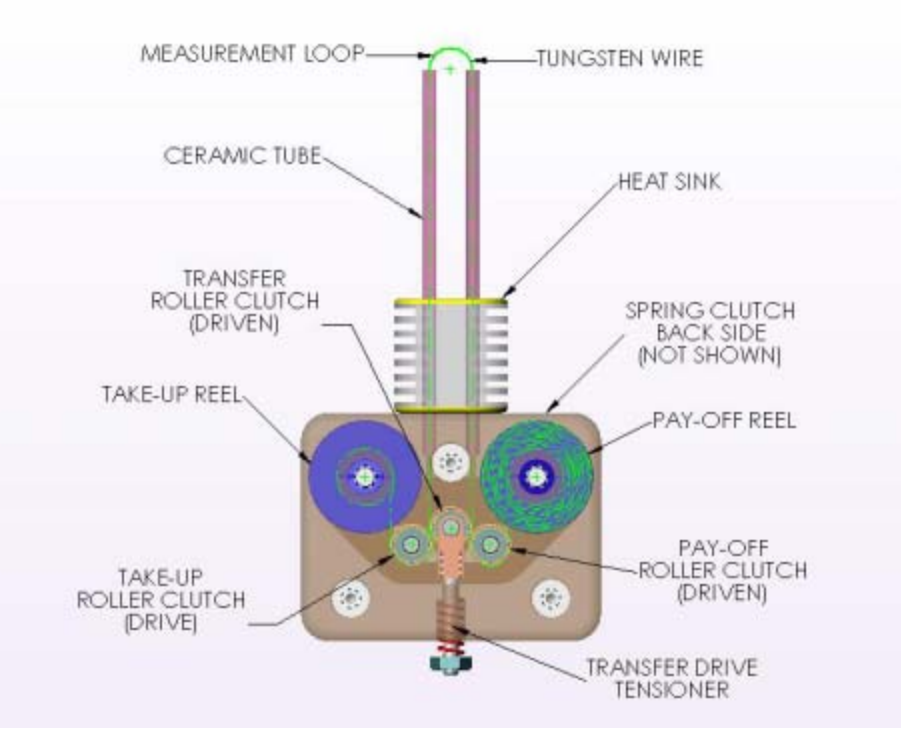


**Fig. 3.11.** Rendering of "moving-wire" Langmuir Probe prototype being fabricated by the ECD Model shop to allow continuous or periodic measurements of plasma properties in the presence of deposition.

## TASK 8: Yield Improvements: Substrate Quality

**Gennady Bondarenko** (ECD), **Gary Di Dio** (United Solar)

### 4.1 Introduction, Background and Summary

From a production point of view, throughput and yield are even more important than efficiency. In this Task ECD/United Solar are working on improving the yield of the 30 MW equipment. We have studied improving the yield by developing an improved substrate cleaning system – an in-line plasma cleaning process that would not only improve the substrate cleanliness, but also allow us to eliminate the wet chemical Washing Machine (WM) [1 of the 4 Front-End Roll-to-Roll processors]. Below is a succinct summary of yield improvement studies to date:

- We have determined that the substrate cleanliness level provided by the present chemical Washing Machine (WM) is sufficient to reduce yield loss resulting from substrate contamination to immeasurable levels for the Al/ZnO backreflector (BR) product produced in the 30 MW manufacturing equipment;
- Substrate cleanliness variations affecting yield for Ag/ZnO BR prototype "space" product produced in the 5 MW manufacturing equipment can be observed; however, sufficient cleanliness can be provided by proper configuration of operating parameters in the present WM.
- Preliminary studies for including the type of plasma-cleaning process we have investigated into the next generation manufacturing equipment show the capital costs would not be reduced, nor would the manufacturing process be simplified. We still, however, believe that capital and cost savings might be realized in beyond-next generation equipment by including an in-line plasma cleaning process.
- The plasma cleaning system developed in this program has been shown to work better than chemical washing for low levels of contamination, but is ineffective for large levels of contamination. Consequently, since we do not know how to economically or adequately specify or ensure the cleanliness of incoming substrate, it may be prudent to keep the WM in the next generation machine even with the addition of a plasma cleaning system.
- There may be more effective types of plasma cleaning (e.g. use of excited oxygen jets) that would require operation at a very different pressure regime than we can obtain in the present BR machine configuration.
- In addition, the WM has the additional function of splicing incoming rolls of substrate into fixed-length (2400 m) coils for the manufacturing process. Even if the WM were eliminated, it would need to be replaced with another Roll-to-Roll machine of only slightly less complexity.

During the course of yield studies carried out over the last 1½ years on the 30 MW/yr manufacturing equipment we have identified the two primary sources of yield loss: substrate surface finish features, and process conditions in the a-Si machine. In the Phase III portion of this program we will focus work on understanding and ameliorating these sources, and to refine our measurement systems to assess substrate quality and Yield.

In the rest of this report we summarize our work in implementing a plasma cleaning system into the present BR machine at United Solar. Effectiveness of plasma cleaning versus wet washing was completely evaluated; the plasma cleaning system was implemented and evaluated in 30 MW BR machine. The system has been partially optimized for BR production process.

## 4.2 Evaluation of Plasma Cleaning Versus Chemical Cleaning

Evaluation of the effectiveness of plasma cleaning versus chemical cleaning included:

- Preparation of a small vacuum system to conduct offline plasma cleaning experiments;
- Initial plasma cleaning experiments to determine optimal cleaning parameters, which could be used in production process;
- Plasma cleaning experiments with deliberately contaminated substrate to test the limits of the cleaning technique, and comparison of these results with the effectiveness of chemical cleaning;
- Plasma cleaning experiments with un-cleaned substrate directly from vendor, and comparison of these results with effectiveness of chemical cleaning; and
- Plasma cleaning experiments with subsequent testing of substrate adhesiveness.

### *4.2.1 Offline Plasma Cleaning Test System*

All off-line experiments have been conducted in the small vacuum system shown in Fig. 4.1.

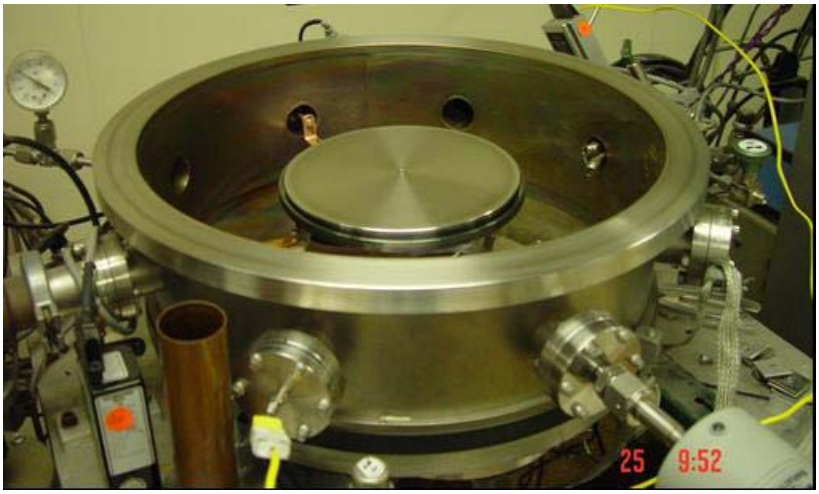


**Fig. 4.1.** View inside plasma cleaning vacuum chamber

This chamber has an 8” diameter stainless steel electrode, positively biased, approximately 1.5” from the grounded substrate attached to the lid of the chamber. The lid had an integral heater behind the substrate and a thin foil thermocouple was placed under the substrate to monitor the temperature.

The chamber pressure during plasma cleaning was fixed at 40 mtorr with a gas flow of 20 sccm (standard cc per minute) (this would be a typical pressure in the plasma chamber in the 30 MW production back reflector system). The temperature was set to 130 °C.

Two types of gas were used: an argon-oxygen mixture and pure argon.

The chamber vacuum background was typically 2-4 x $10^{-6}$ Torr prior to the tests.

The plasma voltage was 350 and 400 V at a current of 4.5 – 5.0 A.

### *4.2.2 Optimization of plasma cleaning parameters*

In this set of optimization experiments, the plasma voltage was fixed at 350 or 400 V while varying the plasma exposure duration between 15 and 30 s. These durations were longer than the current duration of substrate exposure to the cleaning plasma in the production BR machine; there are, however, potential hardware modifications that could extend the plasma treatment from current 5 s to as high as 15 s. The mixture of argon and 20 or 30% oxygen was used as the plasma forming gas.

We also tested the ability of the plasma to remove carbon bearing oily residues that in some cases might be present on the stainless steel substrate as received from the vendor. In this test, we spread pump oil on the stainless steel coupons and wiped off the excess with a lint free towel to simulate a thin covering of oil on the surface. Following the experiments, the samples were placed in a clean vacuum desiccator and sent for Auger spectroscopy analysis. Table 4-I displays the levels of contaminants observed by Auger analysis on the surface of the samples versus the plasma cleaning parameters.

**Table 4-I.** Results of Auger analysis after plasma cleaning

| SAMPLE | | | %C | %O | %Fe | %Cr | %Si | Thick. Oxide | Thick. Carbon |
|---|---|---|---|---|---|---|---|---|---|
| Thin oil | | | 72.8 | 16.2 | 0.0 | 0.0 | 11.0 | 117 | 163 |
| 350V | 20%$O_2$ | 15sec | 25.8 | 42.7 | 14.7 | 9.2 | 6.8 | 61 | 14 |
| 350V | 20%$O_2$ | 30sec | 18.5 | 46.1 | 14.4 | 9.7 | 10.6 | 72 | 15 |
| 400V | 20%$O_2$ | 15sec | 23.5 | 45.4 | 16.6 | 7.9 | 5.0 | 74 | 11 |
| 400V | 20%$O_2$ | 30sec | 18.6 | 50.9 | 16.5 | 8.2 | 5.0 | 80 | 13 |
| 350V | 30%$O_2$ | 15sec | 22.3 | 47.0 | 14.2 | 9.5 | 5.2 | 66 | 15 |
| 350V | 30%$O_2$ | 30sec | 22.8 | 50.4 | 11.9 | 8.1 | 5.6 | 68 | 13 |
| 400V | 30%$O_2$ | 15sec | 12.6 | 53.2 | 17.2 | 8.6 | 7.8 | 87 | 11 |
| 400V | 30%$O_2$ | 30sec | 17.5 | 50.6 | 16.4 | 8.2 | 6.3 | 104 | 11 |

Auger sputter profiling (ASP) was used to evaluate the effectiveness of the plasma treatment. Figure 4.2 displays the profile for the surface following oil contamination before plasma cleaning; Fig. 4.3 displays the profile for the surface following oil contamination after plasma cleaning. The actual thickness of the oil layer as measured by ASP was uncertain as the absolute sputter rate for the oil was unknown and would be difficult to measure. However, we can make relative comparisons to determine the most effective parameters.

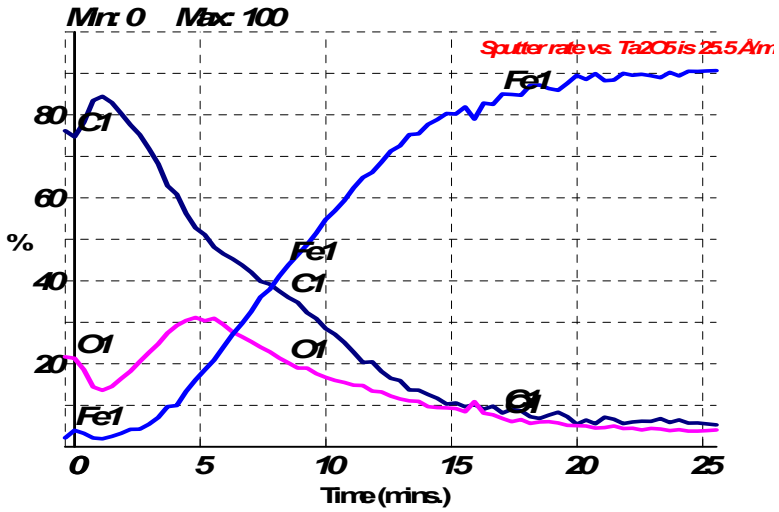


**Fig. 4.2.** Profile of oil contaminant before sputter cleaning.

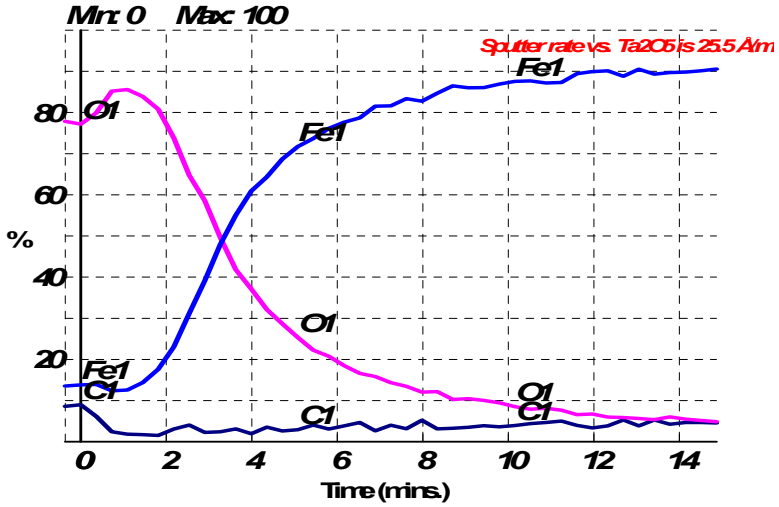


**Fig. 4.3**. Profile of oil contaminant after plasma cleaning. (400 V, 30%$O_2$, 15s).

Table 4-I clearly indicates that the percentage and thickness of carbon (and to a lesser degree, the percentage of silicon) can serve as a good measure of surface contamination. The data shows that an Ar + $O_2$ plasma effectively reduced level and thickness of hydrocarbon and silicon parts of the oil contaminant. As expected, the plasma removed the organic (hydrocarbon) parts of the contaminant much faster than its non-organic (silicon) component.

Figure 4.3 displays the thickness of the surface oxide following plasma treatment. The plasma treatment increased the oxygen on the surface of the substrate and removed the carbon.

It was not known whether the oxidation occurs in the plasma, or during subsequent exposure to atmosphere. It is well known that sputter cleaning can leave the surface a very reactive state, especially the chrome in the alloy. The fact that oxygen level and thickness grow even in case of wet cleaning and pure argon plasma, where no $O_2$ present, indicated that oxidation probably took place after the cleaning due to atmospheric oxidation of the chemically or plasma activated surface. Higher oxygen concentration increased the effectiveness of plasma

cleaning. Therefore at this stage we could consider plasma parameters of 400 V and Ar + 30% $O_2$ as optimal. While a further increase of oxygen concentration in plasma gas might increase the cleaning effectiveness, it was not desirable since it might compromise the safety of the gas pumping systems in both the experimental chamber and the production machine. Higher voltages also increased cleaning efficiency. Arcing limited the voltage used in the experimental chamber; the 30 MW Back Reflector Glow Chamber, however, allows operation with voltages up to 1500 V. Consequently, we could expect to see better results in the production equipment than we observed in the experimental equipment.

### *4.2.3 Tests of the limits of the plasma cleaning technique*

*Thick Films*

Further plasma cleaning experiments were intended to explore some extreme elements of the production environment, including heavier oily contamination of substrate and shortening of the plasma exposure duration. A drop of machine oil was put on the SS substrate sample and covered with the vendor's paper interleaf and another piece of SS. This "sandwich" was then compressed for an hour to simulate worst possible oily contamination. After removing top SS and interleaf, the remaining thick oily film was cleaned in an Ar + $O_2$ plasma.

We found that these thick oily films could not be removed with reasonable cleaning durations -- even with cleaning durations up to 1 hr. The film was removed only on few small spots within the main spot where the film was obviously thinner. The remaining film turned silver-white in color and stopped reacting with the plasma. [See Fig. 4.4]. It could be explained by the fact that at a pressure of 40 mtorr ion bombardment prevails over plasma activated chemical reactions in the plasma cleaning process. This can lead to molecular cross linking in deeper layers of thick contaminant with the formation of a hard to clean substance.

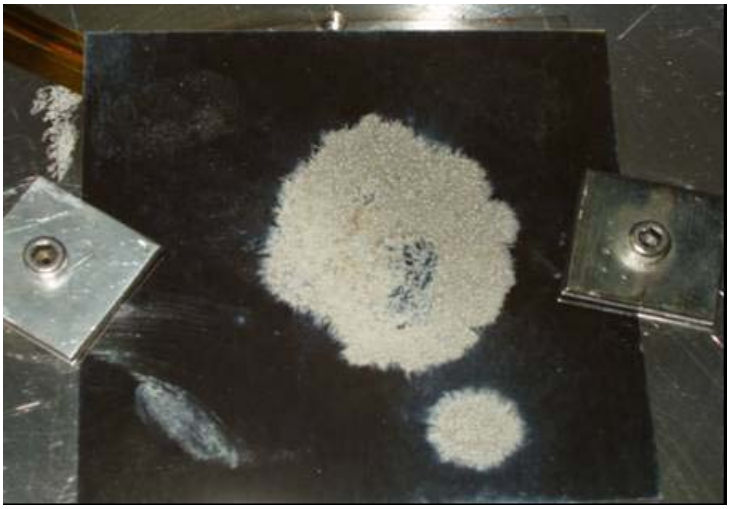

**Fig. 4.4.** Thick oily film after extended plasma treatment.

*Thin Films*

The plasma cleaning technique was found to be much more effective for the removal of thinner oily films, such as oily fingerprints (machine oil was used to wet fingers). In this set of experiments the plasma voltage was fixed at 400 V and the plasma exposure duration was varied (5, 15 and 30 s). One set of experiments used a pure argon plasma and another set used a mixture of argon and 30% of oxygen. We found that even a 5 s Ar + $O_2$ plasma treatment significantly reduced the thickness of the film and a 30 s treatment removed the fingerprints almost completely. The same tests with a pure Ar plasma showed that the cleaning process was about 3 times more effective with addition of oxygen. See Figs. 4.5-7 for the Ar plasma and Figs. 4.8-10 for the Ar +$O_2$ plasma treatment experiments.

These experiments have shown that plasma cleaning was not effective for removal of thick oily substrate contaminants. It may be said that wet chemical cleaning is more appropriate for such work. On the other hand, the removal of thick oil contaminants would require a higher concentration of the chemical cleaning agent in the current substrate washing process. And that, in its turn, can leave significant residues on the surface of substrate. Removal of that kind of contaminant would require extended rinse of the substrate, and that would reduce production capacity of the current washing machine. Regarding removal of thinner oily films, it may be said that plasma cleaning has clear advantages over wet chemical cleaning. Plasma process does not leave any detergent residues and due to the improved cleaning effect caused by the addition of oxygen, removes contaminations such as finger prints completely. Wet cleaning, despite of ability to remove the “greasy” component of finger prints, leave imprinted pattern of them on the substrate surface.

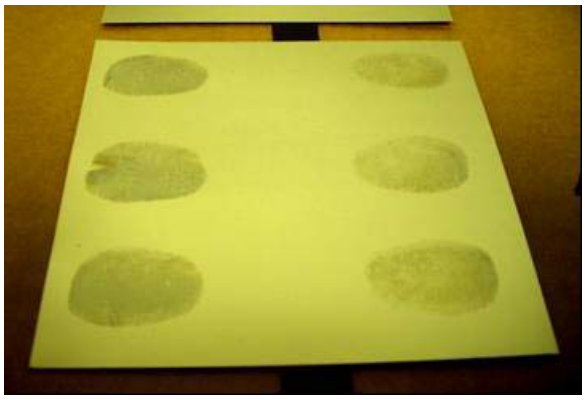

**Fig. 4.5** – Ar plasma, 5 seconds


**Fig. 4.6** – Ar plasma, 15 seconds


**Fig. 4.7** – Ar plasma, 30 seconds

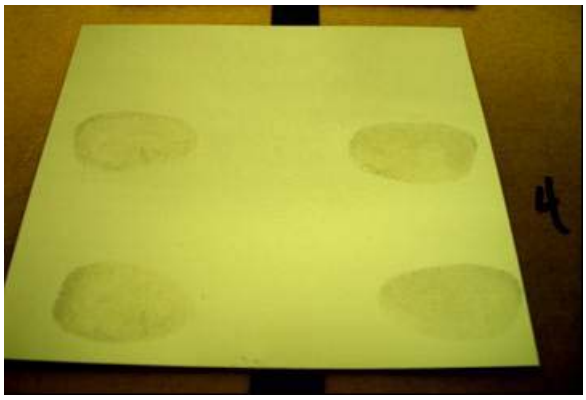


**Fig. 4.8** – Ar+$O_2$ plasma, 5 seconds


**Fig. 4.9** – Ar+$O_2$ plasma, 15 seconds


**Fig. 4.10** – Ar+$O_2$ plasma, 30 second

*4.2.4 Plasma cleaning of "as from vendor" substrate*

After the optimal plasma cleaning parameters were determined we performed additional plasma cleaning experiments (both Ar + $O_2$ and Ar) with plasma exposure times of 5 s to 30 s. The 5 s duration corresponded to the exposure time in the 30 MW BB Glow Chamber as it is currently configured; the 30 s duration corresponded to what can be potentially reached with hardware modifications. In these experiments the plasma voltage was fixed at 400 V while the plasma exposure duration was set at 5, 15 and 30 s. One set of experiments was done with pure argon plasma and another set involved a mixture of argon and 30% of oxygen. None of the samples used for plasma cleaning had any preliminary cleaning or deliberate contamination. The samples were cut off substrate rolls as received directly from the vendor. Each experiment was done with two or more samples to minimize data inconsistency and fluctuations. Along with these plasma treated samples, samples of washed (current wet cleaning process) and unwashed (as from vendor) SS substrate were sent for Auger tests to obtain data for comparison of plasma cleaning versus chemical cleaning or no cleaning. Average Auger data was calculated from multiple samples for each experiment. See Table 4-II.

**Table 4-II.** Auger Analysis Results

| SAMPLE | %C | %O | %Fe | %Cr | %Si | Thick. Oxide | Thick. Carbon |
|---|---|---|---|---|---|---|---|
| **Thin oil (1)** | **72.8** | 16.2 | 0.0 | 0.0 | 11.0 | 117 | **163** |
| **Unwashed (average of 4)** | 37.6 | 35.0 | 10.6 | 8.7 | 4.0 | 53 | 27 |
| **Washed (4)** | 26.0 | 43.6 | 13.8 | 10.6 | 4.7 | 62 | 17 |
| **Plasma Ar 5 s (2)** | 9.9 | 52.1 | 11.6 | 10.6 | 12.3 | 55 | - |
| **Plasma Ar 15 s (2)** | 10.8 | 50.6 | 11.4 | 9.2 | 13.0 | 69 | - |
| **Plasma Ar 30 s (2)** | 14.2 | 52.1 | 11.1 | 8.3 | 8.5 | 76 | - |
| **Plasma Ar+$O_2$ 5 s (5)** | 15.0 | 50.4 | 13.5 | 9.0 | 6.9 | 86 | 11 |
| **Plasma Ar+$O_2$ 15 s (3)** | 9.2 | 54.8 | 13.4 | 8.9 | 9.2 | 78 | 3 |
| **Plasma Ar+$O_2$ 30 s (3)** | 13.6 | 51.7 | 13.2 | 7.6 | 7.4 | 99 | 3 |

As shown in Table 4-II, again we see that both Ar and Ar + $O_2$ plasmas effectively reduced the level and thickness of the main contaminant (hydrocarbon) on the substrate surface. Even the shortest possible plasma treatment cleaned the substrate surface roughly two times better than the chemical wash. The Ar + $O_2$ plasma and chemical washing showed a higher percentage of surface iron than the Ar plasma. That might be interpreted as a "deeper" cleaning of the stainless steel substrate from the enhanced cleaning ability of the Ar + $O_2$ plasma.

Silicon atomic percentage was lower after Ar + $O_2$ plasma cleaning than after Ar plasma treatment. But the fact that chemically washed and plasma cleaned samples had higher percentage of silicon than unwashed substrate from vendor should be investigated further.

Table 4-II clearly indicates that silicon component of oily contaminant was significantly reduced by plasma treatment.

### *4.2.5 Substrate adhesiveness after plasma cleaning*

We also performed some experiments to check substrate adhesiveness after plasma cleaning. Unwashed substrate samples were exposed to plasma as in the experiments described in previous paragraph; then aluminum film was deposited on each of them by evaporating Al in vacuum. After that all samples were heated to 300 $^{o}$C and kept hot for a day, followed by a cool-down. Then very sticky packing tape was applied to each sample. The tape came off without peeling the aluminum film off any of the samples. Therefore, we could see that plasma cleaning does not reduce adhesiveness of the stainless steel substrate.

### *4.2.6 Conclusions*

All described experiments have proven that:

- Plasma cleaning has a twice higher effectiveness for cleaning “as from vendor” substrate than chemical washing.
- Plasma cleaning has higher effectiveness for cleaning substrate of thin oily contaminations (such as fingerprints) than chemical washing.
- Plasma cleaning has lower effectiveness on cleaning substrate with thick oily contaminations than chemical washing. Since thick oily contaminations of SS substrate have never been reported in real 30 MW photovoltaic production environment plasma cleaning may be considered as a substitute replacement for the existing wet chemical cleaning process.

## 4.3 Evaluation Of On Line Techniques for Measuring Substrate Cleanliness

The goal of this work was to evaluate existing techniques for measuring surface contamination levels on stainless steel substrate, currently used in the 30 MW photovoltaic production line. Use of online continuous cleanliness monitoring might improve production yield and help prevent downstream equipment contamination due to unexpectedly high levels of substrate contaminants.

Evaluation of the techniques for measuring substrate cleanliness included:

- A listing of known surface quality analytical techniques;
- Selection of the most suitable technique based on goals, applicability in the current production conditions and cost; and
- Description of selected technique and aspects of its implementation

### *4.3.1 Listing of surface analytical techniques*

Common surface quality analytical techniques are listed below:

- TXRF and VPD-TXRF - Total Reflection X-Ray Fluorescence and Vapor Phase Decomposition + TXRF
- XPS / ESCA - X-Ray Photoelectron Spectroscopy
- SIMS - Secondary Ion Mass Spectroscopy and sub techniques ULE-SIMS, TOF-SIMS, SNMS
- RBS / Channeling - Rutherford Backscattering Spectrometry
- NRA / ERD - Nuclear Reaction Analysis, Elastic Recoil Detection
- AES - Auger Electron Spectroscopy
- AFM and STM - Atomic Force Microscopy and Scanning Tunneling Microscopy
- FTIR - Fourier Transform Infrared Spectroscopy
- SEM and EDS - Scanning Electron Microscopy and Energy Dispersive Spectroscopy
- Raman Spectroscopy
- SPD - Surface Potential Difference
- Optical Ellipsometry
- OSEE - Optically Stimulated Electron Emission

### *4.3.2 Selection of the appropriate technique*

Selection of the cleanliness monitoring technique was dictated by restrictions of its application in the existing 30 MW PV production BR machine. Therefore, ability to build-in hardware components of the technique into the production system was the primary condition for the selection. The following factors have been considered:

- Current BR production QA-QC standards do not require precision analysis of the substrate surface composition. Therefore, qualitative contamination monitoring may be used along with quantitative detection of the contamination degree.
- There are three 14” wide SS substrates continuously moving roll to roll at process speed of 180 cm/min. Cleanliness should be monitored across entire width of each substrate on their deposition (bottom) sides.
- Contamination detection must be immediate to prevent significant yield decrease.
- If sensors of the selected cleanliness monitor are to be placed in close proximity to the substrate, then the sensors should withstand low process pressure of 40 mtorr.
- Also, depending in which chamber of the BR machine the sensors will be installed, the vertical distance for placement of the sensors is restricted by 7 or 17 in.
- Cleanliness monitoring techniques which involves very precision distancing between sensor and substrate may not be used due to machine vibrations and insignificant imperfections of substrate’s flatness.

These factors provided a very restrictive filter which could help to easily remove all but one technique from the list above.

Techniques which use electron and ion beams (SIMS, RBS/Channeling, NRA and ERD, AES, SEM/EDS) might not be used because:

- Use of the beams require pressures significantly lower than the 40 mtorr pressure and implementation of bulky focusing and accelerating systems which cannot be accommodated in existing BR machine.
- Very small analyzed areas.
- Very high cost of such systems.

Techniques which use X-ray, Infrared and Laser Spectroscopy (TXRF, VPD – TXRF, XPS / ESCA, FTIR, Raman) as well as Ellipsometry also might not be used because:

- These systems commonly have very small analysis areas and would require implementation of bulky mechanical scanning systems which cannot be accommodated in existing BR machine.
- These system have a variety of negatives such as slowness of XPS / ESCA, the need of pretreatment for VPD – TXRF or the inability to detect lighter elements as in TXRF
- These systems have a relatively high cost.

Techniques such as AFM and STM or SPD might not be used because require very precision distancing between substrate and the probe.

Therefore, only one suitable technique was left: OSEE - Optically Stimulated Electron Emission.

### *4.3.3 Description of selected technique and aspects of its implementation*

The OSEE uses ultra-violet light from a mercury discharge lamp to photo-emit electrons from the surface under study. A biased grid collects these electrons across the air gap, and the total current is displayed. According to OSEE experience, contaminants virtually always reduce photo-emission from a conducting substrate. There is no exact science, however, that relates the reduction in photo-current to the thickness or type of contaminant. The technique was developed in early 90's by NASA Langley Research Center to provide manufacturing control and documentation of bonding surfaces prior to bonding. Many configurations of OSEE Surface Quality monitors are manufactured by Photo Emission Tech. Inc. (CA). Such a system consists of control unit and sensor head. The sensor for 6" x 1/4" inspected area is shown in Fig. 4.11.

The Sensor and Controlling unit provide an analog output, which we monitored with a ***LabView*** program during initial tests. Variations in this signal can be used as the signal for contamination presence and contamination degree. The maximum sensor width is 6"; consequently, two or three sensors per substrate will be required – 6 or 9 total. The monitor's output signal varies immediately in accordance with the presence of a contaminant. The signal can be processed in the BR machine control computer for immediate alarming, real-time data representation and historian data logging. The device is sensitive to substrate-to-sensor distance (the photo-emitted electron current decays exponentially with distance from the surface in air). But in this technique the sensor–substrate distancing does not need to be ultra-precise as in AFM, STM or SPD. Placement of the sensors right under one of the substrate magnetic rollers, or a capstan roller in the take-up chamber would reduce signal distortions due to machine vibration and imperfections of substrate flatness. The UV lamp intensity

degrades over time with about a 5500 hour half-life. According to the manufacturer the lamp intensity degradation can be compensated with the optional high frequency, high voltage power supply for the lamp. It was recognized that main challenge of OSEE implementation would be functionality of the sensor in vacuum.

**Fig. 4.11.** The PET 6-in wide OSEE sensor head used in the Pay-Off and Take-Up chambers of the 30 MW Washing Machine.

While the OSEE has shown potential for both optimizing the cleaning process, and as an online QA device, it was not clear that it is cost effective.

- Sections of poor yield traced to substrate contamination are rare. Even in instances in which they have been observed it would have been a mistake to stop the process, as the poor yield section was relatively short.
- Diagnostics cost money to install, maintain, and to monitor. It is not clear that these costs would be recouped in production.
- Diagnostics are not perfect: yield problems directly traced to substrate contamination have been quite rare – possibly on the same order as the probability of a “false alarm” or diagnostic malfunction.

### *4.3.4 Conclusion*

The OSEE Surface Quality Monitor can be potentially used for measuring substrate cleanliness in the existing 30MW Back Reflector machine. Additional off-line tests for functionality in vacuum were found necessary. The cost-effectiveness, however, is not clear.

## 4.4 Implementation of Plasma Cleaning System into the 30 MW Roll-To-Roll Production Manufacturing Process

The goal was to implement effective plasma cleaning process in the production 30 MW BR machine and consecutively improve yield, or if possible, to simplify the production process by eliminating the wet chemical cleaning process step – one of the four Front-End Roll-to-Roll Machines. The following activities under the task have been conducted:

- Evaluation of existing BR machine plasma cleaning hardware for efficiency of the process;
- Design and manufacture of hardware to improve efficiency of the BR machine plasma cleaning process;
- Installation and optimization of the plasma cleaning hardware
- Initial evaluation of effectiveness of plasma cleaning process in BR machine

### *4.4.1 Evaluation of existing BR machine plasma cleaning hardware.*

The BR machine has plasma cleaning glow chamber located between pay-off chambers and the aluminum sputtering-deposition chamber as shown in Fig. 4.12. A thorough investigation of the hardware's design and observation of its working during a regular production run were carried out. The existing plasma cleaning reactor was a 50 in x 8 in x 5 in open-top box, assembled from aluminum panels. A stainless steel 1" thick solid cathode rested on 8 plastic spacers installed on the grounded bottom of the box. Three SS web substrates move roll-to-roll 0.5 in above the reactor box; the distances between the substrates were 2 in. The cathode was under variable 0 - 3 kV negative potential and the reactor box and substrates were grounded.

This existing design could not be considered as plasma tight. Plasma escaped through the 0.5" gap between cathode box and the substrates as well as through wide openings between the substrates. As the result we had plasma broadly dispersed around the top of the reactor box and above the substrates. Since the plasma was not confined strictly under the substrates it resulted in lost plasma cleaning efficiency. To eliminate plasma leakages, installation of a plasma confining mask was suggested.

The distance between the existing cathode and substrates was 3.75". It was decided to reduce the distance to obtain more intense plasma. Since rising of the cathode would involve significant modification of the existing design and prolonged down time of the production machine, installation of a secondary build-up cathode was suggested.

It was already mentioned that plasma cleaning reactor included a negative electrode, which served as a cathode and grounded substrates, which served as an anode. The cathode received negative potential from a power supply. It is well known that plasma cleaning basically consists of two processes. One of them is plasma chemical reactions, which have neutrals involved. Another process is ion bombardment. At the existing BR machine process pressure of 40 mtorr the ion bombardment significantly prevailed. Therefore, hardware arrangement where substrates were charged positive relative to another electrode utilized only plasma chemical reaction for substrate cleaning and the main cleaning process due to ion bombardment affected only the cathode. It was obvious after inspection of the plasma reactor: the cathode's top surface was shiny and slightly eroded due to the sputtering process caused by ion bombardment; on the contrary, the inner surfaces of the reactor box walls (they were, as

the substrates, under anode potential) were covered with the black deposits, which were the product of the cathode sputtering. Therefore, turning the cathode into the anode by changing its polarity from negative to positive was suggested.

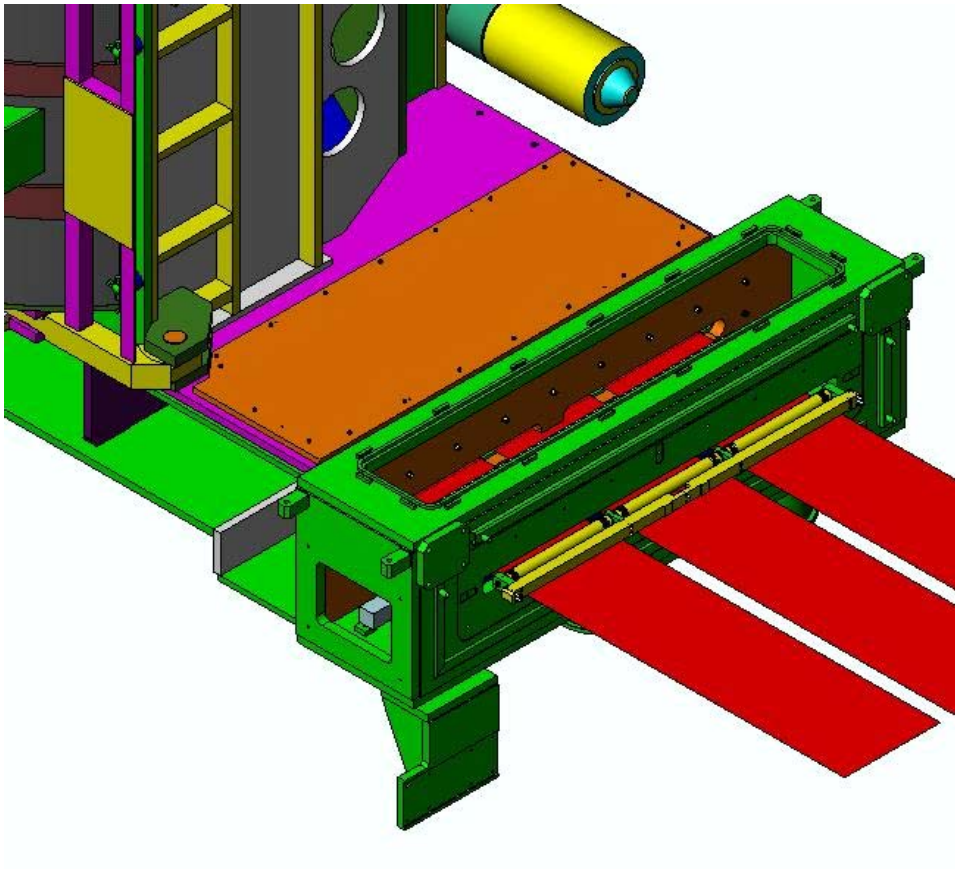

**Fig. 4.12.** BR plasma cleaning Glow Chamber

### *4.4.2 Design and manufacturing of the hardware to improve plasma cleaning efficiency*

Design and manufacturing of stainless steel plasma confining mask

The mask, shown in Fig. 4.13, closed openings between the substrates and formed a 0.25 in tall, 2 in long tunnel for the substrates to enter and exit the plasma reactor. The 0.25 in height of the tunnels resulted in 0.125 in gaps between substrates and tunnel's top and bottom and that distance was within plasma "dark space". Therefore, the plasma was supposed to be fully confined within the plasma reactor.

The height of the mask setting could be adjusted with the set screws. It allowed precise adjustment to eliminate any scratching of the substrate as it entered and exited the reactor.

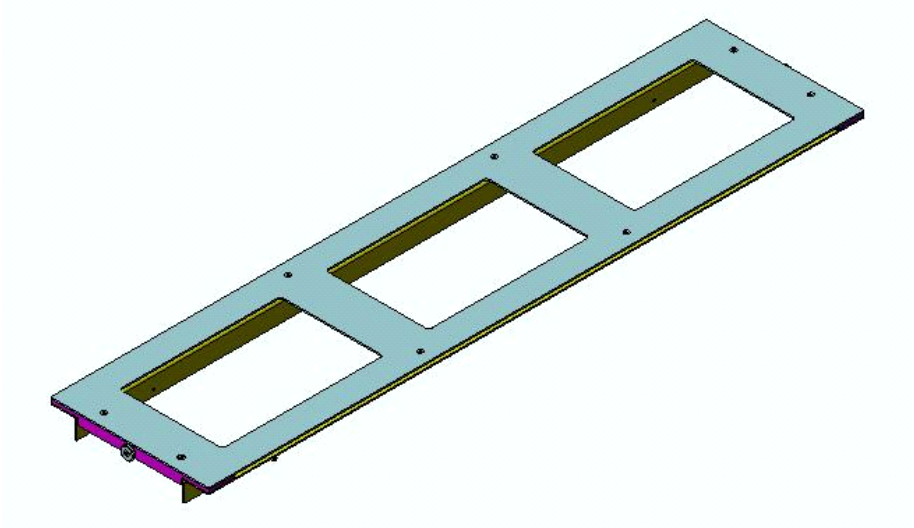

**Fig. 4.13.** Plasma confining mask assembly

Design and manufacturing of the secondary cathode

The secondary cathode was a temporary design to reduce the distance between the original cathode and the substrates with the goal of producing more intensive plasma. The secondary cathode was a 47.7 in x 7 in x 2.5 in hollow stainless steel box which would rest on the existing cathode.

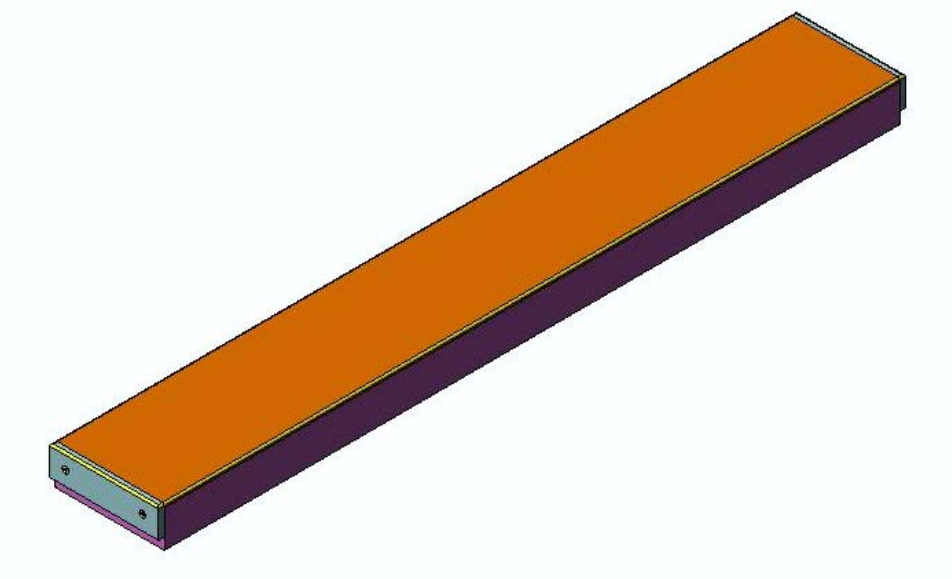

**Fig. 4.14.** Secondary plasma cleaning cathode

Since the secondary cathode had the same electric potential as the main cathode, its top, which was much closer to the substrates, served as a new cathode surface. The gaps between the sides of the box and plasma reactor's walls were less than 0.25 in wide and provided a "dark space" for the plasma.

*4.4.3 Installation and optimization of the plasma cleaning hardware.*

The plasma confining mask was installed first since manufacturing of the secondary cathode took a longer time. The mask worked exactly as expected: the plasma was fully confined within the reactor box without escaping. No significant heat-caused warping of the mask occurred during a prolonged production run. The substrates entered and exited the plasma reactor through the tight tunnels without any scratches.

At the same time it was decided to change polarity on the cathode from negative to positive. An attempt to do that and turn the cathode into anode resulted in surprising effect: plasma relocated from anode box to the space between bottom of the anode box and bottom of the glow chamber. Some spots of significantly brighter plasma were noticed in the middle of the plasma body. It turned out that grounded bottom of the anode box had six holes into which the anode supporting plastic spacers were inserted. This design flaw allowed anode plasma to completely escape from the reactor. Apparently attempts to use the anode versus cathode hardware configuration resulted in a much less “tamable” plasma. Since only the anode plasma could be considered as working in the sense of plasma cleaning at the glow process pressure, we expected that obtaining an intense stable anode plasma could be a serious, challenging task.

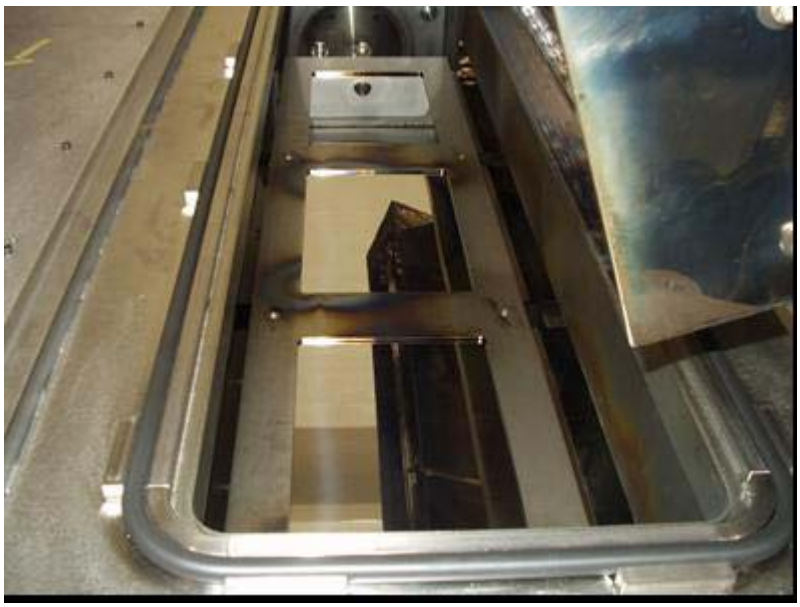

**Fig. 4.15.** Front view of the BR Glow camber with plasma confining mask installed

After the secondary anode was manufactured it was installed inside the plasma reactor box on the top of existing anode plate. At the same time the spacer holes in the grounded bottom of the reactor box were blocked by a thin sheet of stainless steel. Applying a positive voltage to the secondary anode did not result in any plasma leakages beneath the plasma reactor this time. It was obvious that these short paths for the plasma were reliably blocked, but, unfortunately, plasma did not start between the secondary anode and the substrates either. Instead plasma found another short path and started around power cable connecting the anode and electrical vacuum feed-through connector within the glow chamber. It was found

that the cable was not a coaxial cable typically used for such applications; rather, a piece of copper wire with alumina beads was used as the cable. Since there was no any grounded shielding on the wire it started to serve as another plasma igniter when at a high positive potential. The feed-through connector also found to be not suitable for this application. The distance between its grounded and electrically hot parts was about 1 in -- greater than the plasma “dark space” distance and consequently guaranteed a plasma between the two. The traces of plasma were found on the inner walls of insulating plastic cup, which was put on the connector. Therefore, the existing power cable along with feed through connector need to be replaced by a reliable coaxial cable similar to those used in previous generations of vacuum equipment designed by ECD.

After a proper coaxial cable and a new vacuum feed-through were manufactured and installed, another attempt to start the anode plasma took place. The secondary anode was removed from the test in order to evaluate the changes separately. This time the test went successfully. The plasma ignited at 250 V and stayed stable at currents of up to 3 A and a voltage of up to 750 V. This resulted in stable plasma power of up to 2 kW which is in four times higher than they could reach with the negative cathode while using old power cable and it feed-through. It is also worth noting that the anode plasma was very stable while the cathode plasma flickered and displaced. The plasma power was limited by the power supply’s current limit of 3 A.

An overnight BR plasma cleaning test was conducted. Since the previous year’s running of cathode plasma had significantly contaminated the inner walls of the plasma reactor (up to 0.2 mm thick matte black deposits), it was decided to leave the reactor deliberately dirty to estimate anode plasma’s cleaning abilities and at the same time to clean the reactor for the future tests on surface cleaning. The plasma ran at power of 1.5 kW for 12 hours. The results of the test might be considered promising. The matte solid contaminant became shiny and porous. In the lower part of the reactor, closer to the anode, the pores grew deep and wide enough to form clusters and as a result there were spots of bare aluminum. The ceiling of the reactor formed by the substrates and confining mask became rather contaminated than cleaned.

These observations allowed us to think that plasma’s density was much higher in the lower part of the reactor, closer to the anode, and not strong enough in reactor’s upper part to effectively fight deposition of the sputtered contaminant on the mask and substrates. All that called for immediate testing of the secondary anode to reduce the distance between the anode and substrate. The secondary anode was reinstalled and tested. The plasma would not ignite at voltage of up to 1.2 kV; instead an arcing started at 1.2 kV. This might be explained by a poor contact between main and secondary anodes. A test to identify the problem was conducted. After further investigation of the problem it was assumed that the gap between the secondary anode and substrate, approximately 1 in, was too small for effective ionization of the gas at the operating pressure, 40 mtorr. To verify this assumption the plasma confining mask was removed consequently exposing the anode to the more remote grounded surface of the substrate heater between the substrates. The distance between the anode and the heater was approximately 2.5” through the openings between the webs. As a result plasma ignited at 300 V and burnt between the webs and inside the chamber. That fact eliminated assumption of poor contact between main and secondary cathode and confirmed that too small a distance between secondary cathode and substrates was to blame.

A new design of the secondary anode was suggested. Instead of using a hollow block, a 0.75 in thick aluminum plate with four vertical 1 in thick aluminum ribs was designed as shown in Fig. 4.16. The design provided two different distances between the anode's electrically hot surface and substrates: 3 in between the ribs and 1.5 in above the ribs. Therefore, the dips between the ribs would serve as plasma igniters and top of the ribs as plasma "concentrators".

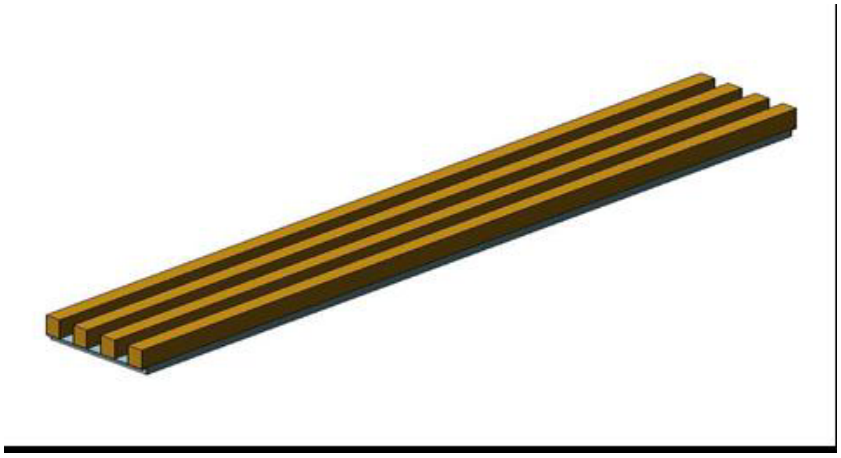

**Fig. 4.16.** Ribbed anode assembly

After fabrication of the new secondary anode it was installed in the BR glow chamber. Plasma started at 400 V. The voltage gradually increased to 1500 V with the current of 1 A. The cleaning plasma was left on overnight to see if previously contaminated confining mask could be cleaned. The test resulted in 70% cleaning of the previously contaminated area. Study of logged Historian data of the test showed though that after one hour of stable plasma cleaning, the plasma current started to degrade and gradually decreased to 30% of initial current down to 0.3 Amp. This resulted in a decrease of plasma power from 1.5 kW to 0.45 kW.

Another test was conducted and this time plasma current started to degrade right after plasma was started and maximum current reached. It was noticed that increase of substrate speed partially brought plasma current back and reduced the speed of the current degradation. Visual investigation of the ribbed anode discovered some discouraging signs: the two side ribs were coated with a dark film and previously cleaned areas of the mask above the ribs also got coated. It allowed us to conclude that cleaning plasma stopped burning above the side ribs.

It is expected that in order to reproduce plasma cleaning efficiency similar to the efficiency reached in off-line experiments that the plasma power in BR glow reactor should be in the range of 4-6 kW. Therefore, any degradation of the power can cause plasma to lose its cleaning ability. Therefore, it was decided to remove the secondary anode and try to reach maximum plasma power with primary anode only since the earlier tests indicated that primary anode plasma did not degrade during overnight run. This test was conducted. Plasma started at 300 V and remained stable for two hours with the current of 3 A at 600 V. The substrate was moving slow at 1/15 of the process speed. Visual inspection of the confining mask found that coated areas located above the side ribs of the secondary anode were cleaned. The plasma power in the test was limited by the 3 A current limit of the power supply. It was decided to use another power supply with a higher current limit. The maximum power reached

was 4 kW and that could be considered as high enough to obtain plasma cleaning efficiency similar to one in off-line experiments.

### *4.4.4 Initial evaluation of effectiveness of plasma cleaning process in BR machine*

Despite the fact that ribbed secondary anode could not provide steady plasma parameters during overnight testing, the test could be considered successful: 70% of the contaminated area was etched through the thick contaminant to the bare stainless steel.

**Fig. 4.17.** Inner surface of the confining mask

In Fig. 4.17 it can be seen that large rectangular dark areas between the mask's windows were significantly cleaned. These areas were exposed to the same cleaning plasma as the substrates. Dark areas on the ends of the mask accumulated sputtered contaminant from initial cleaning experiments. These areas of the mask, as well as the narrow strips along short sides of the mask windows, were not exposed to plasma but exposed to deposits of sputtered contaminant.

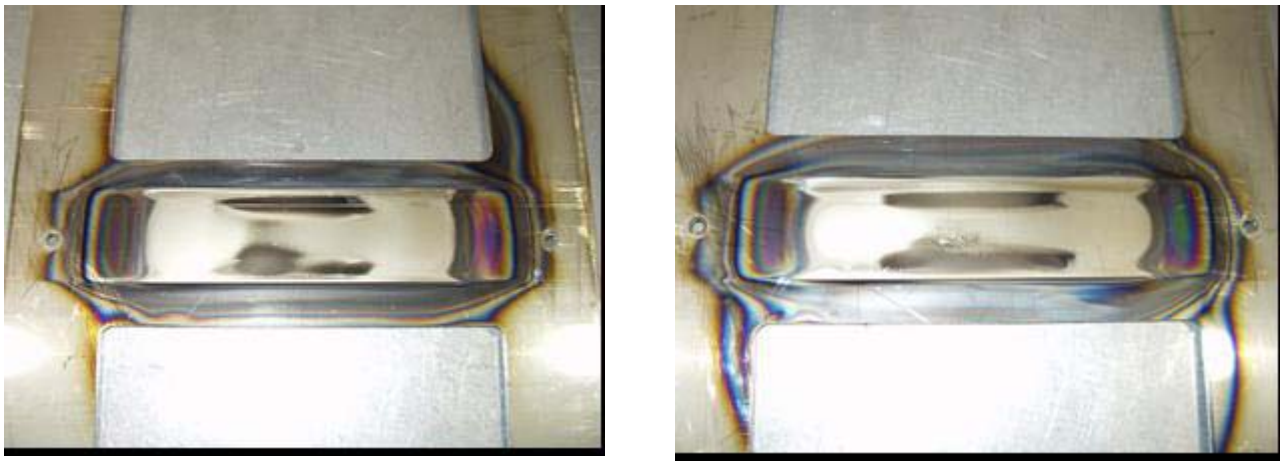

**Fig. 4.18.** Closer view of cleaned areas on the mask

The next overnight cleaning test at lower power cleaned the contaminated areas to 99% of bare stainless steel. It should be realized that such thick and visible deposits of contaminant in the non-plasma exposed areas were result of intensive sputtering during initial plasma cleaning experiments. The contaminant accumulated on the plasma reactor's walls over a period longer than a year. Initial plasma cleaning experiments resulted in intensive transfer of the contaminant from areas with the dense plasma (lower part of the reactor) to areas with the weaker plasma (mask and substrates). Since the proper modifications of the plasma reactor have been performed there will be no contamination of reactor walls and substrates anymore. Contamination of non-plasma exposed areas should not significantly affect plasma cleaning process and will require just regular infrequent (3-4 times a year) sandblasting. The high power (4 kW) plasma obtained during these tests without a secondary anode installed allowed us to reach plasma density similar to the density of the secondary anode plasma.

## 4.5 Off-Line Vacuum Testing of the OSEE Monitor for Implementation in BR

According to the manufacturer, the OSEE sensor could work in vacuum at pressures as low as 40 mtorr. Nevertheless, it was decided to test the sensor in a small vacuum chamber. The sensor assumingly may be used as a substrate cleanliness monitor in the production BR machine. The special hardware was designed and manufactured for the tests. The hardware included a vacuum plate with two sealed OSEE sensor feed through connectors and a table of adjustable height for precision placement of substrate sample above the OSEE sensor.

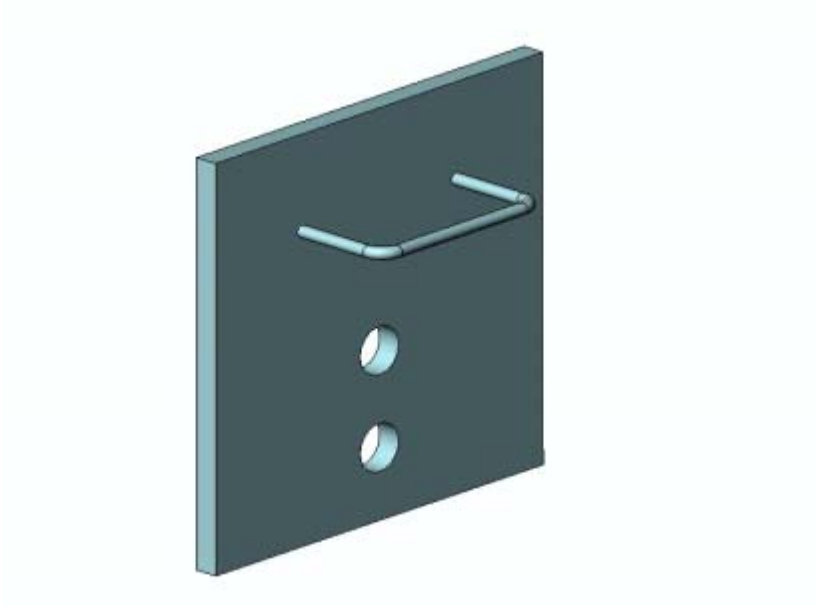

**Fig. 4.19.** Vacuum plate with the holes for two sealed OSEE sensor's feed through connectors.

**Fig. 4.20.** OSEE sensor sample table.

The plate was installed on the front of a small vacuum chamber, where the OSEE sensor and sample table were placed. The distance between the OSEE sensor and the sample was adjusted to 1mm, at atmospheric pressure which proved a strong OSEE signal even with lowest setting of the sensor's gain.

The initial tests indicated that low pressure did not cause any mechanical damage to components of the OSEE sensor. The OSEE signal grew roughly by a factor of 30 as the pressure was decreased from 760 torr to 1 torr. When pressure dropped bellow 1 torr, the OSEE signal became very unstable and at pressure of about 50 mtorr the signal dropped

down to very low reading. After some investigation it was found that arcing on the vacuum side of OSEE sensor's feed trough connector was to blame. The voltage for OSEE sensor's UV lamp is about 350 V while the starting voltage is up to 800 V. That was high enough to cause electric arcing at low enough pressures as well as some undesirable plasma. A special high voltage vacuum sealed connector was installed for the next test. The high voltage cable was replaced with the shielded coaxial cable to prevent ignition of plasma around the cable, and the UV lamp's leads were electrically sealed with the Torrseal alumina-based epoxy compound.

Further tests showed that all these measures could not solve the problem of the OSEE signal instability. The fact that the OSEE signal was extremely sensitive to the slightest arcing or discharge around the sensor could make the use of the sensor in vacuum doubtful.

Nevertheless, it was decided to continue the sensor tests in vacuum. Since after the above mentioned modifications of the sensor no visible traces of arcing or plasma were found, the aluminum vacuum plate was replaced with the plate made from a transparent plastic. It would allow observation of factors, if visible, caused the instability of the OSEE signal at pressures lower than 1 torr.

Observations of OSEE sensor work trough the vacuum transparent plate allowed us to see that there was no arcing anymore at the pressures lower than 1 Torr. Instead it was seen that UV lamp discharge extinguished and became very dim at pressure of 100-80 mtorr. It seemed that when chamber pressure was getting close to the lamp vapor pressure the lamp discharge partially moved from inside the lamp to the lamp outer space. To prove this theory the following experiments were done: the UV lamp has a tight wire mesh sleeve on its outer surface. This serves as a collector of photoelectrons. The collector is grounded. The lamp was tested in vacuum, separately from the sensor, with the sleeve on and off the lamp. The lamp without the sleeve did not lose discharge, while the lamp with the sleeve did lose discharge at above mentioned pressure. Since the sleeve is an essential part of the OSEE sensor design, it was hard to plan any of its modifications without risk of serious corruption of the sensor's functions. Nevertheless, it was noticed that further reductions in the system pressure caused the lamp's discharge to gradually return and stabilize. The accurate pressure of the discharge's return was hard to recognize since the chamber had only the Bourden tube pressure gauge. The measurement of the pressure with a high accuracy vacuum gauge helped us to notice that the sensor's UV lamp extinguished at pressure of approximately 1 torr and reignited at pressures of 200-500 mtorr. Those numbers were quite different from the previously recorded, inaccurate readings and allowed us to think that OSEE sensor might be used for our production applications.

There were also reasons to assume that at such low pressures the there may be a significant background signal. Presence of the background signal might be explained by generation of some photoelectrons within the sensor itself in close proximity of the UV lamp. Therefore, tests were conducted with OSEE sensor completely insulated to prevent UV coming out and photoelectrons coming in.

These tests indicated that at a pressure of approximately 200 mtorr the background signal was about 800 at lowest signal gain setting of the OSEE controller. The tests with OSEE sensor open and coupled with SS substrate at 0.125" distance between indicated OSEE signal of 1200 at similar pressure.

The signal of 1200 at the lowest gain indicated that OSEE amplifier was saturated and no further instrumental gain reduction was provided. Therefore, to estimate ratio between substrate and background signals and to adjust the sensor for work at real BR pressure, methods to further reduce of the OSEE summary signal were investigated. It was found that ratio between substrate and background signals was approximately 8:1 at pressures in the region of 200-250 mtorr. The substrate signal sharply grew and saturated amplifier at lower pressures while background signal grew gradually. Therefore, it was impossible to determine the ratio at lower pressures. The sensor was taken apart to investigate the ways for further reduction of the OSEE signal. The following measures can be taken: reducing the OSEE signal electronically by using smaller amplifier's input resistor, reducing accelerating voltage on photoelectron collecting electrodes, or reducing the area of the mesh photoelectron collecting electrode.

It is not clear enough now if installation of OSEE sensor in the production BR machine is feasible. The necessity of its use in the machine is conditioned by effectiveness of BR plasma cleaning and consequently by the scenario when wet washing process is given up. Since the conditions are not known yet it is not clear if the OSEE sensor will be installed in the current BR machine or in a next-generation machine. Therefore, it is not known yet at what pressure the OSEE sensor will work. Since this parameter is essentially important for the functionality of the sensor it was decided that the most appropriate way for reduce of OSEE signal in vacuum would be regulated amplifier's input resistance.

# REPORT DOCUMENTATION PAGE

*Form Approved*
*OMB No. 0704-0188*



**PLEASE DO NOT RETURN YOUR FORM TO THE ABOVE ORGANIZATION.**

| 1. REPORT DATE *(DD-MM-YYYY)* | 2. REPORT TYPE | 3. DATES COVERED *(From - To)* |
|---|---|---|
| February 2005 | Subcontract Report | 1 September 2003–31 August 2004 |

**4. TITLE AND SUBTITLE**
Implementation of a Comprehensive On-Line Closed-Loop Diagnostic System for Roll-to-Roll Amorphous Silicon Solar Cell Production: Annual Report, Year Two, September 2003–31 August 2004

**5a. CONTRACT NUMBER**
DE-AC36-99-GO10337

**5b. GRANT NUMBER**

**5c. PROGRAM ELEMENT NUMBER**

**6. AUTHOR(S)**
T. Ellison

**5d. PROJECT NUMBER**
NREL/SR-520-37660

**5e. TASK NUMBER**
PVB56101

**5f. WORK UNIT NUMBER**

**7. PERFORMING ORGANIZATION NAME(S) AND ADDRESS(ES)**
Energy Conversion Devices, Inc.
1621 Northwood
Troy, Michigan 48084

**8. PERFORMING ORGANIZATION REPORT NUMBER**
ZDO-2-30628-11

**9. SPONSORING/MONITORING AGENCY NAME(S) AND ADDRESS(ES)**
National Renewable Energy Laboratory
1617 Cole Blvd.
Golden, CO 80401-3393

**10. SPONSOR/MONITOR'S ACRONYM(S)**
NREL

**11. SPONSORING/MONITORING AGENCY REPORT NUMBER**
NREL/SR-520-37660

**12. DISTRIBUTION AVAILABILITY STATEMENT**
National Technical Information Service
U.S. Department of Commerce
5285 Port Royal Road
Springfield, VA 22161

**13. SUPPLEMENTARY NOTES**
NREL Technical Monitor: R. Mitchell

**14. ABSTRACT** *(Maximum 200 Words)*

Energy Conversion Devices, Inc. (ECD) has developed and built 7 generations of roll-to-roll amorphous silicon PV production equipment. In the ECD/United Solar Ovonic production process, we deposit about a 1-μm-thick, 12-layer coating consisting of a metal/oxide backreflector, a - layer a-Si/a-SiGe alloy triple-junction solar cell, and a top transparent conductive oxide coating onto 125-μm-thick, 35.5-cm-wide stainless steel webs in a series of three roll-to-roll deposition machines. ECD has now completed the Phase II work for this program. In the following report, we summarize the Phase II work in each of these tasks. We have involved United Solar production personnel in each of these Tasks. This is important for two reasons: Firstly, the collaboration of ECD and United Solar personnel keeps the projects responsive to the developing needs at United Solar. Secondly, most of the tasks affect operations and consequently need the support of United Solar production and QA/QC managers. In the process, we have developed a good working relationship between the production personnel and good balance between optimizing production, while also “adiabatically” improving the manufacturing equipment.

**15. SUBJECT TERMS**
PV; module; solar cells; manufacturer; roll-to-roll amorphous silicon; production equipment; back reflector; transparent conductive oxide (TCO) coating; triple junction; PV capacitive diagnostic (PVCD); metal/oxide back backreflector; stainless steel webs;

| 16. SECURITY CLASSIFICATION OF: | | | 17. LIMITATION OF ABSTRACT | 18. NUMBER OF PAGES | 19a. NAME OF RESPONSIBLE PERSON |
|---|---|---|---|---|---|
| a. REPORT | b. ABSTRACT | c. THIS PAGE | | | |
| Unclassified | Unclassified | Unclassified | UL | | 19b. TELEPONE NUMBER (*Include area code)* |

**Standard Form 298** (Rev. 8/98)
Prescribed by ANSI Std. Z39.18